# รายงานวิจัยฉบับสมบูรณ์

โครงการ

**การศึกษาการตอบสนองของเซลล์ท่อไตต่อการเกาะจับของผลึกแคลเซี่ยมอ๊อกซาเลทที่เป็นกลไกสำคัญในการเกิดโรคนิ่วในไตโดยใช้เทคนิคทางโปรตีโอมิกส์**


โดย

**นายแพทย์ วิศิษฏ์ ทองบุญเกิด**



**มิถุนายน พ.ศ. 2552**

สัญญาเลขที่ **RMU4980040**

# รายงานวิจัยฉบับสมบูรณ์

โครงการ

**การศึกษาการตอบสนองของเซลล์ท่อไตต่อการเกาะจับของผลึกแคลเซี่ยมอ๊อกซาเลทที่เป็นกลไกสำคัญในการเกิดโรคนิ่วในไตโดยใช้เทคนิคทางโปรตีโอมิกส์**

ผู้วิจัย

**นายแพทย์ วิศิษฏ์ ทองบุญเกิด**

**หน่วยโปรตีโอมิกส์ทางการแพทย์ สถานส่งเสริมการวิจัย**

**คณะแพทยศาสตร์ศิริราชพยาบาล มหาวิทยาลัยมหิดล**

**สนับสนุนโดยสำนักงานคณะกรรมการการอุดมศึกษา**

**และสำนักงานกองทุนสนับสนุนการวิจัย**

## กิตติกรรมประกาศ

ผู้วิจัยขอขอบคุณพระคุณสำนักงานกองทุนสนับสนุนการวิจัย (สกว.) และ สำนักงานคณะกรรมการการอุดมศึกษา (สกอ.) ที่สนับสนุนเงินทุนวิจัยสำหรับดำเนินงานโครงการวิจัยเรื่องนี้ ซึ่งจะเกิดขึ้นไม่ได้เลยหากปราศจากการสนับสนุนเงินทุนวิจัยดังกล่าว ขอขอบพระคุณคณะแพทยศาสตร์ศิริราชพยาบาล และมหาวิทยาลัยมหิดล สำหรับการสนับสนุนในทุกๆ ด้านจากไม่ว่าจะเป็นเรื่องสถานที่ทำการวิจัย โครงสร้างพื้นฐาน เครื่องมือ และอุปกรณ์วิจัย ขอขอบคุณผู้ร่วมงานทุกท่านทุกระดับในทีมวิจัยที่ร่วมกันทำวิจัย สร้างองค์ความรู้ใหม่ และผลิตผลงานวิจัยที่มีคุณภาพและเป็นประโยชน์ต่อสังคมโดยรวม

## บทคัดย่อ

**รหัสโครงการ** RMU4980040

**ชื่อโครงการ** การศึกษาการตอบสนองของเซลล์ท่อไตต่อการเกาะจับของผลึกแคลเซี่ยมอ๊อกซาเลทที่เป็นกลไกสำคัญในการเกิดโรคนิ่วในไตโดยใช้เทคนิคทางโปรตีโอมิกส์

**ชื่อนักวิจัย** นพ. วิศิษฏ์ ทองบุญเกิด
คณะแพทยศาสตร์ศิริราชพยาบาล มหาวิทยาลัยมหิดล

**E-mail address** vthongbo@yahoo.com

**ระยะเวลาโครงการ** 3 ปี (1 กรกฎาคม พ.ศ. 2549 ถึง 30 มิถุนายน พ.ศ. 2552)

**เนื้อหางานวิจัย**

โรคนิ่วในไตยังคงเป็นปัญหาสาธารณสุขที่พบบ่อยทั่วโลก โดยองค์ประกอบของก้อนนิ่วส่วนใหญ่คือผลึกแคลเซี่ยมอ๊อกซาเลท และการเกาะจับของผลึกแคลเซี่ยมอ๊อกซาเลทบนเซลล์ท่อไตเป็นเหตุสำคัญทำให้เกิดการตอบสนองของเซลล์จนพัฒนาเป็นก้อนนิ่วในที่สุด อย่างไรก็ตามกลไกระดับโมเลกุลของการตอบสนองดังกล่าวยังไม่เป็นที่ทราบแน่ชัด ผู้วิจัยจึงทำการศึกษาการตอบสนองของเซลล์ท่อไตต่อการเกาะจับของผลึกแคลเซี่ยมอ๊อกซาเลทชนิดโมโนไฮเดรต (COM) และผลึกแคลเซี่ยมอ๊อกซาเลทชนิดไดไฮเดรต (COD) โดยดูจากการเปลี่ยนแปลงการแสดงออกของโปรตีนโดยใช้เทคนิคทางโปรตีโอมิกส์ชนิดเจล ทำการทดลองโดยเลี้ยงเซลล์ท่อไตชนิด MDCK ในภาวะที่มีผลึก COM หรือ COD (100 ไมโครกรัมต่อ 1 มิลลิลิตรของสารอาหารเลี้ยงเซลล์) เป็นระยะเวลา 48 ชั่วโมงเปรียบเทียบกับภาวะที่ไม่มีผลึกดังกล่าว การวัดจำนวนเซลล์ตายโดยวิธี annexin V/propidium iodide double staining แสดงผลร้อยละของเซลล์ตายพอๆกันในทุกตัวอย่าง จากนั้นจึงทำการสกัดโปรตีนออกจากเซลล์ แยกโดยเจลอิเล็กโตรโฟรีซิสสองระนาบ และดูด้วยสีสำหรับย้อมโปรตีนทั้งหมด phosphoproteins หรือ glycoproteins (จำนวน 5 แผ่นเจลต่อกลุ่มตัวอย่าง) การวิเคราะห์เชิงปริมารและสถิติแสดงการเปลี่ยนแปลงอย่างมีนัยสำคัญของระดับของโปรตีนทั้งหมด 20 ชนิด phosphoproteins 20 ชนิด และ glycoproteins 5 ชนิดจากการเหนี่ยวนำโดยผลึก COM และพบการเปลี่ยนแปลงอย่างมีนัยสำคัญของระดับของโปรตีนทั้งหมด 11 ชนิด phosphoproteins 11 ชนิด และ glycoproteins 18 ชนิดจากการเหนี่ยวนำโดยผลึก COD จากนั้นจึงวิเคราะห์ชนิดของโปรตีนที่เปลี่ยนแปลงดังกล่าวโดยเทคนิคแมสสเปคโตรเมตรี้ โดยโปรตีนที่เปลี่ยนแปลงดังกล่าวเกี่ยวข้องกับ transcription, translation, signal transduction, cellular metabolism, nuclear membrane structure, cellular transport, cellular structure, stress response, biosynthesis, enzyme activation และ growth regulation ข้อมูลที่ได้เหล่านี้อาจนำไปสู่ความรู้ความเข้าใจถึงการตอบสนองของเซลล์ท่อไตส่วนปลายต่อการเกาะจับของผลึกแคลเซี่ยมอ๊อกซาเลทที่ดียิ่งขึ้น

**คำหลัก**
แคลเซี่ยมอ๊อกซาเลท; การเกาะจับของผลึก; โรคนิ่วในไต; โปรตีโอม; โปรตีโอมิกส์

## ABSTRACT

**Project code** RMU4980040

**Project title** Proteomic analysis of responses in renal tubular cells to calcium oxalate crystal adhesion: Implications for stone formation

**Investigator** Visith Thongboonkerd, MD

Faculty of Medicine Siriraj Hospital, Mahidol University

**E-mail address** vthongbo@yahoo.com

**Project period** 3 years (1 July 2006 – 30 June 2009)

**Research contents**

Kidney stone disease remains a common public health problem worldwide. Major composition of kidney stones is calcium oxalate (CaOx) crystals. Adhesion of CaOx crystals to renal tubular cells is an important event that triggers a cascade of responses, leading to the development of kidney stones. However, molecular mechanisms of these cellular responses remain largely unknown. We therefore performed gel-based, differential proteomics study to examine cellular responses (as determined by altered protein expression) in renal tubular cells induced by CaOx monohydrate (COM) and CaOx dihydrate (COD) crystal adhesion. Madin-Darby canine kidney (MDCK) cells were cultivated in culture medium with or without COM or COD crystals (100 μg crystals per 1 mL culture medium) for 48 h. Cell death assay using annexin V/propidium iodide double staining showed that all these samples had comparable % cell death. Cellular proteins were then extracted, resolved with two-dimensional polyacrylamide gel electrophoresis (2-D PAGE), and visualized using dyes that could stain total proteins, phosphoproteins, or glycoproteins (n = 5 gels per group). Quantitative intensity analysis and statistics revealed significantly altered levels of 20 proteins, 20 phosphoproteins, and 5 glycoproteins induced by COM crystal adhesion, and 11 proteins, 11 phosphoproteins, and 18 glycoproteins induced by COD crystal adhesion. These altered proteins were then identified by mass spectrometry, including those involved in transcription, translation, signal transduction, cellular metabolism, nuclear membrane structure, cellular transport, cellular structure, stress response, biosynthesis, enzyme activation and growth regulation. These data may lead to better understanding of cellular responses in distal renal tubular cells upon CaOx crystal adhesion.

**Keywords**

Calcium oxalate; Crystal adhesion; Kidney stone disease; Proteome; Proteomics

## INTRODUCTION

Kidney stone disease remains a common public health problem worldwide. The stone has originated by nucleation of crystals (due to supersaturation of calcium and oxalate ions in renal tubular fluid), followed by their retention and accretion in the kidney [1]. The major composition of kidney stones is calcium oxalate (CaOx) crystal, particularly CaOx monohydrate (COM), which is the most thermodynamically stable hydrate form that has the most potent adhesive capability to the renal tubular cell surface [2, 3]. A number of crystal-binding molecules on tubular cell surface have been identified, including CD44 [4, 5], hyaluronan [4, 5], osteopontin (OPN) [4, 5], annexin II [6], nucleolin-related protein (NRP) [7, 8], and sialic acid-containing glycoprotein [9].

Several recent studies have suggested that adhesion of crystals to the surface of renal tubular cells is probably the most critical step for kidney stone formation [7, 10, 11]. COM crystals can induce cellular oxidative stress, both *in vitro* and *in vivo*, that leads to overproduction of free radicals and reactive oxygen species (ROS), *i.e.* superoxide ($O_2^{\bullet -}$) and hydrogen peroxide ($H_2O_2$) [12]. These molecules play important roles as mediators of signal transduction pathways that can activate several signaling molecules, *i.e.* p38 mitogen-activated protein kinase (p38-MAPK); transcription factor, *i.e.* nuclear factor kappa B (NF-ĸB); and activation protein-1 (AP-1) [13]. On the other hand, renal tubular epithelial cells can generate inflammatory mediators that, in turn, cause an infiltration of phagocytes around the interstitial crystals. For example, monocyte chemoattractant protein-1 (MCP-1), which is a potent chemoattractant for monocytes and macrophages that plays a crucial role in the pathogenesis of a variety of crystal deposition disease, is overexpressed in renal tubular epithelial cells exposed to COM crystals [14]. Even with the aforementioned knowledge, the molecular mechanisms of cellular responses to COM crystal adhesion remain largely unknown.

In the post-genomic era, several biotechnologies have been developed to utilized genomic information to explain the biology and physiology of cell, tissue, or organ. One of the post-genomic studies is proteomics, which has recently been applied to several aspects of biomedical research. History of proteomics began in 1994 when Marc Wilkins first coined the term ‘proteome’ (set of proteins expressed by the genome) in the public at the Siena electrophoresis conference [15]. Since then, there have been several definitions for proteomics, which can be simply defined as the subject to study the proteome. Perhaps, the best definition for proteomics is *“the systematic analysis of proteins for their identity, quantity, and function”* described by Peng and Gygi [16]. The rapid progress of the proteomics field

during the past decade is based primarily on the success of: (i) genomics, especially when the Human Genome Project was completed – because proteins can be identified on genomic-scale basis; (ii) protein separation techniques, either gel-based (two-dimensional polyacrylamide gel electrophoresis, 2-D PAGE) or gel-free (liquid chromatography, LC); and (iii) mass spectrometry, which is the core technique in protein identification. The data obtained from proteomic analysis are complementary to those obtained from genomic analysis and other 'OMICS' studies (e.g. transcriptomics, metabolomics, interactomics, lipomics, glycomics, etc.).

Western blot analysis and other immunological methods have been utilized successfully to examine various proteins for a long time. Immunological methods are, however, limited in some instances because: (i) only a small number of proteins can be simultaneously studied in a single experiment; (ii) the specific antibody must be existing and available; and (iii) the proteins of interest are based entirely on *a priori* assumption. Proteomic analysis can be utilized to examine a larger number of proteins simultaneously and does not require any antibody. Additionally, protein identification in proteomic analysis is based on molecular mass data, not prior results. Therefore, both expected (previously determined) and unexpected (previously undetermined) proteins can be explored and characterized. These strengths of proteomic analysis will thus lead to rapid determination of potential candidates of proteins that are involved in the pathogenesis and pathophysiology of diseases and to biomarker discovery. Moreover, the proteomic approach may lead to uncovering the pathogenic mechanisms that were previously hidden in analyses of proteins using conventional methods.

The aim of our present study, therefore, was to investigate cellular responses (as determined by alterations in protein expression) in Madin-Darby canine kidney (MDCK) cells (distal renal tubular epithelial cells) during COM crystal adhesion. Specific aims included:

1) To identify quantitative and qualitative changes of a set of proteins (proteome) in renal tubular cells in response to COM crystal adhesion.

2) To identify quantitative and qualitative changes of a set of proteins (proteome) in renal tubular cells in response to COD crystal adhesion.

3) To determine differential cellular responses to crystal adhesion with different types of CaOx crystals – COM vs. COD.

## MATERIALS AND METHODS

### Crystal generation

COM crystals were generated by adding 5 mM $CaCl_2 \cdot 2H_2O$ to 0.5 mM $Na_2C_2O_4$ in Tris-HCl (pH 7.3). The solution was then mixed gently for 30 sec and incubated overnight at 25ºC. The COM crystals were then collected, washed with methanol and allowed to air-dry. The dried crystals were weighed, exposed to UV light for 30 min, and added into the culture medium (200 µg crystals per 1 mL culture medium). Thereafter, crystal morphology was evaluated using scanning electron microscopy.

COD crystals were produced by adding 6.4 mM $Na_2C_2O_4$ to 25.08 mM $CaCl_2 \cdot 2H_2O$ in a buffer containing 19.26 mM $Na_3C_6H_5O_7$, 23.1 mM $MgSO_4$ and 127.4 mM KCl (pH 6.5). The solution was then mixed gently for 30 sec and incubated overnight at 25ºC. The COD crystals were then collected, washed with methanol and allowed to air-dry. The dried crystals were weighed, exposed to UV light for 30 min, and added into the culture medium (200 µg crystals per 1 mL culture medium). Thereafter, crystal morphology was evaluated using scanning electron microscopy.

### Cell cultivation

The MDCK cell line subclone NBL-2 was used throughout this study. The MDCK cell line was initially isolated in 1958 by S. H. Madin and N. B. Darby [17], and characterized by Gaush [18]. This cell line was isolated from the kidney cortex of an apparently normal adult female Cocker Spaniel dog without intentional exposure to carcinogens [18]. Their physiologic and morphologic properties indicate that they were derived from cells of the thick ascending limb of the loop of Henle, distal convoluted tubule and cortical collecting duct [19-21]. The MDCK cells were maintained in a humidified incubator at 37°C with 5%$CO_2$. Culture medium containing COM or COD crystals (200 µg crystals per 1 ml culture medium) was added into the cultured T75 flasks confluent with MDCK cells and further incubated for 24 h. The cells were then washed three times with 1X PBS prior to further investigations.

### Quantitative analysis of cell death

To quantitate cell apoptosis and necrosis that might occur during exposure to COM or COD crystals, annexin V-FITC and propidium iodide double staining was performed to measure cell death in our model. After crystal adhesion for 48 h, MDCK cells were scrapped and further washed twice with ice-cold PBS. The cells were then resuspended

with annexin V buffer at a final concentration of 500,000 cells/mL. Thereafter, annexin V-FITC was added with a ratio of 1:50 and incubated on ice in the dark for 15 min. Propidium iodide was then added to the final concentration of 10 µL/mL prior to flow cytometric analysis. A monolayer of MDCK cells treated with 2 µg/mL camptothecin served as a positive control [22].

**Protein extraction**

Cellular proteins were extracted using a lysis buffer containing 7 M urea, 2 M thiourea, 20 mg/mL CHAPS (3-[(3-cholamidopropyl)dimethyl-ammonio]-1-propanesulfonate), 2% (v/v) ampholytes, and 120 mM dithiothreitol (DTT). Protein concentrations were measured by spectrophotometry using Bradford's method.

**2-D PAGE**

Immobilized pH gradient (IPG) strips, nonlinear pH 3-10, 7-cm-long (GE Healthcare) were rehydrated overnight with 200 µg proteins using rehydration buffer containing 8 M urea, 2% CHAPS, 0.01 M DTT, 2% ampholytes and bromophenol blue. The first dimensional separation (IEF) was performed in Ettan IPGphor II Isoelectric Focusing Unit (GE Healthcare) at 20ºC, using stepwise mode to reach 9,083 volt.hours. After completion of the IEF, the samples were equilibrated with a buffer containing 6 M urea, 130 mM DTT, 30% glycerol, 112 mM Tris base, 4% sodium dodecyl sulfate (SDS), 0.002% bromophenol blue and acetic acid, and then with another buffer containing 6 M urea, 135 mM iodoacetamide, 30% glycerol, 112 mM Tris base, 4% SDS, 0.002% bromophenol blue and acetic acid. The focused IPG strips were then transferred onto 12% acrylamide slab gel (8 x 9.5 cm) and the second dimensional separation was performed in Hoefer miniVE system (GE Healthcare) with the current of 20 µA/gel for 1.5 h.

**Staining of total proteins, phosphoproteins and glycoproteins, and gel imaging**

For staining of total proteins, the slab gel was fixed in 10% methanol and 7% acetic acid for 30 min. The fixing solution was removed and 100-200 mL SYPRO Ruby total protein stain (Invitrogen – Molecular Probes) was added to each gel and incubated on a continuous rocker at room temperature in the dark for 18 h. For phosphoproteins and glycoproteins, the gels were stained with Pro-Q Diamond (Invitrogen – Molecular Probes) and Pro-Q Emerald (Invitrogen – Molecular Probes), respectively. All fluorescence-stained gels were imaged using Typhoon laser scanner (GE Healthcare).

**Spot matching and quantitative intensity analysis**

Image Master 2D Platinum (GE Healthcare) software was used for matching and analysis of protein spots on gels. A reference gel was created from an artificial gel combining all of the spots presenting in different gels into one image. The intensity volume in pixel unit (or summation of optical densities of each spot), which represents protein concentration or the amount of protein per spot, was used for quantification. Average mode of background subtraction was performed to normalize the intensity volume of each spot for the compatibility of intensity units across different gels. The reference gel was then used for determination of existence and difference of protein expression among different gels.

**Statistical analysis**

Although several proteins were examined simultaneously, each protein spot was analyzed individually to define "*differential protein expression*". Our hypothesis was not to define that expression levels of all proteins were different among each individual sample but we aimed to examine whether there was(were) any protein(s) that was(were) differentially expressed between the two different groups (MDCK cells cultured with or without CaOx crystals in culture medium). Unpaired t-test was performed to determine differences in intensity volume of each corresponding spot between two groups of samples. P values less than 0.05 were considered statistically significant.

**In-Gel Tryptic Digestion**

The protein spots whose intensity levels significantly differed between groups were excised from 2-D gels, washed twice with 200 µL of 50% acetonitrile (ACN)/25 mM $NH_4HCO_3$ buffer (pH 8.0) at room temperature for 15 min, and then washed once with 200 µL of 100% ACN. After washing, the solvent was removed, and the gel pieces were dried by a SpeedVac concentrator (Savant; Holbrook, NY) and rehydrated with 10 µL of 1% (w/v) trypsin (Promega; Madison, WI) in 25 mM $NH_4HCO_3$. After rehydration, the gel pieces were crushed with siliconized blue stick and incubated at 37°C for at least 16 h. Peptides were subsequently extracted twice with 50 µL of 50% ACN/5% trifluoroacetic acid (TFA); the extracted solutions were then combined and dried with the SpeedVac concentrator. The peptide pellets were resuspended with 10 µL of 0.1% TFA and purified using $ZipTip_{C18}$ (Millipore; Bedford, MA). The peptide solution was drawn up and down in the $ZipTip_{C18}$ for ten times and then washed with 10 µL of 0.1% formic acid by drawing up and expelling the

washing solution for three times. The peptides were finally eluted with 5 μL of 75% ACN/0.1% formic acid.

**Protein Identification by MALDI-Q-TOF MS and MS/MS Analyses**

The proteolytic samples were premixed 1:1 with the matrix solution (5 mg/mL α-cyano-4-hydroxycinnamic acid (CHCA) in 50% ACN, 0.1% v/v TFA and 2% w/v ammonium citrate) and spotted onto the 96-well sample stage. The samples were analyzed by the Q-TOF Ultima™ mass spectrometer (Micromass; Manchester, UK), which was fully automated with predefined probe motion pattern and the peak intensity threshold for switching over from MS survey scanning to MS/MS, and from one MS/MS to another. Within each sample well, parent ions that met the predefined criteria (any peak within the *m/z* 800–3000 range with intensity above 10 count ± include/exclude list) were selected for CID MS/MS using argon as the collision gas and a mass dependent ± 5 V rolling collision energy until the end of the probe pattern was reached.

The combined MS and MS/MS ion meta data were searched in concert against the NCBI mammalian protein database using the ProteinLynx™ GlobalSERVER 2.0 workflow. The search algorithm employed a Hidden Markov Model that incorporates empirically determined fragmentation characteristics to increase the efficacy of the search. Additionally, the MS and MS/MS data were extracted and outputted as the searchable *.txt* and *.pkl* files, respectively, for independent searches using the MASCOT search engine (*http://www.matrixscience.com*), assuming that peptides were monoisotopic, oxidized at methionine residues, and carbamidomethylated at cysteine residues. Only 1 missed trypsin cleavage was allowed, and peptide mass tolerances of 100 and 50 ppm were used for peptide mass fingerprinting and MS/MS ions search, respectively.

**Validation of proteomic data by 2-D Western blot analysis**

To confirm the results of MS and/or MS/MS protein identification, 2-D Western blot analysis was performed. Proteins derived from MDCK cells (100 μg total protein for each sample; extraction was performed as for 2-D PAGE analysis) were resolved by 2-D PAGE and transferred onto nitrocellulose membranes (Whatman, Dassel, Germany) using a semi-dry transfer apparatus (Bio-Rad, Milano, Italy) at 75 mA for 1 h. Nonspecific binding was blocked with 5% milk in PBS at room temperature for 1 h. The membranes were then incubated with rabbit polyclonal anti-GRP94 antibody (Santa Cruz Biotechnology, Inc., Santa Cruz, CA) (1:100 in 5% milk/PBS) or goat polyclonal anti-annexin II antibody (Santa

Cruz Biotechnology) (1: 500 in 5% milk/PBS) at 4°C overnight. After washing, the membranes were further incubated with corresponding secondary antibody conjugated with horseradish peroxidase (Dako; FortCollins, CO) (1:1000 in 5% milk/PBS) at room temperature for 1 h. Immunoreactive protein spots were then visualized with SuperSignal® West Pico chemiluminescence substrate (Pierce Biotechnology, Inc., Rockford, IL).

## RESULTS

### Generation of typical COM and COD crystals

Using preparative conditions as described in “Materials and Methods”, we successfully generated COM crystals with typical monoclinic prismatic shape (**Figure 1A**) and COD crystals with typical tetragonal bipyramidal shape (**Figure 1B**) as demonstrated by scanning electron microscopy.

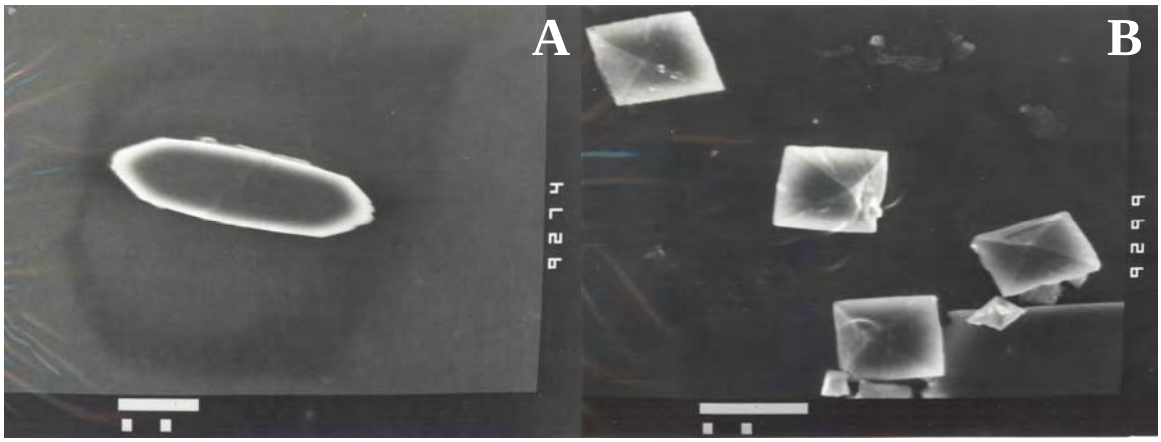


**Figure 1. Scanning electron microscopy of typical COM (A) and COD (B) crystals in culture medium.**

### Cultivation of MDCK cells with or without COM or COD crystal adhesion

The MDCK cell line subclone NBL-2 was used throughout this study. The MDCK cells were derived from cells of the thick ascending limb of the loop of Henle, distal convoluted tubule and cortical collecting duct. They were maintained in a humidified incubator at 37°C with 5% $CO_2$. Culture medium containing COM or COD crystals (100 µg crystals per 1 mL culture medium) was added into the cultured T75 flasks confluent with MDCK cells and further incubated for 48 h. The cells were then washed three times with PBS prior to further investigations. Having done these procedures, our results demonstrated that COM and COD successfully adhered to the cultured MDCK cells (**Figure 2**). The morphology of MDCK cells with or without adhered cells appeared normal (**Figure 2**).

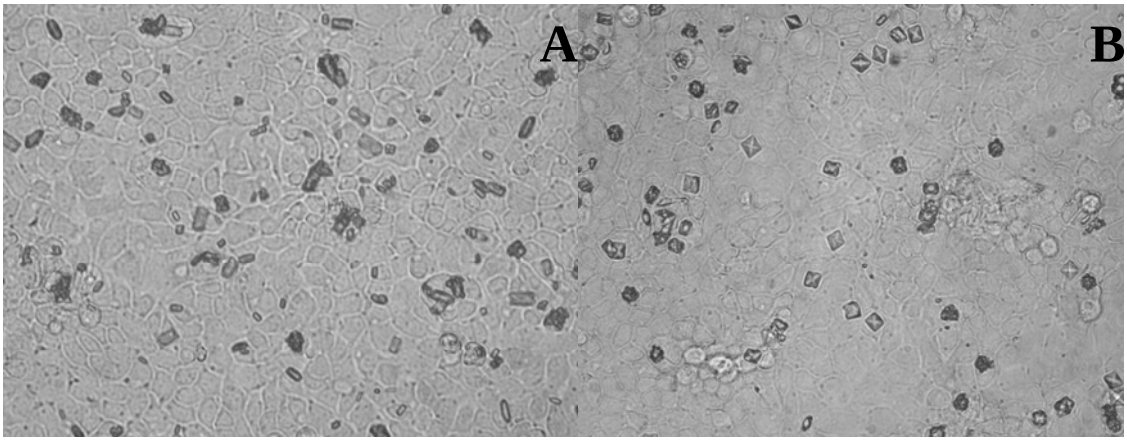


**Figure 2. Phase-contrast microscopy demonstrates COM (A) and COD (B) crystals adhered to MDCK cells.** Culture medium containing COM or COD crystals (100 µg/mL in culture medium) was added into the cultured T75 flask confluent with MDCK cells and further incubated for 48 h. The cells were then washed three times with 1X PBS. Magnification power = 400X.

## Quantitative analysis of cell death (both apoptosis and necrosis)

To quantitate cell apoptosis and necrosis that might occur during exposure to COM or COD crystals (100 µg/mL in culture medium), flow cytometry was performed using annexin V-FITC and propidium iodide double staining. **Figure 3** shows that percentages of cell death were comparable among the three conditions; including 1) control MDCK cells without crystal adhesion, 2) MDCK cells with COM crystal adhesion, and 3) MDCK cells with COD crystal adhesion (all had cell death < 20%).

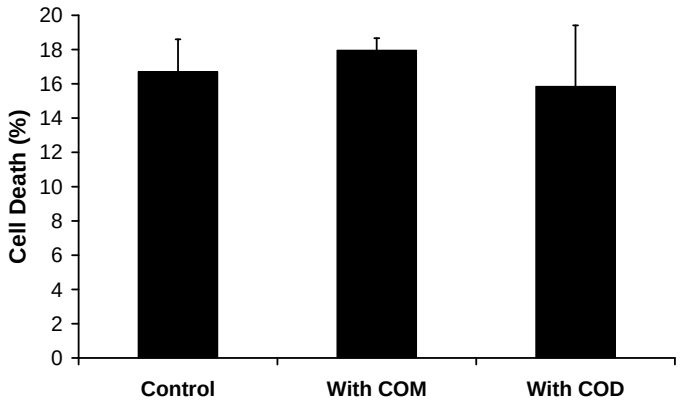


**Figure 3. Quantitative analysis of cell death.** Both apoptosis and necrosis were quantitated by flow cytometry using annexin V-FITC and propidium iodide double staining (n = 3 measurements for each condition).

**Proteomic analysis of altered cellular proteome induced by COM or COD crystal adhesion**

Although several proteins were examined simultaneously, each protein spot was analyzed individually to define "*differential protein expression*". Our hypothesis was not to define that expression levels of all proteins were different among each individual sample but we aimed to examine whether there was (were) any protein(s) that was (were) differentially expressed among groups. **Figure 4** shows all 2-D gels of proteins derived from MDCK cells without (A), with COM (B), or with COD (C) crystal adhesion. Proteins were extracted from these cultured cells and equal amount of total protein (200 μg) was resolved in each 2-D gel (non-linear pH gradient of 3-10). The resolved proteins were then visualized with SYPRO Ruby stain (n = 5 gels for each group). Quantitative intensity analysis revealed a total of 20 protein spots that were significantly altered by COM crystal adhesion, whereas 11 protein spots were significantly altered by COD crystal adhesion. **Figure 5** shows the 2-D proteome maps of all significantly differed proteins, which are also summarized in **Tables 1 and 2**. Comparing between changes induced by COM crystal adhesion to those affected by COD crystal adhesion, these alterations (as the responses to crystal adhesion) totally differed, indicating that each type of CaOx crystals caused different cellular responses. These significantly differed proteins were then identified by Q-TOF MS and/or MS/MS analyses (**Table 3**). Subsequently, all the identified proteins were subjected to bioinformatic (using the SwissProt/TrEMBL protein database) and literature search to obtain additional protein information (focusing on functional classification). **Table 4** summarizes functional categories of all significantly differed proteins identified in this study.

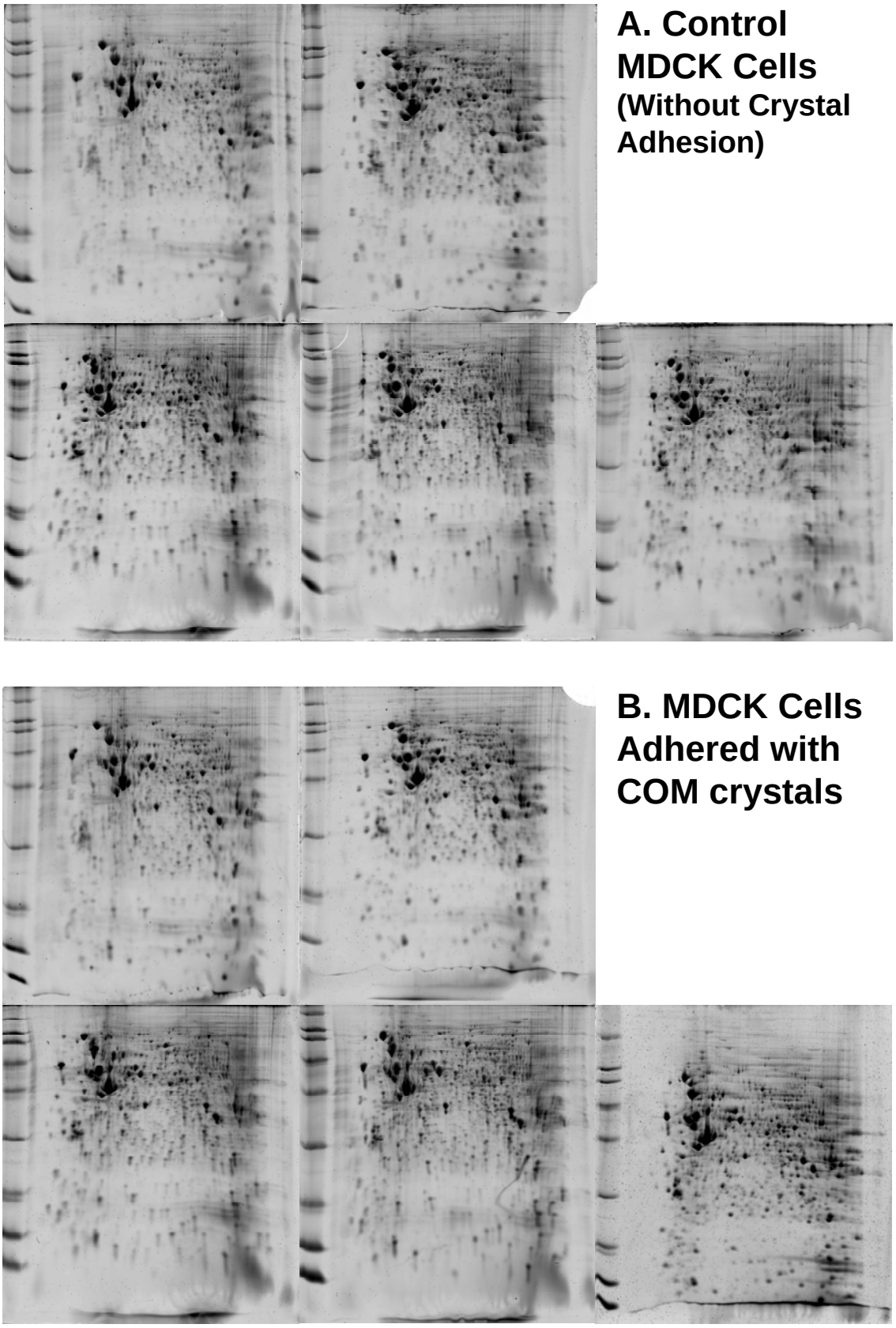


Figure 4 (cont.)

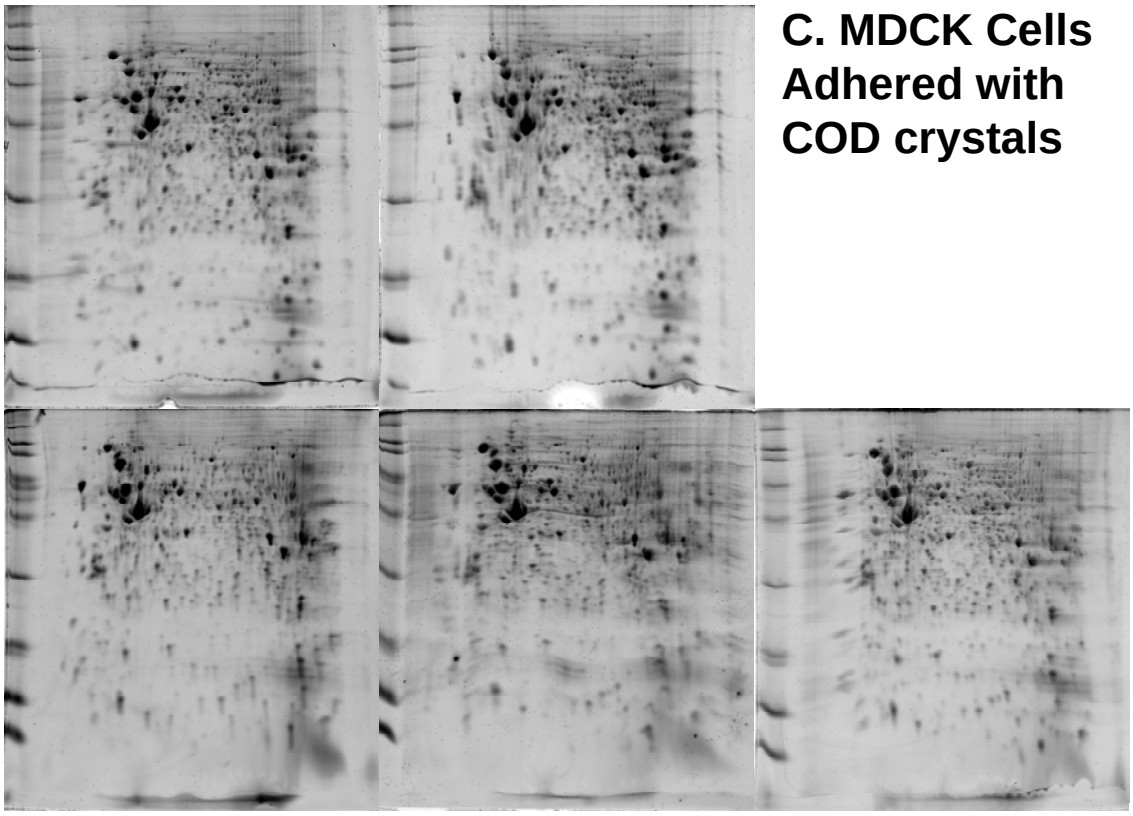


**Figure 4. 2-D PAGE of proteins derived from MDCK cells without (A), with COM (B), or with COD (C) crystal adhesion.** Proteins were extracted from these cultured cells and equal amount of total protein (200 µg) was resolved in each 2-D gel (non-linear pH gradient of 3-10). The resolved proteins were then visualized with SYPRO Ruby stain (n = 5 gels for each group).

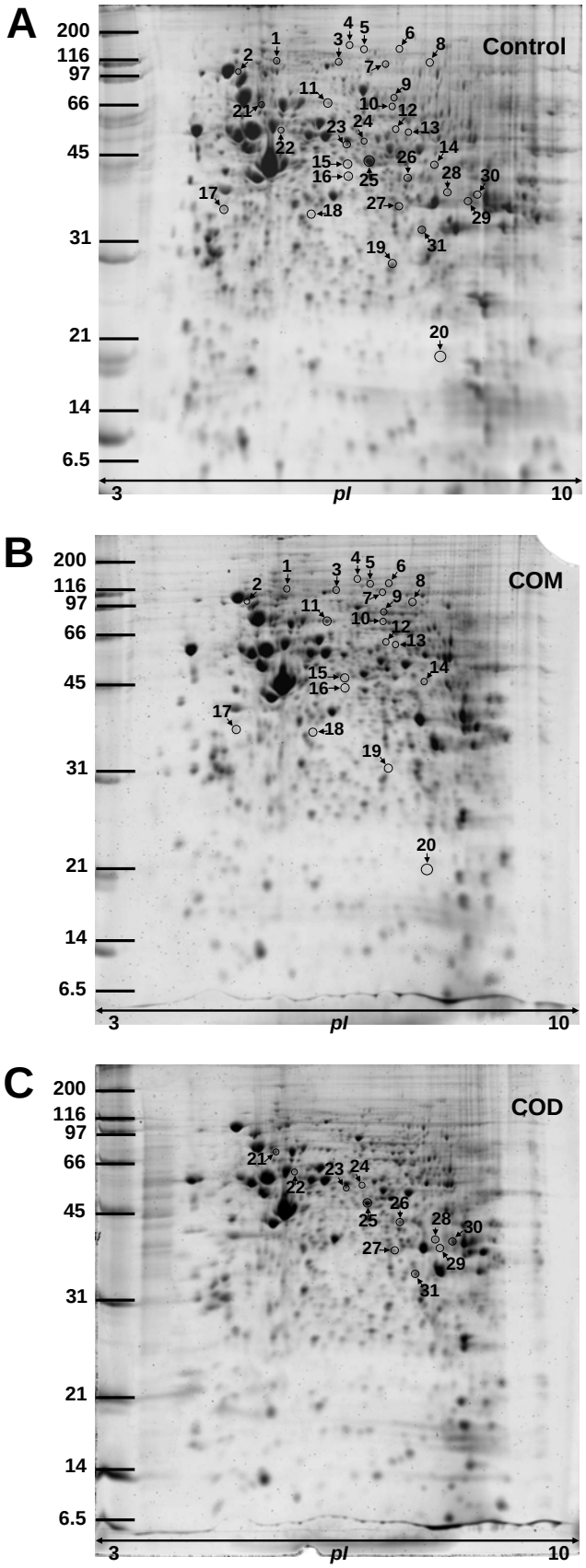


**Figure 5. The 2-D proteome map of all significantly differed proteins.** (A) = MDCK cells without crystal adhesion; (B) MDCK cells with COM crystal adhesion; and (C) MDCK cells with COD crystal adhesion.

**Table 1: Protein spots whose intensity levels were significantly altered during COM crystal adhesion.**

| Spot no. | Intensity levels (Mean ± SEM) | | Comparison (p value) |
|---|---|---|---|
| | Control | COM | COM vs. Control |
| 1 | 0.0644 ± 0.0059 | 0.0406 ± 0.0042 | 0.011 |
| 2 | 0.0417 ± 0.0169 | 0.0007 ± 0.0007 | 0.042 |
| 3 | 0.0419 ± 0.0045 | 0.0588 ± 0.0053 | 0.042 |
| 4 | 0.0116 ± 0.0031 | 0.0294 ± 0.0036 | 0.006 |
| 5 | 0.0207 ± 0.0034 | 0.0393 ± 0.0062 | 0.029 |
| 6 | 0.0215 ± 0.0012 | 0.0312 ± 0.0039 | 0.044 |
| 7 | 0.0054 ± 0.0033 | 0.0320 ± 0.0050 | 0.002 |
| 8 | 0.0525 ± 0.0045 | 0.0351 ± 0.0058 | 0.046 |
| 9 | 0.0494 ± 0.0060 | 0.0740 ± 0.0058 | 0.018 |
| 10 | 0.0410 ± 0.0074 | 0.0626 ± 0.0052 | 0.043 |
| 11 | 0.0507 ± 0.0083 | 0.0713 ± 0.0026 | 0.046 |
| 12 | 0.0102 ± 0.0030 | 0.0213 ± 0.0029 | 0.028 |
| 13 | 0.0113 ± 0.0050 | 0.0268 ± 0.0031 | 0.030 |
| 14 | 0.0420 ± 0.0020 | 0.0695 ± 0.0087 | 0.015 |
| 15 | 0.0486 ± 0.0041 | 0.0719 ± 0.0057 | 0.011 |
| 16 | 0.0247 ± 0.0072 | 0.0484 ± 0.0062 | 0.038 |
| 17 | 0.0962 ± 0.0147 | 0.0545 ± 0.0088 | 0.041 |
| 18 | 0.0269 ± 0.0048 | 0.0395 ± 0.0023 | 0.046 |
| 19 | 0.0329 ± 0.0018 | 0.0185 ± 0.0048 | 0.023 |
| 20 | 0.0000 ± 0.0000 | 0.0436 ± 0.0097 | 0.002 |

**Table 2: Protein spots whose intensity levels were significantly altered during COD crystal adhesion.**

| Spot no. | Intensity levels (Mean ± SEM) | | Comparison (p value) |
|---|---|---|---|
| | Control | COD | COD vs. Control |
| 21 | 0.1423 ± 0.0094 | 0.0913 ± 0.0114 | 0.009 |
| 22 | 0.0361 ± 0.0039 | 0.0200 ± 0.0036 | 0.016 |
| 23 | 0.0466 ± 0.0036 | 0.0833 ± 0.0142 | 0.037 |
| 24 | 0.0212 ± 0.0025 | 0.0131 ± 0.0014 | 0.024 |
| 25 | 0.2715 ± 0.0291 | 0.3817 ± 0.0211 | 0.015 |
| 26 | 0.0483 ± 0.0097 | 0.0949 ± 0.0160 | 0.037 |
| 27 | 0.0421 ± 0.0174 | 0.0987 ± 0.0125 | 0.030 |
| 28 | 0.0352 ± 0.0010 | 0.0544 ± 0.0052 | 0.006 |
| 29 | 0.0146 ± 0.0064 | 0.0670 ± 0.0143 | 0.010 |
| 30 | 0.1969 ± 0.0176 | 0.1244 ± 0.0240 | 0.041 |
| 31 | 0.2723 ± 0.0161 | 0.2022 ± 0.0200 | 0.026 |

**Table 3: Identification of altered proteins by Q-TOF MS and/or MS/MS analyses.**

| Spot no. | Protein name | NCBI ID | Identified by | MOWSE/Ions scores | pI | MW (kDa) |
|---|---|---|---|---|---|---|
| 1 | Alanyl-tRNA synthetase (Alanine-tRNA ligase) (AlaRS) isoform 1 | gi\|73957022 | MS/MS | −/60 | 5.27 | 107.45 |
| 2 | Protein kinase (GRP94) | gi\|984249 | MS, MS/MS | 83/76 | 4.76 | 93.09 |
| 3 | Transcriptional repressor BSR/RACK7/PRKCBP1 | gi\|119905994 | MS | 56/− | 6.04 | 122.29 |
| 4 | Armadillo repeat containing 3 (ARMC3) | gi\|63488113 | MS | 50/− | 5.95 | 97.06 |
| 5 | Leucine-rich PPR motif-containing protein (Lrpprc) | gi\|73970116 | MS | 113/− | 6.46 | 158.93 |
| 6 | Metalloprotease 1 (MP1) | gi\|73949192 | MS | 82/− | 6.60 | 117.74 |
| 7 | Minichromosome maintenance complex 8 (MCM8) | gi\|39644544 | MS | 53/− | 6.11 | 82.17 |
| 8 | RP3-398G3.1 (spectrin repeat containing, nuclear envelope 1) | gi\|57162570 | MS | 57/- | 5.78 | 110.45 |
| 9 | Lamin A/C (70 kDa lamin) isoform 4 | gi\|73960920 | MS | 68/− | 6.57 | 74.47 |
| 10 | Succinate dehydrogenase (SDH) [ubiquinone] Flavoprotein subunit of complex II isoform 1 | gi\|74003064 | MS, MS/MS | 107/64 | 7.29 | 74.09 |
| 11 | ALB protein | gi\|74267962 | MS, MS/MS | 110/112 | 5.88 | 71.19 |
| 12 | Unidentified | – | – | – | – | – |
| 13 | Elongation protein 3 homolog (ELP3) isoform 1 | gi\|114619483 | MS/MS | −/36 | 8.93 | 61.03 |
| 14 | Methionine aminopeptidase 1 (MetAP 1) | gi\|74002259 | MS | 52/- | 6.96 | 40.40 |
| 15 | Unidentified | – | – | – | – | – |
| 16 | Plakophilin 4 isoform CRA_g | gi\|119631836 | MS | 75/− | 9.11 | 10.10 |
| 17 | HSPC263, otubain 1 | gi\|6841176 | MS, MS/MS | 106/48 | 4.90 | 31.95 |
| 18 | Unidentified | – | – | – | – | – |
| 19 | Parvalbumin | gi\|31980767 | MS | 84/− | 5.02 | 11.92 |
| 20 | Unidentified | – | – | – | – | – |
| 21 | Lamin B | gi\|293689 | MS, MS/MS | 71/44 | 5.14 | 66.95 |
| 22 | Chaperonin isoform 4 | gi\|114582392 | MS, MS/MS | 92/244 | 8.13 | 50.73 |
| 23 | Heterogeneous nuclear ribonucleoprotein H1 | gi\|5031753 | MS, MS/MS | 97/280 | 5.89 | 49.48 |
| 24 | Cytokeratin 7 (CK 7) | gi\|73996579 | MS | 70/- | 6.21 | 51.65 |
| 25 | Ornithine aminotransferase, mitochondrial precursor isoform 1 | gi\|73998800 | MS, MS/MS | 195/315 | 6.44 | 48.75 |
| 26 | Branched-chain-amino-acid aminotransferase (Placental protein 18) (PP18) | gi\|73948032 | MS | 114/- | 7.14 | 44.93 |
| 27 | Unidentified | – | – | – | – | – |
| 28 | Alcohol dehydrogenase | gi\|73977957 | MS, MS/MS | 70/59 | 7.12 | 36.90 |
| 29 | Annexin A2 (annexin II) | gi\|50950177 | MS, MS/MS | 159/55 | 6.92 | 38.92 |
| 30 | Glyceraldehyde-3-phosphate dehydrogenase | gi\|50978862 | MS, MS/MS | 87/162 | 8.20 | 36.07 |
| 31 | Galactose-specific lectin | gi\|114653156 | MS/MS | -/83 | 8.26 | 37.99 |

**Table 4: Subcellular localizations and functions of the altered proteins.**

| Altered proteins | Subcellular localization | Function |
|---|---|---|
| ***By COM crystal adhesion*** | | |
| Transcriptional repressor BSR/RACK7/PRKCBP1 | Cytoplasm | Transcription regulator |
| ARMC 3 | Cytoplasm | Signal transduction |
| Lrpprc | Nucleus | RNA binding protein |
| MP 1 | Mitochondrial | Metabolic enzyme |
| MCM8 | Nucleus | DNA replication |
| Nuclear envelope 1 | Inner nuclear membrane | Nuclear membrane structure |
| Lamin A/C isoform 4 | Inner nuclear membrane | Nuclear membrane structure |
| SDH | Mitochondrial | Metabolic enzyme |
| ALB protein | Secreted protein | Carrier protein |
| ELP3 isoform 1 | Nucleus | Transcription regulator |
| Plakophilin 4, isoform CRA_ g | Adheren junctions | Cellular structure |
| AlaRS | Cytoplasm | Protein biosynthesis |
| GRP94 | ER | Chaperone |
| MetAP 1 | Cytoplasm | Metabolic enzyme |
| HSPC263 | Cytoplasm | Metabolic enzyme |
| Parvalbumin | Cytoplasm | Growth regulation |
| | | |
| ***By COD crystal adhesion*** | | |
| hnRNP-H1 | Nucleus | RNA metabolism |
| Oat, mitochondrial precursor isoform 1 | Mitochondrial | Metabolic enzyme |
| Placenta protein 18 | Mitochondrial | Metabolic enzyme |
| Alcohol dehydrogenase | Mitochondrial | Metabolic enzyme |
| Annexin A2 | Cytosol (monomeric)/ nucleus (heteromeric) | Signal transduction |
| Lamin B | Intermediate filament | Cellular structure |
| Chaperonin isoform 4 | Mitochondrial | Protein biosynthesis |
| CK 7 | Intermediate filament | Cellular structure |
| G3PDH | Cytoplasm | Metabolic enzyme |
| Galactose-specific lectin | Cell membrane | Adherence molecule |

**Validation of proteomic data by 2-D Western blot analysis**

To validate protein identification by Q-TOF MS and/or MS/MS analyses, 2-D Western blot analysis of GRP94 (whose level was significantly decreased by COM crystal adhesion) and annexin II (whose level was significantly increased by COD crystal adhesion) was performed. Briefly, proteins resolved by 2-D PAGE were transferred onto nitrocellulose membrane. Non-specific bindings were blocked with 5% skim milk in PBS. The membrane was incubated with rabbit polyclonal anti-GRP94 or goat polyclonal anti-annexin II antibody and then with their respective secondary antibodies conjugated with horseradish peroxidase. The immunoreactive proteins were then detected using chemiluminescence substrate. **Figure 6** shows that the decreased level of GRP94 during COM crystal adhesion and the increased level of annexin II during COD crystal adhesion were nicely confirmed by 2-D Western blot analysis.

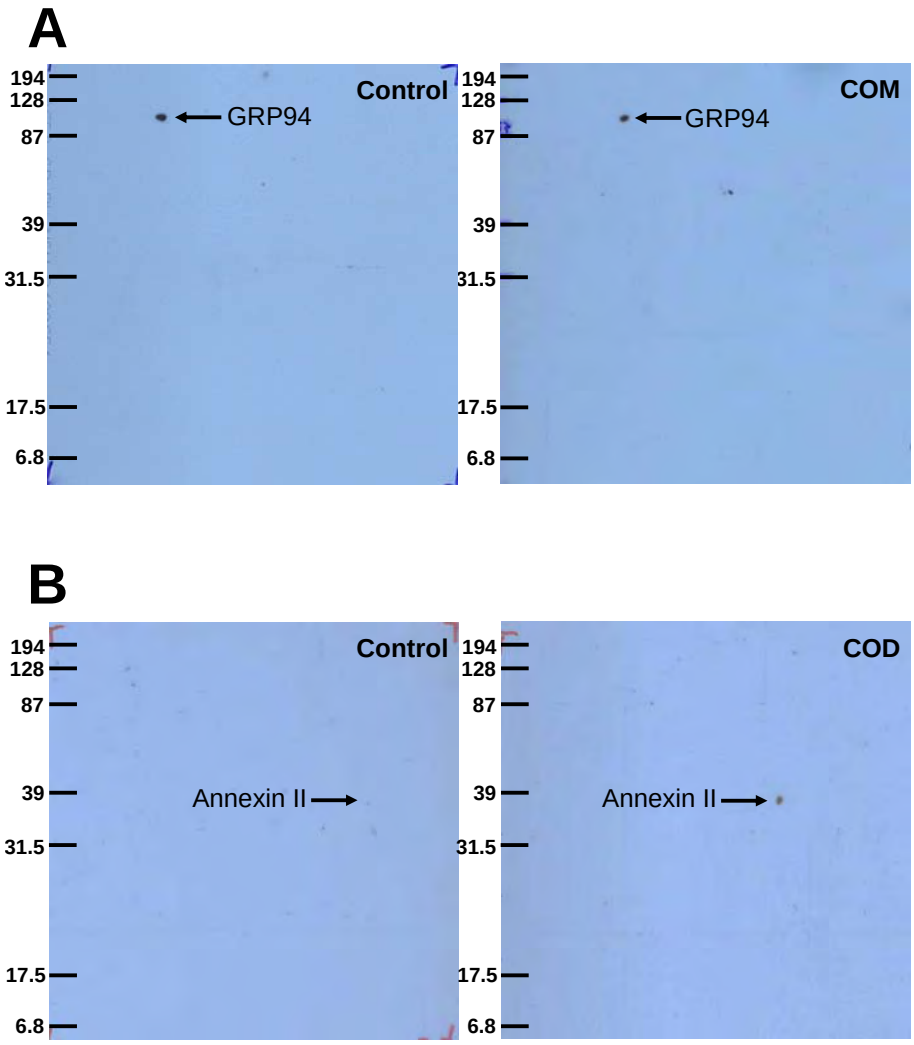


**Figure 6. 2-D Western blot analysis of glucose-regulated protein 94 kDa (GRP94) (A) and annexin II (B).** The decreased level of GRP94 during COM crystal adhesion and the increased level of annexin II during COD crystal adhesion were nicely confirmed by 2-D Western blot analysis.

**Proteomic analysis of phospho- and glyco-proteins that were altered by COM or COD crystal adhesion**

In addition to analysis of whole cellular proteome, we also examined changes in phospho- and glycol-proteins induced by COM or COD crystal adhesion. After 2-D PAGE, the slab gel was fixed in 10% methanol and 7% acetic acid for 30 min. The fixing solution was removed and 100-200 mL Pro-Q Diamond (phospho-stain) or Pro-Q Emerald (glyco-stain) (Invitrogen – Molecular Probes) was added to each gel and incubated on a continuous rocker at room temperature in the dark for 18 h. Phospho- and glycol-proteins were then visualized using Typhoon laser scanner (GE Healthcare).

**Figure 7** shows representative 2-D gels of phospho- (A and B) and glyco-proteins (C and D) derived from MDCK cells without (A and C) or with COM crystal adhesion (B and D) (n = 5 gels for each group). Quantitative and statistical analyses revealed 20 phospho- and 5 glyco-proteins that were significantly altered by COM crystal adhesion (**Tables 5 and 6**, respectively).

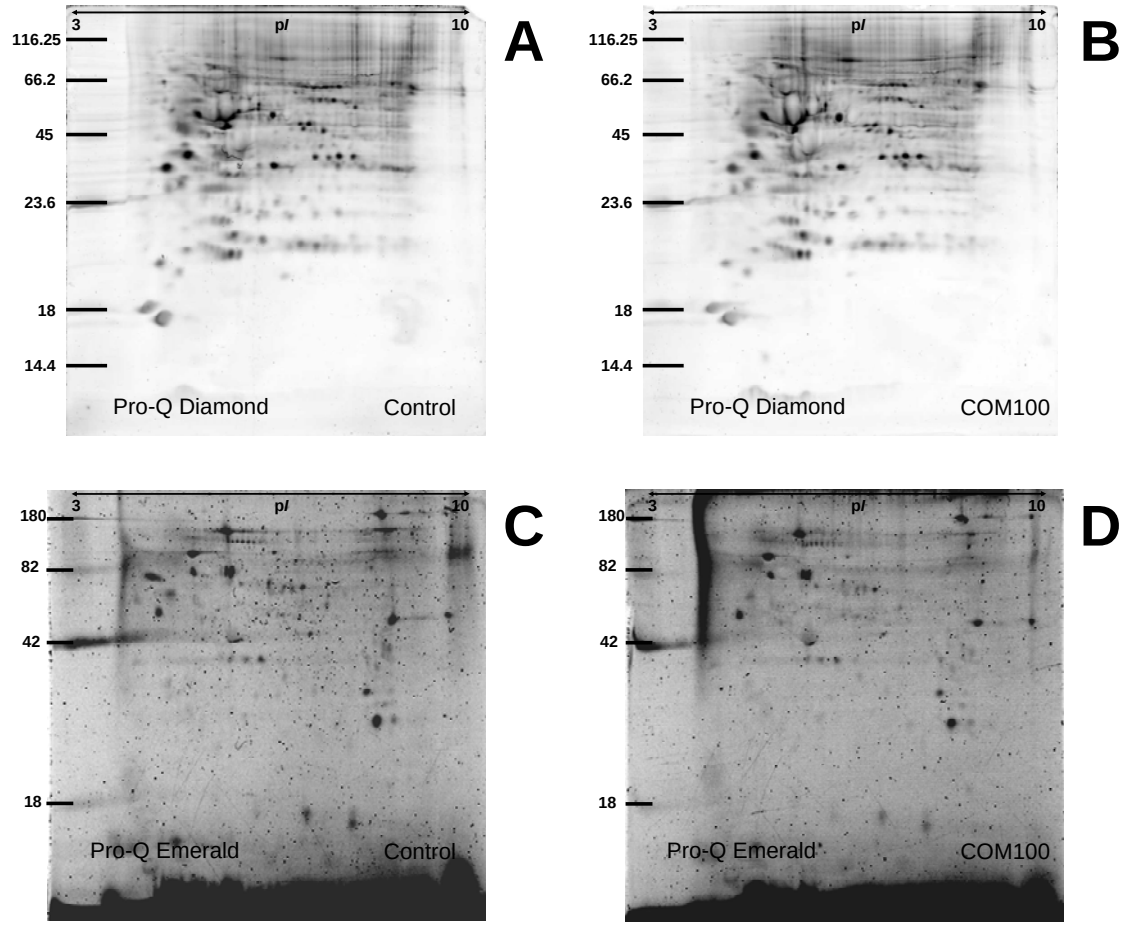


**Figure 7. Representative 2-D gels of proteins derived from MDCK cells without (A and C) or with COM (B and D) crystal adhesion.** Proteins were extracted from these cultured cells and equal amount of total protein (200 µg) was resolved in each 2-D gel (non-linear pH gradient of 3-10). The resolved proteins were then visualized with Pro-Q Diamond (phospho-stain) or with Pro-Q Emerald (glyco-stain). (n = 5 gels for each group).

**Table 5: Phosphoprotein spots whose intensity levels were significantly altered during COM crystal adhesion.**

| Spot no. | Intensity (Mean ± SEM) | | Ratio (COM/ Control) | *p* values |
|---|---|---|---|---|
| | Control | COM | | |
| 387 | 0.0387 ± 0.0254 | 0.1496 ± 0.0301 | 3.86 | 0.0226 |
| 392 | 0.0682 ± 0.0457 | 0.2804 ± 0.0389 | 4.11 | 0.0076 |
| 585 | 0.0640 ± 0.0296 | 0.1547 ± 0.0220 | 2.42 | 0.0393 |
| 587 | 0.0509 ± 0.0273 | 0.1252 ± 0.0153 | 2.46 | 0.0450 |
| 588 | 0.0825 ± 0.0096 | 0.1183 ± 0.0066 | 1.43 | 0.0150 |
| 604 | 0.1249 ± 0.0614 | 0.3148 ± 0.0340 | 2.52 | 0.0269 |
| 725 | 0.0286 ± 0.0137 | 0.0755 ± 0.0055 | 2.64 | 0.0130 |
| 733 | 0.1486 ± 0.0202 | 0.0350 ± 0.0215 | 0.24 | 0.0049 |
| 775 | 0.1466 ± 0.0438 | 0.2983 ± 0.0288 | 2.04 | 0.0201 |
| 848 | 0.0939 ± 0.0082 | 0.0508 ± 0.0132 | 0.54 | 0.0244 |
| 1038 | 0.3784 ± 0.0707 | 0.7368 ± 0.0882 | 1.95 | 0.0132 |
| 1043 | 0.0532 ± 0.0218 | 0.1169 ± 0.0157 | 2.20 | 0.0452 |
| 1091 | 0.3715 ± 0.0444 | 0.6295 ± 0.0710 | 1.69 | 0.0151 |
| 1172 | 0.2264 ± 0.0617 | 0.4367 ± 0.0400 | 1.93 | 0.0211 |
| 1418 | 0.3430 ± 0.0379 | 0.2342 ± 0.0155 | 0.68 | 0.0290 |
| 2008 | 0.0551 ± 0.0338 | 0.1800 ± 0.0289 | 3.27 | 0.0228 |
| 2017 | 0.0425 ± 0.0196 | 0.1116 ± 0.0108 | 2.63 | 0.0151 |
| 2018 | 0.1549 ± 0.0278 | 0.0381 ± 0.0244 | 0.25 | 0.0134 |
| 2020 | 0.1589 ± 0.0639 | 0.0000 ± 0.0000 | 0.00 | 0.0377 |
| 2066 | 0.0000 ± 0.0000 | 0.1159 ± 0.0482 | #DIV/0! | 0.0428 |

**Table 6: Glycoprotein spots whose intensity levels were significantly altered during COM crystal adhesion.**

| Spot no. | Intensity (Mean ± SEM) | | Ratio (COM/ Control) | *p* values |
|---|---|---|---|---|
| | Control | COM | | |
| 84 | 0.0627 ± 0.0386 | 0.2054 ± 0.0441 | 3.28 | 0.0409 |
| 90 | 0.0413 ± 0.0413 | 0.3634 ± 0.0829 | 8.80 | 0.0083 |
| 110 | 0.0000 ± 0.0000 | 0.0659 ± 0.0284 | #DIV/0! | 0.0489 |
| 334 | 0.0000 ± 0.0000 | 0.1026 ± 0.0314 | #DIV/0! | 0.0114 |
| 689 | 0.0000 ± 0.0000 | 0.1519 ± 0.0527 | #DIV/0! | 0.0204 |

**Figure 8** shows representative 2-D gels of phospho- (A and B) and glyco-proteins (C and D) derived from MDCK cells without (A and C) or with COD crystal adhesion (B and D) (n = 5 gels for each group). Quantitative and statistical analyses revealed 11 phospho- and 18 glyco-proteins that were significantly altered by COD crystal adhesion (**Tables 7 and 8**, respectively).

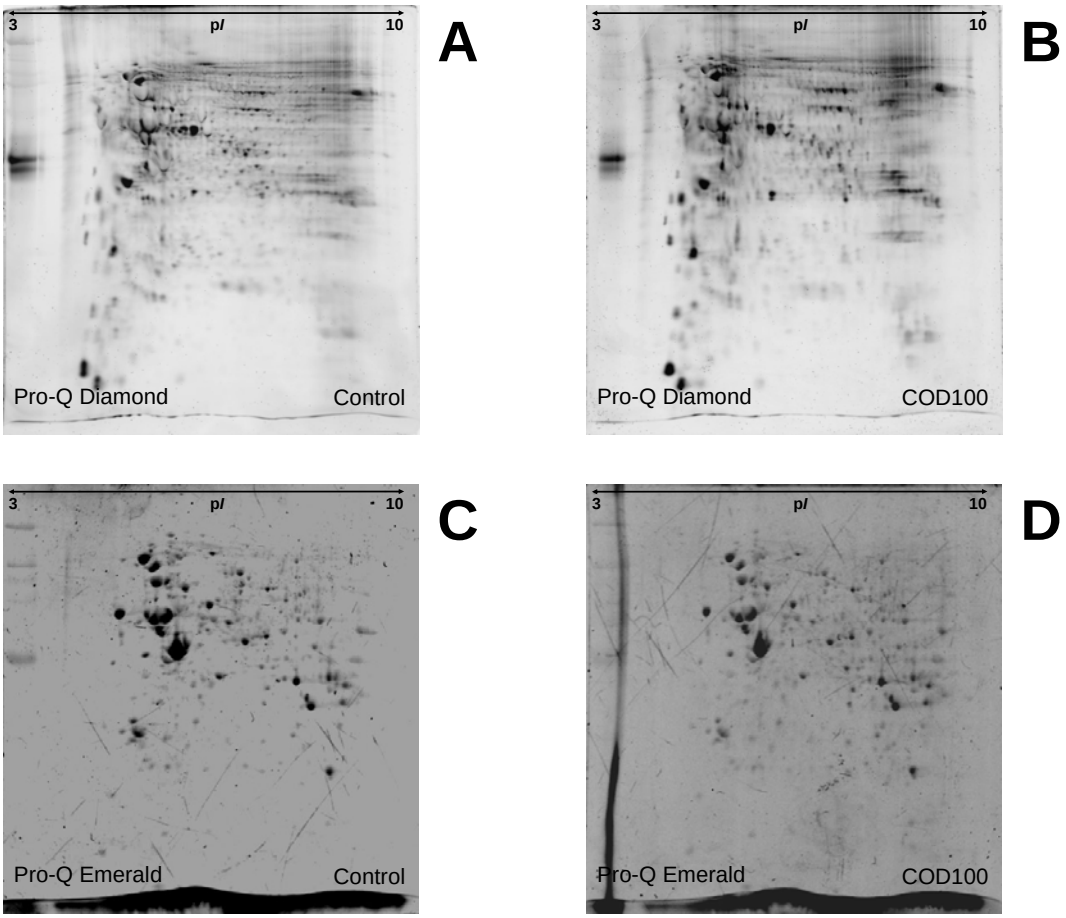


**Figure 8. Representative 2-D gels of proteins derived from MDCK cells without (A and C) or with COD (B and D) crystal adhesion.** Proteins were extracted from these cultured cells and equal amount of total protein (200 µg) was resolved in each 2-D gel (non-linear pH gradient of 3-10). The resolved proteins were then visualized with Pro-Q Diamond (phospho-stain) or with Pro-Q Emerald (glyco-stain). (n = 5 gels for each group).

**Table 7: Phosphoprotein spots whose intensity levels were significantly altered during COD crystal adhesion.**

| Spot no. | Intensity (Mean ± SEM) | | Ratio (COD/ Control) | *p* values |
|---|---|---|---|---|
| | Control | COD | | |
| 1795 | 0.0068 ± 0.0056 | 0.0507 ± 0.0119 | 7.43 | 0.0261 |
| 1880 | 0.0852 ± 0.0058 | 0.1169 ± 0.0050 | 1.37 | 0.0097 |
| 1943 | 0.0606 ± 0.0048 | 0.0865 ± 0.0035 | 1.43 | 0.0071 |
| 1970 | 0.2018 ± 0.0285 | 0.3388 ± 0.0382 | 1.68 | 0.0471 |
| 2073 | 0.3064 ± 0.0744 | 0.5342 ± 0.0170 | 1.74 | 0.0408 |
| 2109 | 0.0602 ± 0.0096 | 0.1149 ± 0.0134 | 1.90 | 0.0268 |
| 2243 | 0.0688 ± 0.0077 | 0.1036 ± 0.0047 | 1.51 | 0.0138 |
| 2245 | 0.2094 ± 0.0086 | 0.2745 ± 0.0118 | 1.31 | 0.0065 |
| 2254 | 0.0949 ± 0.0043 | 0.1202 ± 0.0064 | 1.27 | 0.0283 |
| 2653 | 0.1764 ± 0.0123 | 0.1374 ± 0.0029 | 0.78 | 0.0355 |
| 2751 | 0.0622 ± 0.0024 | 0.0851 ± 0.0064 | 1.37 | 0.0249 |

**Table 8: Glycoprotein spots whose intensity levels were significantly altered during COD crystal adhesion.**

| Spot no. | Intensity (Mean ± SEM) | | Ratio (COD/ Control) | *p* values |
|---|---|---|---|---|
| | Control | COD | | |
| 393 | 0.0879 ± 0.0540 | 0.2731 ± 0.0561 | 3.11 | 0.045 |
| 423 | 0.0704 ± 0.0311 | 0.1784 ± 0.0266 | 2.54 | 0.030 |
| 625 | 0.3117 ± 0.0601 | 0.0549 ± 0.0341 | 0.18 | 0.006 |
| 828 | 0.4358 ± 0.0495 | 0.2689 ± 0.0323 | 0.62 | 0.022 |
| 837 | 0.4068 ± 0.1093 | 0.1321 ± 0.0417 | 0.32 | 0.047 |
| 890 | 0.0104 ± 0.0104 | 0.1495 ± 0.0479 | 14.32 | 0.022 |
| 960 | 0.0000 ± 0.0000 | 0.0904 ± 0.0384 | #DIV/0! | 0.047 |
| 961 | 0.0132 ± 0.0132 | 0.2655 ± 0.0568 | 20.11 | 0.003 |
| 967 | 0.0399 ± 0.0246 | 0.1902 ± 0.0560 | 4.77 | 0.039 |
| 1042 | 0.0070 ± 0.0070 | 0.1547 ± 0.0465 | 22.06 | 0.014 |
| 1045 | 0.0132 ± 0.0132 | 0.0925 ± 0.0245 | 6.99 | 0.022 |
| 1059 | 0.6623 ± 0.0752 | 0.4305 ± 0.0399 | 0.65 | 0.026 |
| 1066 | 0.0000 ± 0.0000 | 0.2723 ± 0.0453 | #DIV/0! | 0.000 |
| 1118 | 0.9071 ± 0.0476 | 0.6283 ± 0.0779 | 0.69 | 0.016 |
| 1134 | 0.0000 ± 0.0000 | 0.0733 ± 0.0235 | #DIV/0! | 0.014 |
| 1139 | 0.3483 ± 0.0970 | 0.0000 ± 0.0000 | 0.00 | 0.007 |
| 1378 | 0.0538 ± 0.0330 | 0.2769 ± 0.0275 | 5.15 | 0.001 |
| 1387 | 0.0000 ± 0.0000 | 0.2225 ± 0.0645 | #DIV/0! | 0.009 |

## DISCUSSION

We have successfully performed an *in vitro* study for evaluation of cellular responses of distal renal tubular cells during COM and COD crystal adhesion. Flow cytometry using annexin V/propidium iodide double staining clearly showed that incubation of MDCK cells with 100 μg/mL COM crystals for up to 48 h did not significantly increase % cell death (**Figure 3**). Additionally, the total cell numbers were not significantly altered by crystal adhesion at this 48-h time-point, implicating that there was no significant effect of crystal adhesion on cell division, using the conditions described herein. Thus, the experimental condition used herein was suitable for examining cellular responses to COM and COD crystal adhesion. Gel-based differential proteomics study revealed alterations in abundance of 20 and 11 proteins in MDCK cells induced by COM and COD crystal adhesion, respectively (**Figure 5; Tables 1-3**). Functional roles of some of these altered proteins are highlighted as follows.

GRP94 (also known as tumor rejection antigen 1 or gp96) is the most abundant chaperone located in the endoplasmic reticulum (ER) lumen, a place to restore or correct folding of the misfolded/misassembled proteins and target them for degradation by coupling to the proteasome [23, 24]. GRP94 regulates cellular homeostasis [25, 26] and apoptosis in several mammalian cell lines [27]. In the presence of various stresses, the final state or survival of cells may mainly depend on the ability of the cells to resist to the stresses. GRP94 regulates cell fate by maintaining the intracellular calcium balance among cytosol, ER and mitochondria [28]. In the present study, we observed a marked decrease in abundance of GRP94 in the COM-interacting MDCK cells. The data obtained from 2-D Western blot analysis clearly confirmed the proteomic data (**Figure 6A**). However, it should be noted that Western blot analysis is more sensitive than the detection of protein spots by gel staining. Mechanisms of visualization of protein spots by antibody-chemiluminescence enhancement obviously differ from those of the detection by staining. These may explain the differential magnitudes of changes observed by these two different methods. The detection of another (smaller) GRP94 spot in **Figure 6A** might be simply explained by the higher sensitivity of Western blot analysis. Our data was consistent with those obtained from a previous study, which showed significant down-regulation of heat shock protein 25 (HSP25), HSP 70 and heme oxygenase-1 expression in COM-treated MDCK cells [29]. The mechanistic basis for the decrease of these proteins during COM crystal adhesion remains unclear. Perhaps, the decreased levels of chaperones may simply reflect the damaged

renal epithelial cells caused by COM-mediated ROS and decreased anti-oxidant glutathione concentrations [30].

HSPC263, also known as otubain 1, contained ubiquitin-interaction motifs and ubiquitin-associated domains, which are generally found in the proteins involved in the ubiquitin pathway [31, 32]. Otubain 1 is also a deubiquitinating enzyme cysteine protease, which precisely cleaves the polyubiquitin chains from the defective proteins [33]. Moreover, it has putative nuclear localization signals and a consensus LxxLL motif (where L is leucine and x is any amino acid), which is known to mediate the binding of transcriptional co-activators to liganded nuclear receptors [34]. The data from a previous study have suggested that otubain 1 may play a significant role in tumor necrosis factor (TNF) signaling pathway [33]. However, ubiquitination pathway has exerted in a wide spectrum of biological processes including cell cycle progression, transcriptional activation, signal transduction, apoptosis and DNA repair [35, 36]. In our present study, HSPC263 protein was decreased in the COM-interacting cells. The role of decreased HSPC263 in MDCK cells during COM crystal adhesion remains unclear and deserves further investigation.

Transcriptional repressor BSR/RACK7/PRKCBP1 or protein kinase C (PKC)-binding protein 1 is a member of the receptors for activated C-kinase (RACK) family. Upon activation, most PKC isoenzymes are translocated to the cellular site of activity and bind to a specific receptor for RACK [37, 38]. The PKC-beta 1 interacts specifically with the carboxy-terminus of PRKCBP1 (protein kinase C binding protein 1) and increases both its phosphorylation and the duration of its activation. In the present study, we found that interactions with COM crystals increased level of this PKC-binding protein, which is a specific receptor of activated PKC-beta 1 in MDCK cells. This cellular response was consistent with the data reported in several previous studies, which demonstrated that COM can induce up-regulation and/or activation of several signaling molecules; *i.e.* PKC, c-Jun N-terminal kinase (JNK), p38, and mitogen-activated protein (MAP) kinase, as well as transcription factors, leading to the up-regulation of several genes and proteins, *i.e.* OPN, fibronectin and TGF-$\beta_1$ [13, 39, 40].

Succinate dehydrogenase (SDH) or succinate-coenzyme Q reductase is an enzyme complex composed of four subunits, including SDHA, SDHB, SDHC and SDHD. It is also known as complex II in an electron transport chain bound to the inner mitochondrial membrane [41-43]. SDHA acts by oxidizing succinate into fumarate, while passing electrons onto flavin adenine dinucleotide (FAD), which is then reduced to $FADH_2$ [41-43]. $FADH_2$ then passes its electrons onto the iron-sulfur centers found in the SDHB of the protein. After

passing through the iron-sulfur centers, electrons are then passed into either a heme molecule or ubiquinone, which is bound to SDHC/SDHD dimer, where they are transported out of this complex and onto the next step of electron transport [41-43]. The fundamental role of SDH in the electron transport chain of mitochondria makes it vital in most multicellular organisms. Our present study identified a significant increase in SDH abundance in response to COM crystal adhesion. We have proposed that this increase is a cascade cellular response to the overproduction of ROS that is one of the most important effects of cell-crystal interactions [12].

Anx II is a 36-kDa calcium-dependent phospholipids-binding protein, which can be present in monomeric and heterotetrameric forms [44]. Anx II is involved in several cellular processes; *i.e.* cell adhesion, endocytosis, exocytosis, cell motility, actin assembly, cell-matrix interactions and fibrinolysis [44]. In the present study, we observed a marked increase in abundance of Anx II in the COD-interacting MDCK cells. The data obtained from 2-D immunoblot analysis confirmed the proteomic data (**Figure 6B**). Recently, Anx II has been identified as a CaOx crystal-binding molecule on the surface of MDCK cells [6]. These findings may imply that the increased level of Anx II may mediate the adhesion of COD crystals onto the surface of MDCK cells.

hnRNP H1 is a member of heterogeneous nuclear ribonucleoproteins (hnRNPs) family, which contains RNA recognition motifs and supplementary domains with atypical amino acid distributions [45]. The former motifs bind to pre-mRNA, while the latter domains contribute to various functions, including annealing and splicing of RNA [46]. More than 20 proteins have been identified as the members in the hnRNPs family and are designated with letters from A to U [47]. Among these, hnRNP H1 plays an essential role in manipulating gene expression. Previous studies have shown that hnRNP H1 participates in alternative splicing of genes encoding $\beta$-tropomyosin and thyroid hormone receptor [48, 49]. Alterations in hnRNP H1 expression levels are associated with various cell differentiation processes. Additionally, hnRNP H1 acts as a gene regulatory protein and represses the expression of certain genes in mesenchymal cells. Throughout the differentiation process of smooth muscle cells, the decreased expression level of hnRNP H1 leads to the increased expression of smooth muscle cell proteins; *i.e.* $\alpha$-actin, desmin and myosin [50]. Our present study found that the level of hnRNP H1 protein was significantly increased in the COD-interacting cells. This finding might implicate the central function of hnRNP H1 in regulation of expression of genes and their products during COD crystal adhesion.

However, precise role of hnRNP H1 in kidney stone formation remains unknown and deserves further investigation.

The 48-kDa OAT is well characterized as a mitochondrial matrix enzyme that is normally present in liver and kidney tissues [51]. The OAT enzymatic activity reversibly converts L-ornithine to α-ketoglutarate, producing glutamic-γ-semialdehyde and glutamate. OAT plays an essential role in driving L-ornithine to the oxidative pathway for energy production via the TCA cycle [52]. L-ornithine is a pivotal molecule in several metabolic pathways in L-proline, L-glutamate, L-glutamine, L-citrulline and L-arginine biosynthesis. Our present study identified a significant increase in OAT protein in response to COD crystal adhesion. We hypothesize that the increase in this mitochondrial protein is involved in altered metabolism as a response to COD crystal adhesion. Nevertheless, the precise role of increased OAT in the COD-interacting cells needs to be elucidated.

Lectins are sugar-binding proteins that bind to sugar molecules, which are highly specific for their sugar moieties [53]. These proteins are present on cell surfaces of mammalian cells and can mediate cell-cell interactions by combining with complementary carbohydrates on apposing cells [53]. In addition to cell-cell interactions, they also play role in other several cellular functions including glycoprotein synthesis. One type of lectins specifically recognizes galactose residues on cell surface and functions to remove particular type of glycoproteins from the circulation. Unlike Anx II, which is a crystal-binding protein that had increased level during COD crystal adhesion, we found that a galactose-specific lectin (Gal-specific lectin) was significantly decreased in the COD-interacting cells. The mechanism of this decrease during COD crystal adhesion remains unknown. A recent study showed that lipopolysaccharide antigen can suppress the expression of Gal/GalNAc-specific lectin, which acts as an endocytosis receptor of macrophage [54]. The data suggested that the decrease in lectin level may drive a negative signal to balance the lipopolysaccharide-stimulated signals mediated by proinflammatory cytokines [54]. Based on this assumption, we propose that, perhaps, the engagement of COD crystal may elicit a negative signal that results to the decreased expression level of the Gal-specific lectin as well. Moreover, as lectins play important role in cell-cell interactions, we also hypothesize that COD crystals while reduce the level of a lectin in renal tubular cells may somehow disrupt interactions of the affected renal tubular cell to the adjacent cells. However, further functional study is required to unravel this mysterious pathogenic mechanism.

In addition to changes in levels of total proteins, we also examined alterations in levels of phospho- and glycol-proteins in response to COM and COD crystal adhesion. The data revealed that these post-translationally modified proteins were also involved in cellular responses of renal tubular cells to COM and COD crystal adhesion.

Interestingly, there was no overlapping of changes in cellular proteome (either total proteins or their modified forms) induced by COM crystals compared to those induced by COD crystals. This indicated that renal tubular cells responded to the two crystal types differently. It should be noted that COM is the most common crystalline composition found in kidney stones with a frequency of up to 78% [55], whereas COD is the second most common found with a frequency of up to 43% [55]. While previous studies have shown that COD can nucleate and adhere to renal tubular epithelial cells [56-58], several lines of evidence have indicated that COM has more potent adhesive capability and can induce toxic effects to renal tubular cells [2, 39, 59, 60]. The differential responses as determined by altered cellular proteome might therefore reflect their differential physico-chemical properties and pathogenic roles in kidney stone disease.

## CONCLUSIONS

In summary, we have identified a number of altered proteins in MDCK cells in response to COM crystal adhesion. These altered proteins were known to involve in transcription, translation, signal transduction, cellular metabolism, nuclear membrane structure, cellular transport, cellular structure, stress response, biosynthesis, enzyme activation and growth regulation. Further functional study on these altered proteins would lead to better understanding of the molecular mechanisms underlying kidney stone formation.

## REFERENCES


1. Asplin, J. R., Parks, J. H., Chen, M. S., Lieske, J. C. et al, Reduced crystallization inhibition by urine from men with nephrolithiasis. *Kidney Int.* 1999, *56,* 1505-1516.
2. Tomazic, B. B., Nancollas, G. H., The dissolution of calcium oxalate kidney stones. A kinetic study. *J. Urol.* 1982, *128,* 205-208.
3. Tomazic, B. B., Nancollas, G. H., A study of the phase transformation of calcium oxalate trihydrate-monohydrate. *Invest Urol.* 1979, *16,* 329-335.
4. Verkoelen, C. F., van der Boom, B. G., Romijn, J. C., Identification of hyaluronan as a crystal-binding molecule at the surface of migrating and proliferating MDCK cells. *Kidney Int.* 2000, *58,* 1045-1054.
5. Verhulst, A., Asselman, M., Persy, V. P., Schepers, M. S. et al, Crystal retention capacity of cells in the human nephron: involvement of CD44 and its ligands hyaluronic acid and osteopontin in the transition of a crystal binding- into a nonadherent epithelium. *J Am. Soc. Nephrol.* 2003, *14,* 107-115.
6. Kumar, V., Farell, G., Deganello, S., Lieske, J. C., Annexin II is present on renal epithelial cells and binds calcium oxalate monohydrate crystals. *J Am. Soc. Nephrol.* 2003, *14,* 289-297.
7. Sorokina, E. A., Kleinman, J. G., Cloning and preliminary characterization of a calcium-binding protein closely related to nucleolin on the apical surface of inner medullary collecting duct cells. *J Biol. Chem.* 1999, *274,* 27491-27496.
8. Sorokina, E. A., Wesson, J. A., Kleinman, J. G., An acidic peptide sequence of nucleolin-related protein can mediate the attachment of calcium oxalate to renal tubule cells. *J Am. Soc. Nephrol.* 2004, *15,* 2057-2065.
9. Kramer, G., Steiner, G. E., Prinz-Kashani, M., Bursa, B. et al, Cell-surface matrix proteins and sialic acids in cell-crystal adhesion; the effect of crystal binding on the viability of human CAKI-1 renal epithelial cells. *BJU. Int.* 2003, *91,* 554-559.
10. Lieske, J. C., Spargo, B. H., Toback, F. G., Endocytosis of calcium oxalate crystals and proliferation of renal tubular epithelial cells in a patient with type 1 primary hyperoxaluria. *J Urol.* 1992, *148,* 1517-1519.
11. Verkoelen, C. F., van der Boom, B. G., Schroder, F. H., Romijn, J. C., Cell cultures and nephrolithiasis. *World J Urol.* 1997, *15,* 229-235.
12. Huang, H. S., Ma, M. C., Chen, J., Chen, C. F., Changes in the oxidant-antioxidant balance in the kidney of rats with nephrolithiasis induced by ethylene glycol. *J Urol.* 2002, *167,* 2584-2593.

13. Koul, H. K., Menon, M., Chaturvedi, L. S., Koul, S. et al, COM crystals activate the p38 mitogen-activated protein kinase signal transduction pathway in renal epithelial cells. *J Biol. Chem.* 2002, *277,* 36845-36852.
14. Umekawa, T., Chegini, N., Khan, S. R., Increased expression of monocyte chemoattractant protein-1 (MCP-1) by renal epithelial cells in culture on exposure to calcium oxalate, phosphate and uric acid crystals. *Nephrol. Dial. Transplant.* 2003, *18,* 664-669.
15. Wilkins, M. R., Sanchez, J. C., Gooley, A. A., Appel, R. D. et al, Progress with proteome projects: why all proteins expressed by a genome should be identified and how to do it. *Biotechnol. Genet. Eng Rev.* 1996, *13,* 19-50.
16. Peng, J., Gygi, S. P., Proteomics: the move to mixtures. *J. Mass Spectrom.* 2001, *36,* 1083-1091.
17. MADIN, S. H., DARBY, N. B., Jr., Established kidney cell lines of normal adult bovine and ovine origin. *Proc Soc. Exp. Biol. Med.* 1958, *98,* 574-576.
18. Gaush, C. R., Hard, W. L., Smith, T. F., Characterization of an established line of canine kidney cells (MDCK). *Proc Soc. Exp. Biol. Med.* 1966, *122,* 931-935.
19. Rindler, M. J., Taub, M., Saier, M. H., Jr., Uptake of 22Na+ by cultured dog kidney cells (MDCK). *J Biol. Chem.* 1979, *254,* 11431-11439.
20. Rindler, M. J., Chuman, L. M., Shaffer, L., Saier, M. H., Jr., Retention of differentiated properties in an established dog kidney epithelial cell line (MDCK). *J Cell Biol.* 1979, *81,* 635-648.
21. Saier, M. H., Jr., Growth and differentiated properties of a kidney epithelial cell line (MDCK). *Am. J Physiol* 1981, *240,* C106-C109.
22. Steinhusen, U., Weiske, J., Badock, V., Tauber, R. et al, Cleavage and shedding of E-cadherin after induction of apoptosis. *J Biol. Chem.* 2001, *276,* 4972-4980.
23. Macario, A. J., Heat-shock proteins and molecular chaperones: implications for pathogenesis, diagnostics, and therapeutics. *Int. J Clin. Lab Res.* 1995, *25,* 59-70.
24. Csermely, P., Schnaider, T., Soti, C., Prohaszka, Z. et al, The 90-kDa molecular chaperone family: structure, function, and clinical applications. A comprehensive review. *Pharmacol. Ther.* 1998, *79,* 129-168.
25. Parsell, D. A., Taulien, J., Lindquist, S., The role of heat-shock proteins in thermotolerance. *Philos. Trans. R. Soc. Lond B Biol. Sci* 1993, *339,* 279-285.

26. Parsell, D. A., Lindquist, S., The function of heat-shock proteins in stress tolerance: degradation and reactivation of damaged proteins. *Annu. Rev. Genet.* 1993, *27,* 437-496.
27. Kubota, H., Suzuki, T., Lu, J., Takahashi, S. et al, Increased expression of GRP94 protein is associated with decreased sensitivity to X-rays in cervical cancer cell lines. *Int. J Radiat. Biol.* 2005, *81,* 701-709.
28. Liu, H., Miller, E., van de, W. B., Stevens, J. L., Endoplasmic reticulum stress proteins block oxidant-induced Ca2+ increases and cell death. *J Biol. Chem.* 1998, *273,* 12858-12862.
29. Patel, A. B., Robertson, W. G., Choong, S., Hothersall, J. S., Heat-shock protein 25 ameliorates calcium oxalate crystal-mediated oxidative stress in renal epithelial cells. *BJU. Int.* 2006, *98,* 1094-1099.
30. Khand, F. D., Gordge, M. P., Robertson, W. G., Noronha-Dutra, A. A. et al, Mitochondrial superoxide production during oxalate-mediated oxidative stress in renal epithelial cells. *Free Radic. Biol. Med.* 2002, *32,* 1339-1350.
31. Hofmann, K., Bucher, P., The UBA domain: a sequence motif present in multiple enzyme classes of the ubiquitination pathway. *Trends Biochem. Sci* 1996, *21,* 172-173.
32. Hofmann, K., Falquet, L., A ubiquitin-interacting motif conserved in components of the proteasomal and lysosomal protein degradation systems. *Trends Biochem. Sci* 2001, *26,* 347-350.
33. Balakirev, M. Y., Tcherniuk, S. O., Jaquinod, M., Chroboczek, J., Otubains: a new family of cysteine proteases in the ubiquitin pathway. *EMBO Rep.* 2003, *4,* 517-522.
34. Heery, D. M., Kalkhoven, E., Hoare, S., Parker, M. G., A signature motif in transcriptional co-activators mediates binding to nuclear receptors. *Nature* 1997, *387,* 733-736.
35. Baek, K. H., Conjugation and deconjugation of ubiquitin regulating the destiny of proteins. *Exp. Mol. Med.* 2003, *35,* 1-7.
36. Wilkinson, K. D., Regulation of ubiquitin-dependent processes by deubiquitinating enzymes. *FASEB J* 1997, *11,* 1245-1256.
37. Mochly-Rosen, D., Smith, B. L., Chen, C. H., Disatnik, M. H. et al, Interaction of protein kinase C with RACK1, a receptor for activated C-kinase: a role in beta protein kinase C mediated signal transduction. *Biochem. Soc. Trans.* 1995, *23,* 596-600.

38. Mochly-Rosen, D., Localization of protein kinases by anchoring proteins: a theme in signal transduction. *Science* 1995, *268,* 247-251.
39. Khan, S. R., Crystal-induced inflammation of the kidneys: results from human studies, animal models, and tissue-culture studies. *Clin. Exp. Nephrol.* 2004, *8,* 75-88.
40. Chaturvedi, L. S., Koul, S., Sekhon, A., Bhandari, A. et al, Oxalate selectively activates p38 mitogen-activated protein kinase and c-Jun N-terminal kinase signal transduction pathways in renal epithelial cells. *J Biol. Chem.* 2002, *277,* 13321-13330.
41. Rustin, P., Munnich, A., Rotig, A., Succinate dehydrogenase and human diseases: new insights into a well-known enzyme. *Eur. J Hum. Genet.* 2002, *10,* 289-291.
42. Lancaster, C. R., Succinate:quinone oxidoreductases: an overview. *Biochim. Biophys. Acta* 2002, *1553,* 1-6.
43. Briere, J. J., Favier, J., El, G., V, Djouadi, F. et al, Succinate dehydrogenase deficiency in human. *Cell Mol. Life Sci* 2005, *62,* 2317-2324.
44. Gerke, V., Moss, S. E., Annexins: from structure to function. *Physiol Rev.* 2002, *82,* 331-371.
45. Krecic, A. M., Swanson, M. S., hnRNP complexes: composition, structure, and function. *Curr. Opin. Cell Biol.* 1999, *11,* 363-371.
46. Biamonti, G., Riva, S., New insights into the auxiliary domains of eukaryotic RNA binding proteins. *FEBS Lett.* 1994, *340,* 1-8.
47. Dreyfuss, G., Matunis, M. J., Pinol-Roma, S., Burd, C. G., hnRNP proteins and the biogenesis of mRNA. *Annu. Rev. Biochem.* 1993, *62,* 289-321.
48. Chen, C. D., Kobayashi, R., Helfman, D. M., Binding of hnRNP H to an exonic splicing silencer is involved in the regulation of alternative splicing of the rat beta-tropomyosin gene. *Genes Dev.* 1999, *13,* 593-606.
49. Hastings, M. L., Wilson, C. M., Munroe, S. H., A purine-rich intronic element enhances alternative splicing of thyroid hormone receptor mRNA. *RNA.* 2001, *7,* 859-874.
50. Liu, J., Beqaj, S., Yang, Y., Honore, B. et al, Heterogeneous nuclear ribonucleoprotein-H plays a suppressive role in visceral myogenesis. *Mech. Dev.* 2001, *104,* 79-87.
51. Dhanakoti, S. N., Brosnan, M. E., Herzberg, G. R., Brosnan, J. T., Cellular and subcellular localization of enzymes of arginine metabolism in rat kidney. *Biochem. J* 1992, *282 ( Pt 2),* 369-375.
52. Mezl, V. A., Knox, W. E., Properties and analysis of a stable derivative of pyrroline-5-carboxylic acid for use in metabolic studies. *Anal. Biochem.* 1976, *74,* 430-440.

53. Sharon, N., Lis, H., Lectins as cell recognition molecules. *Science* 1989, *246,* 227-234.
54. Ma, B. Y., Kaihama, M., Nonaka, M., Oka, S. et al, LPS suppresses expression of asialoglycoprotein-binding protein through TLR4 in thioglycolate-elicited peritoneal macrophages. *Glycoconj. J* 2007, *24,* 243-249.
55. Schubert, G., Stone analysis. *Urol. Res.* 2006, *34,* 146-150.
56. Lieske, J. C., Toback, F. G., Deganello, S., Face-selective adhesion of calcium oxalate dihydrate crystals to renal epithelial cells. *Calcif. Tissue Int.* 1996, *58,* 195-200.
57. Lieske, J. C., Toback, F. G., Deganello, S., Direct nucleation of calcium oxalate dihydrate crystals onto the surface of living renal epithelial cells in culture. *Kidney Int.* 1998, *54,* 796-803.
58. Lieske, J. C., Toback, F. G., Deganello, S., Sialic acid-containing glycoproteins on renal cells determine nucleation of calcium oxalate dihydrate crystals. *Kidney Int.* 2001, *60,* 1784-1791.
59. Guo, C., McMartin, K. E., The cytotoxicity of oxalate, metabolite of ethylene glycol, is due to calcium oxalate monohydrate formation. *Toxicology* 2005, *208,* 347-355.
60. McMartin, K. E., Wallace, K. B., Calcium oxalate monohydrate, a metabolite of ethylene glycol, is toxic for rat renal mitochondrial function. *Toxicol. Sci* 2005, *84,* 195-200.

## OUTPUTS

### Publications

1. Semangoen T, Sinchaikul S, Chen ST, **Thongboonkerd V***.
   Proteomic analysis of altered proteins in distal renal tubular cells in response to calcium oxalate monohydrate crystal adhesion: Implications for kidney stone disease.
   *Proteomics Clin. Appl. 2(7-8): 1099-1109, 2008*
   (2008 Impact Factor = 1.514)
2. Semangoen T, Sinchaikul S, Chen ST, **Thongboonkerd V***.
   Altered proteins in MDCK tubular cells in response to calcium oxalate dihydrate crystal adhesion: A proteomics approach.
   *J. Proteome Res. 7(7): 2889-2896, 2008*
   (2008 Impact Factor = 5.684)
3. **Thongboonkerd V***, Semangoen T, Sinchaikul S, Chen ST.
   Proteomic analysis of calcium oxalate monohydrate crystal-induced cytotoxicity in distal renal tubular cells.
   *J. Proteome Res. 7(11): 4689-4700, 2008*
   (2008 Impact Factor = 5.684)

### Poster presentations in international scientific meetings

1. Human Proteome Organisation (HUPO) 8th Annual World Congress
   26 – 30 September 2009; Toronto, Canada
   Title: “Altered glycoproteins in distal renal tubular cells upon calcium oxalate dihydrate crystal adhesion”
2. American Society of Nephrology (ASN) 42nd Annual Meeting (Renal Week)
   27 October – 1 November 2009; San Diego, USA
   Title: “Calcium oxalate dihydrate crystal causes changes in glycoproteome of distal renal tubular epithelial cells”

# APPENDIX

RESEARCH ARTICLE

# Proteomic analysis of altered proteins in distal renal tubular cells in response to calcium oxalate monohydrate crystal adhesion: Implications for kidney stone disease

*Theptida Semangoen[1, 2], Supachok Sinchaikul[3], Shui-Tein Chen[3, 4] and Visith Thongboonkerd[1]*

[1] Medical Proteomics Unit and Medical Molecular Biology Unit, Office for Research and Development, Faculty of Medicine Siriraj Hospital, Mahidol University, Bangkok, Thailand
[2] Department of Immunology and Immunology Graduate Program, Faculty of Medicine, Siriraj Hospital, Mahidol University, Bangkok, Thailand
[3] Institute of Biological Chemistry and Genomic Research Center, Academia Sinica, Taipei, Taiwan
[4] Institute of Biochemical Sciences, College of Life Science, National Taiwan University, Taipei, Taiwan

Received: November 26, 2007
Revised: January 27, 2008
Accepted: February 4, 2008

Adhesion of calcium oxalate (CaOx) crystals to renal tubular cells is a critical event that triggers a cascade of responses, leading to the development of kidney stones. However, the molecular mechanisms of these cellular responses remain largely unknown. We performed gel-based, differential proteomics study to examine cellular responses (as determined by altered protein expression) in Madin–Darby Canine Kidney (MDCK) cells during CaOx monohydrate (COM) crystal adhesion. Approximately 3-million MDCK cells were inoculated in each culture flask and maintained for 24 h. A total of 10 semiconfluent flasks were then divided into two groups ($n = 5$ *per* group) and the culture medium was replaced by either COM-containing (with 100 μg/mL COM crystals) or COM-free medium. The cells were grown further for 48 h. Crystal adhesion on the cell surface was clearly demonstrated using phase-contrast and scanning electron microscopy. Cell death assay using annexin V/propidium iodide double staining showed that all these samples had comparable % cell death. Cellular proteins were then extracted, resolved with 2-DE, and visualized by SYPRO Ruby staining ($n = 5$ gels *per* group). Quantitative intensity analysis revealed significantly increased abundance of 15 protein spots, whereas the other 5 were decreased. These altered proteins were then identified by quadrupole TOF (Q-TOF) MS and/or MS/MS analyses, including transcription/translation regulators, signal transduction proteins, metabolic enzymes, nuclear membrane proteins, carrier protein, cellular structural protein, chaperones, and proteins involved in biosynthesis, enzyme activation, and growth regulation. These data may lead to better understanding of the cellular responses in distal renal tubular cells during COM crystal adhesion.

**Keywords:**
Calcium oxalate / Cellular response / Crystal adhesion / Renal tubular cells / Stone

**Correspondence:** Dr. Visith Thongboonkerd, Medical Proteomics Unit, Office for Research and Development, 12th Floor Adulyadej Vikrom Building, 2 Prannok Road, Siriraj Hospital, Bangkoknoi, Bangkok 10700, Thailand
**E-mail:** thongboonkerd@dr.com; vthongbo@yahoo.com
**Fax:** +66-2-4184793

**Abbreviations: CaOx,** calcium oxalate; **COM,** CaOx monohydrate; **GRP94,** glucose-regulated protein; **MDCK,** Madin–Darby Canine Kidney; **MEM,** Eagle's minimum essential medium; **NRP,** nucleolin-related protein; **NSS,** normal saline solution; **OPN,** osteopontin; **PKC,** protein kinase C; **PRKCBP1,** protein kinase C binding protein 1; **Q-TOF,** quadrupole TOF; **RACK,** the receptor for activated C-kinase; **SDH,** succinate dehydrogenase; **SEM,** scanning electron microscopy

## 1 Introduction

Kidney stone disease remains a common public health problem worldwide. The stone has originated by nucleation of crystals (due to supersaturations of calcium and oxalate ions in renal tubular fluid), followed by their retention and accretion in the kidney [1]. The major composition of kidney stones is calcium oxalate (CaOx) crystal, particularly CaOx monohydrate (COM), which is the most thermodynamically stable hydrate form that has the most potent adhesive capability to the renal tubular cell surface [2, 3]. A number of crystal-binding molecules on tubular cell surface have been identified, including CD44 [4, 5], hyaluronan [4, 5], osteopontin (OPN) [4, 5], annexin II [6], nucleolin-related protein (NRP) [7, 8], and sialic acid-containing glycoprotein [9].

Several recent studies have suggested that adhesion of crystals to the surface of renal tubular cells is probably the most critical step for kidney stone formation [7, 10, 11]. COM crystals can induce cellular oxidative stress, both *in vitro* and *in vivo*, that leads to overproduction of free radicals and ROS, *i.e.*, superoxide ($O_2^{\bullet -}$) and hydrogen peroxide ($H_2O_2$) [12]. These molecules play important roles as mediators of signal transduction pathways that can activate several signaling molecules, *i.e.*, p38 mitogen-activated protein kinase (p38-MAPK); transcription factor, *i.e.*, nuclear factor kappa B (NF-κB); and activation protein-1 (AP-1) [13]. On the other hand, renal tubular epithelial cells can generate inflammatory mediators that, in turn, cause an infiltration of phagocytes around the interstitial crystals. For example, monocyte chemoattractant protein-1 (MCP-1), which is a potent chemoattractant for monocytes and macrophages that plays a crucial role in the pathogenesis of a variety of crystal deposition disease, is overexpressed in renal tubular epithelial cells exposed to COM crystals [14].

Even with the aforementioned knowledge, the molecular mechanisms of cellular responses to COM crystal adhesion remain largely unknown. The aim of our present study, therefore, was to investigate cellular responses (as determined by alterations in protein expression) in Madin–Darby Canine Kidney (MDCK) cells (distal renal tubular epithelial cells) during COM crystal adhesion. A gel-based differential proteomics approach was employed to identify a set of proteins in MDCK cells that were altered during COM crystal adhesion. These altered proteins were then identified by quadrupole TOF (Q-TOF) MS and/or MS/MS analyses. Implications of these altered proteins in association with the development of kidney stone are also discussed.

## 2 Materials and methods

### 2.1 Preparation of COM crystals

COM crystals were prepared as previously described [15]. Briefly, 10 mM calcium chloride dihydrate ($CaCl_2 \cdot 2H_2O$) was mixed with 10 mM sodium oxalate ($Na_2C_2O_4$) to make final concentrations of 5 and 0.5 mM, respectively, in Tris buffer containing 90 mM NaCl (pH 7.4). The mixture was incubated at 25°C overnight and COM crystals were harvested by centrifugation at 3000 rpm for 5 min. Supernatant was discarded and the crystals were resuspended in methanol. After another centrifugation 3000 rpm for 5 min, methanol was discarded and the crystals were dried at 37°C overnight. The presences of pure COM crystals were confirmed by phase-contrast microscopy and scanning electron microscopy (SEM). After generation and harvesting, COM crystals were decontaminated by UV light radiation for 30 min. They were then added to a complete Eagle's minimum essential medium (MEM; GIBCO™, Invitrogen Corporation, Grand Island, NY) to achieve the final concentrations of 100 μg/mL.

### 2.2 Cell culture and COM crystal adhesion

Approximately $3 \times 10^6$ MDCK cells were inoculated in each 75 $cm^2$ tissue culture flask containing MEM supplemented with 10% FBS, 1.2% penicillin G/streptomycin, and 2 mM glutamine. The cultured cells were maintained in a humidified incubator at 37°C with 5% $CO_2$ for 24 h. A total of 10 semiconfluent flasks were then divided into two groups ($n = 5$ *per* group) and the culture medium was replaced by either COM-containing (with 100 μg/mL COM crystals) or COM-free medium. For the COM-free medium, COM crystals with an equal amount of 100 μg/mL were added into the medium for 30 min, but were finally removed from the medium (as to make the identical concentrations of free calcium and oxalate ions in the medium compared to those of COM-containing medium). The cells were grown further for 48 h, and cell death was quantified using annexin V/propidium iodide double staining. The adhesion of crystals to cell monolayer was also confirmed by phase-contrast microscopy and SEM.

### 2.3 Cell death assay

Apoptosis was detected by the determination of surface phosphatidylserine, which was translocated from the inner side of plasma membranes to outer layer of the cell during apoptotic cell death. After trypsinization, FITC-labeled annexin V, a calcium-dependent phospholipid-binding protein with a high affinity for phosphatidylserine, was added to discriminate healthy from apoptotic cells. Additionally, propidium iodide, a DNA stain, was used simultaneously to detect necrotic cells.

MDCK cells from the monolayer were detached with 0.1% trypsin in 2.5 mM ethylene diamine tetraacetic acid (EDTA) and resuspended in 10 mL MEM. The harvested cells were centrifuged at 1500 rpm, 4°C for 5 min, and washed with PBS. Cell pellets were resuspended with annexin V buffer (10 mM HEPES, 140 mM NaCl, and 2.5 mM $CaCl_2 \cdot 2H_2O$; pH 7.4) at a final concentration of $5 \times 10^5$ cells/mL and then incubated with FITC-labeled

 

annexin V (BD Biosciences, San Jose, CA), on ice for 15 min in the dark. Propidium iodide (BD Biosciences) was added into the samples at a final concentration of 10 μL/mL prior to analysis. The cells were then analyzed by flow cytometry (FACScan, Becton Dickinson Immunocytometry System, San Jose, CA) and a monolayer of MDCK cells treated with 2 μg/mL camptothecin was used as a positive control. This experiment was performed in triplicates. Percentage of cell death (% cell death) = [(number of both apoptotic and necrotic cells/number of all cells) × 100%].

### 2.4 Confirmation of COM crystal adhesion by phase-contrast microscopy and SEM

The confirmation using phase-contrast microscopy was simply performed on an inverted light microscope (Olympus CKX41, Olympus, Tokyo, Japan) after three washes (with PBS) of the MDCK cells incubated with COM crystals (100 μg/mL) in 75 $cm^2$ tissue culture flasks, as mentioned above.

For the evaluation by SEM, the cell culture and COM crystal adhesion were performed exactly as the same as aforementioned, but on cover slips, instead of culture flasks (with approximately $1 \times 10^6$ cells *per* slide at an initial inoculation). After incubation with COM crystals (100 μg/mL), the cover slips were rinsed with normal saline solution (NSS) three times and fixed with 2% glutaraldehyde in NSS at room temperature for 2 h. The cover slips were then rinsed again with NSS three times and dehydrated by a graded ethanol series of 50, 70, 95, and 100% before being air-dried overnight. The cover slips were finally mounted on aluminum stubs and coated with gold particles. The crystal morphology and adhesion were then examined under a scanning electron microscope (JSM-25S, Jeol, Kyoto, Japan).

### 2.5 Protein extraction

After incubation with or without COM crystals, the monolayer of MDCK cells was harvested by directly scraping into the tube containing 0.5 M EDTA in PBS to dissolve the adherent CaOx crystals. After incubation at 4°C for 30 min, EDTA was removed by washing with PBS three times. Cell pellets were resuspended in a buffer containing 7 M urea, 2 M thiourea, 4% 3-[(3-cholamidopropyl) dimethyl-ammonio]-1-propanesulfonate (CHAPS), 120 mM DTT, 2% ampholytes (pH 3–10), and 40 mM Tris-HCl, and further incubated at 4°C for 30 min. Unsolubilized debris and particulate matters were removed by centrifugation at 10 000 rpm for 2 min. Protein concentrations were determined using the Bradford method.

### 2.6 2-DE and staining

Protein solutions (each of 200 μg total protein) derived from individual culture flasks ($n = 5$ for each group) were premixed with a rehydration buffer containing 7 M urea, 2 M thiourea, 2% CHAPS, 120 mM DTT, 40 mM Tris-base, 2% ampholytes (pH 3–10), and a trace of bromophenol blue to make the final volume of 150 μL *per* sample. The mixtures were rehydrated onto Immobiline™ DryStrip (nonlinear pH gradient of 3–10, 7 cm long; GE Healthcare, Uppsala, Sweden) at room temperature for 10–15 h. The first dimensional separation or IEF was performed in Ettan IPGphor II IEF System (GE Healthcare) at 20°C, using a stepwise mode to reach 9000 V·h. After completion of the IEF, the strips were first equilibrated for 15 min in an equilibration buffer containing 6 M urea, 130 mM DTT, 112 mM Tris–base, 4% SDS, 30% glycerol and 0.002% bromophenol blue, and then in another similar buffer, which replaced DTT with 135 mM iodoacetamide, for further 15 min. The second dimensional separation or SDS-PAGE was performed in 12% polyacrylamide gel using SE260 Mini-Vertical Electrophoresis Unit (GE Healthcare) at 150 V for approximately 2 h. Separated proteins were visualized with SYPRO Ruby fluorescence staining (Invitrogen – Molecular Probes, Eugene, OR). Gel images were taken using a Typhoon laser scanner (GE Healthcare).

### 2.7 Matching and analysis of protein spots

Image Master 2D Platinum (GE Healthcare) software was used for matching and analysis of protein spots in 2-D gels. Parameters used for spot detection were (i) minimal area = 10 pixels; (ii) smooth factor = 2.0; and (iii) saliency = 2.0. A reference gel was created from an artificial gel combining all of the spots presenting in different gels into one image. The reference gel was then used for matching the corresponding protein spots between gels. Background subtraction was performed and the intensity volume of each spot was normalized with total intensity volume (summation of the intensity volumes obtained from all spots within the same 2-D gel).

### 2.8 Statistical analysis

Comparisons between the two sets of the samples (*i.e.*, control *vs.* COM-interacting cells) of % cell death and intensity levels of corresponding protein spots were performed using unpaired Student's *t*-test. *P* values less than 0.05 were considered statistically significant. Differentially expressed protein spots, which were statistically significant, were subjected to in-gel tryptic digestion and identification by MS.

### 2.9 In-gel tryptic digestion

The protein spots whose intensity levels significantly differed between groups were excised from 2-D gels, washed twice with 200 μL of 50% ACN/25 mM $NH_4HCO_3$ buffer (pH 8.0) at room temperature for 15 min, and then washed once with 200 μL of 100% ACN. After washing, the solvent was removed, and the gel pieces were dried by a SpeedVac concentrator (Savant, Holbrook, NY) and rehydrated with

 

10 μL of 1% w/v trypsin (Promega, Madison, WI) in 25 mM $NH_4HCO_3$. After rehydration, the gel pieces were crushed with siliconized blue stick and incubated at 37°C for at least 16 h. Peptides were subsequently extracted twice with 50 μL of 50% ACN/5% TFA; the extracted solutions were then combined and dried with the SpeedVac concentrator. The peptide pellets were resuspended with 10 μL of 0.1% TFA and purified using $ZipTip_{C18}$ (Millipore, Bedford, MA). The peptide solution was drawn up and down in the $ZipTip_{C18}$ for ten times and then washed with 10 μL of 0.1% formic acid by drawing up and expelling the washing solution for three times. The peptides were finally eluted with 5 μL of 75% ACN/0.1% formic acid.

### 2.10 Protein identification by MALDI-Q-TOF MS and MS/MS analyses

The proteolytic samples were premixed 1:1 with the matrix solution (5 mg/mL CHCA in 50% ACN, 0.1% v/v TFA, and 2% w/v ammonium citrate) and spotted onto the 96-well sample stage. The samples were analyzed by the Q-TOF Ultima™ mass spectrometer (Micromass, Manchester, UK), which was fully automated with predefined probe motion pattern and the peak intensity threshold for switching over from MS survey scanning to MS/MS, and from one MS/MS to another. Within each sample well, parent ions that met the predefined criteria (any peak within the *m/z* 800–3000 range with intensity above 10 count ± include/exclude list) were selected for CID MS/MS using argon as the collision gas and a mass dependent ±5 V rolling collision energy until the end of the probe pattern was reached. The LM and HM resolution of the quadrupole were both set at 10 to give a precursor selection window of about 4 Da wide. Manual acquisition and optimization for individual samples or peaks was also possible.

The instrument was externally calibrated to <5 ppm accuracy over the mass range of *m/z* 800–3000 using a sodium iodide and PEG 200, 600, 1000, and 2000 mixtures and further adjusted with Glu-Fibrinopeptide B as the near-point lock mass calibrant during data processing. At a laser firing rate of 10 Hz, individual spectra from 5 s integration period acquired for each of the MS survey and MS/MS performed were combined, smoothed, deisotoped (fast option), and centroided using the ProteinLynx™ GlobalSERVER 2.0 data processing software (Micromass). This entailed the identification of the monoisotopic, carbon-12 peaks for MS data, and deconvolution of multiply charged spectra to their singly charged equivalents for MS/MS data. MaxEnt 3™, a maximum-entropy-based technique, has been designed for this purpose and is an integral part of ProteinLynx GlobalSERVER 2.0 [16]. The combined MS and MS/MS ion meta data were searched in concert against the NCBI mammalian protein database using the ProteinLynx GlobalSERVER 2.0 workflow. The search algorithm employed a Hidden Markov Model that incorporates empirically determined fragmentation characteristics to increase the efficacy of the search. Additionally, the MS and MS/MS data were extracted and outputted as the searchable *.txt* and *.pkl* files, respectively, for independent searches using the MASCOT search engine (http://www.matrixscience.com), assuming that peptides were monoisotopic, oxidized at methionine residues and carbamidomethylated at cysteine residues. Only one missed trypsin cleavage was allowed, and peptide mass tolerances of 100 and 50 ppm were used for PMF and MS/MS ions search, respectively.

### 2.11 Immunoblotting

To confirm the results of MS and/or MS/MS protein identification, 2-D Western blot analysis was performed. Proteins derived from MDCK cells (100 μg total protein for each sample; extraction was performed as for 2-DE analysis) were resolved by 2-DE (as described above) and transferred onto NC membranes (Whatman, Dassel, Germany) using a semidry transfer apparatus (BioRad, Milano, Italy) at 75 mA for 1 h. Nonspecific bindings were blocked with 5% milk in PBS at room temperature for 1 h. The membranes were then incubated with rabbit polyclonal antiglucose-regulated protein (GRP94) antibody (Santa Cruz Biotechnology, Santa Cruz, CA) (1:100 in 5% milk/PBS) at 4°C overnight. After washing, the membranes were further incubated with swine antirabbit IgG conjugated with horseradish peroxidase (Dako, FortCollins, CO) (1:200 in 5% milk/PBS) at room temperature for 1 h. Immunoreactive protein spots were then visualized with SuperSignal® West Pico chemiluminescence substrate (Pierce Biotechnology, Rockford, IL).

## 3 Results

We have successfully produced COM crystals using the method described in our previous study [15]. Figures 1A and B show phase-contrast and SEM images, respectively, of these COM crystals, which were present with typical monoclinic prismatic shape that was consistent with the morphology of COM crystals generated in ours [15] and in other previous studies [17, 18]. Figure 2A shows a representative image of phase-contrast microscopy of the COM crystals that were adhered onto the surface of MDCK cells after several washes following the incubation of cells with crystals for 48 h. While Fig. 1B shows COM crystals with sharp borders, Fig. 2B clearly shows the distorted or uneven borders of the COM crystals adhered onto the surface of MDCK cells, indicating the cell–crystal interactions.

We then aimed to identify alterations of a set of proteins in MDCK cells as the cellular responses to COM crystal adhesion. Our aim was not to evaluate for changes in the cell proteome as the results of increased cell death caused by experimental intervention. To achieve our goal, the cell death should not be significantly increased by COM crystal adhesion. Quantitative analysis of cell death, comparing the MDCK cells incubated with COM crystals to those without

 

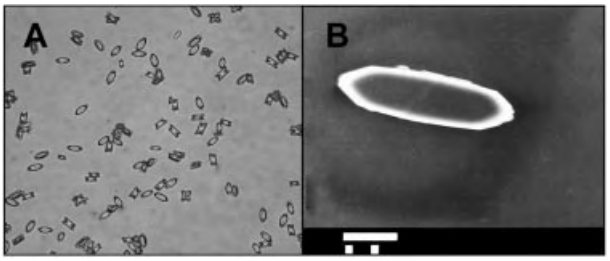


**Figure 1.** Typical monoclinic prismatic shape of COM crystals generated in the present study. Images were taken by phase-contrast microscopy (A) and SEM (B). Some of the COM crystals were present as a twin form. Original magnification power was 400 × in (A) and 2000 × in (B). The bar represents a scale of 1 μm.

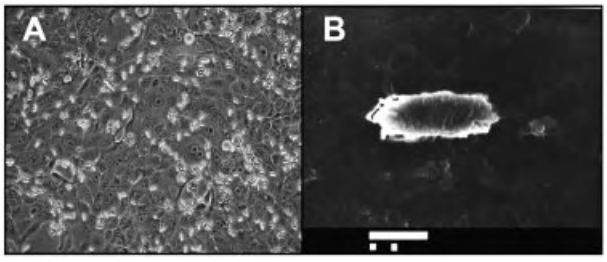


**Figure 2.** Cell–crystal interactions during adhesion of COM crystals onto the surface of MDCK cells. Images were taken by phase-contrast microscopy (A) and SEM (B). Obviously, the distorted or uneven borders of COM crystals were observed, with the background of the monolayer of MDCK cells. Original magnification power was 100 × in (A) and 2000 × in (B). The bar represents a scale of 1 μm.

crystals (control), was thus performed. By light microscopic examination, the obvious morphological hallmarks of apoptotic and/or necrotic cell death (including condensed nuclei, rounding shape, large vacuoles in cytoplasm and floatation of cells) were not observed in any flasks of the cells incubated with COM crystals. Figure 3 shows the time-course study of cell death, as evaluated by annexin V/propidium iodide double staining and flow cytometry. The data clearly demonstrated that % cell death was comparable between the two groups at 12, 24, and 48 h incubation period ($p$ values were not statistically significant; $n = 3$ independent experiments for each condition). We had not extended the incubation period to longer than 48 h as the cells were completely confluent at the 48 h and became overcrowded at later time-points. We also examined the total number of cells at 48 h incubation and the results showed no significant difference in total number of cells between the two groups ($177.9 \pm 0.8$ *vs.* $183.4 \pm 15.5 \times 10^3$ cells/cm$^2$ for control versus COM-interacting cells, respectively; $p$ value was not statistically significant; $n = 3$ independent experiments for each condition). We therefore selected the time-point of 48 h incubation (with or without COM crystals) for all other experiments in the present study. At this 48 h time-point, crystal binding was found in $32.4 \pm 2.1$% of cells in the COM-containing flasks.

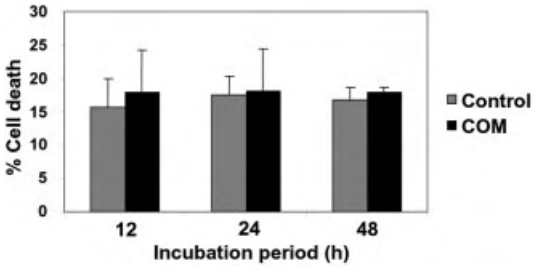


**Figure 3.** Evaluation of time-course cell death. Flow cytometry using annexin V/propidium iodide double staining of MDCK cells showed no significant difference of % cell death in the MDCK cells incubated with or without COM crystals ($p$-values were not statistically significant for the comparisons between the control and COM-interacting cells). The data are reported as Mean (+SD) and each bar represents the results obtained from three independent experiments.

Gel-based differential proteomics study was performed to compare the cellular proteome of MDCK cells incubated with COM crystals with that of cells cultured without crystals (control). Proteins derived from MDCK cells of each cultured flak were resolved in each 2-DE gel ($n = 5$ gels derived from five individual flasks in each group). Figure 4 shows representative 2-DE gel images of the proteome of control and COM-interacting cells. Approximately 1000–1200 protein spots were visualized in each 2-DE gel using SYPRO Ruby stain. From these, quantitative intensity analysis revealed 20 protein spots whose abundance levels were significantly altered by COM crystal adhesion (Fig. 4 and Table 1). These altered protein spots (15 were increased, whereas the other 5 were decreased) were then excised and subjected to identification by Q-TOF MS and/or MS/MS analyses.

Of the 20 altered protein spots, 16 proteins were successfully identified by Q-TOF MS and/or MS/MS (Table 1). These proteins included transcription/translation regulators, signal transduction proteins, metabolic enzymes, nuclear membrane proteins, carrier protein, cellular structural protein, chaperones, and proteins involved in biosynthesis, enzyme activation, and growth regulation. Other four proteins could not be identified because they were the small spots with faint staining by SYPRO Ruby. All these four unidentified spots provided poor mass spectra by Q-TOF MS and/or MS/MS analyses, most likely due to their low abundance levels in MDCK cells. Functional roles and subcellular localizations of the 16 altered proteins identified by Q-TOF MS and/or MS/MS analyses were summarized in Table 2. Moreover, the decreased level of GRP94 (spot #2) was clearly confirmed by 2-D Western blot analysis (Fig. 5).

## 4 Discussion

We have successfully performed an *in vitro* study for an evaluation of cellular responses of distal renal tubular cells during COM crystal adhesion. Flow cytometry using annexin

 

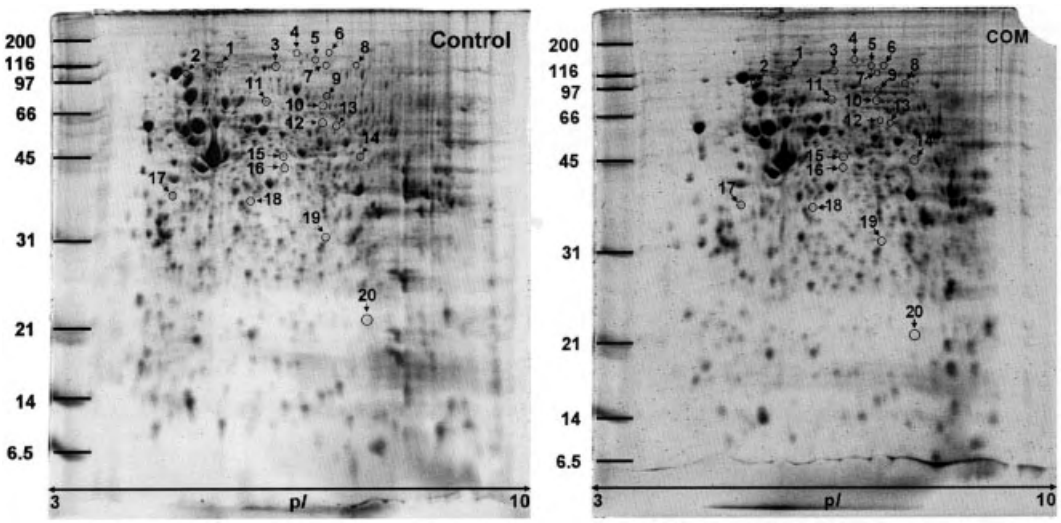


**Figure 4.** Representative 2-DE gel images of proteins derived from the control and COM-interacting MDCK cells. Proteins were resolved with 2-DE using a pH gradient of 3–10 (nonlinear) for the IEF and 12% polyacrylamide SDS-PAGE for the second dimensional separation. The resolved protein spots were then visualized with SYPRO Ruby stain. Each gel contained 200 μg total protein extracted from each culture flask ($n = 5$ for each group; total $n = 10$ gels were used for quantitative intensity analysis). The spots labeled with numbers are those whose intensity levels significantly differed between the two groups. These differentially expressed proteins were subsequently identified by Q-TOF MS and/or MS/MS analyses (see Table 1).

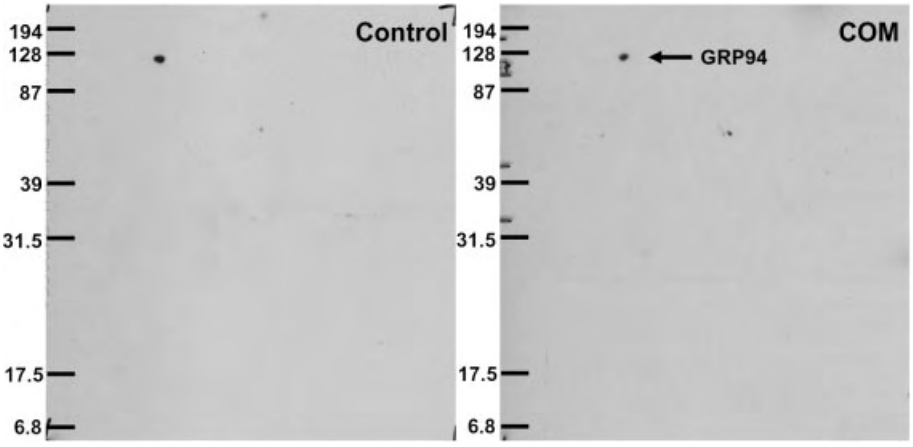


**Figure 5.** Validation of the proteomic data by 2-D Western blot analysis. Proteins derived from MDCK cells (100 μg total protein for each sample; extraction was performed as for 2-DE analysis) were resolved by 2-DE and transferred onto NC membranes. After blocking nonspecific bindings, the membranes were incubated with rabbit polyclonal anti-GRP94 antibody and then with swine antirabbit IgG conjugated with horseradish peroxidase. Immunoreactive protein spots were then visualized with chemiluminescence substrate. The 2-D Western blot data clearly confirmed that GRP94 level was decreased in the COM-interacting cells.

V/propidium iodide double staining clearly showed that incubation of MDCK cells with 100 μg/mL COM crystals for up to 48 h did not significantly increase % cell death (Fig. 3). Additionally, the total cell numbers were not significantly altered by COM crystal adhesion at this 48 h time-point, implicating that there was no significant effect of crystal adhesion on cell division, using the conditions described herein. Moreover, SEM analysis clearly showed the cell–crystal interactions as demonstrated by the distorted or uneven borders of the COM crystals incubated with MDCK cells for 48 h (Fig. 2B). Thus, the experimental conditions used herein were suitable for examining cellular responses to COM crystal adhesion. Gel-based differential proteomics study revealed alterations in abundance levels of 20 proteins, most of which were increased in MDCK cells during COM crystal adhesion (Fig. 4 and Table 1). Functional roles of some of these altered proteins are highlighted as follows.

 

**Table 1.** Summary of differentially expressed proteins, whose abundance levels were significantly altered during COM crystal adhesion

| Spot no. | Protein | NCBI ID | Identified by | MOWSE/ Ions scores | % Cov[a)] | No. of matched peptides | p*I* | MW (kDa) | Intensity levels (Arbitrary unit) (Mean ± SEM) | | Ratio (COM/ control) | *p*-values |
|---|---|---|---|---|---|---|---|---|---|---|---|---|
| | | | | | | | | | Control | COM | | |
| 1 | Alanyl-tRNA synthetase (alanine-tRNA ligase) (AlaRS) isoform 1 | gi\|73957022 | MS/MS | –/60 | 2 | 2 | 5.27 | 107.45 | 0.0644 ± 0.0059 | 0.0406 ± 0.0042 | 0.63 | 0.011 |
| 2 | Protein kinase (GRP94) | gi\|984249 | MS, MS/MS | 83/76 | 24/4 | 16/3 | 4.76 | 93.09 | 0.0417 ± 0.0169 | 0.0007 ± 0.0007 | 0.02 | 0.042 |
| 3 | Transcriptional repressor BSR/RACK7/ PRKCBP1 | gi\|119905994 | MS | 56/– | 12 | 11 | 6.04 | 122.29 | 0.0419 ± 0.0045 | 0.0588 ± 0.0053 | 1.40 | 0.042 |
| 4 | Armadillo repeat containing 3 (ARMC3) | gi\|63488113 | MS | 50/– | 13 | 7 | 5.95 | 97.06 | 0.0116 ± 0.0031 | 0.0294 ± 0.0036 | 2.54 | 0.006 |
| 5 | Leucine-rich PPR motif-containing protein (Lrpprc) | gi\|73970116 | MS | 113/– | 22 | 18 | 6.46 | 158.93 | 0.0207 ± 0.0034 | 0.0393 ± 0.0062 | 1.90 | 0.029 |
| 6 | Metalloprotease 1 (MP 1) | gi\|73949192 | MS | 82/– | 17 | 17 | 6.60 | 117.74 | 0.0215 ± 0.0012 | 0.0312 ± 0.0039 | 1.45 | 0.044 |
| 7 | Minichromosome maintenance complex 8 (MCM 8) | gi\|39644544 | MS | 53/– | 21 | 9 | 6.11 | 82.17 | 0.0054 ± 0.0033 | 0.0320 ± 0.0050 | 5.90 | 0.002 |
| 8 | RP3-398G3.1 (spectrin repeat containing, nuclear envelope 1) | gi\|57162570 | MS | 57/– | 16 | 14 | 5.78 | 110.45 | 0.0351 ± 0.0058 | 0.0525 ± 0.0045 | 1.49 | 0.046 |
| 9 | Lamin A/C (70 kDa lamin) isoform 4 | gi\|73960920 | MS | 68/– | 20 | 13 | 6.57 | 74.47 | 0.0494 ± 0.0060 | 0.0740 ± 0.0058 | 1.50 | 0.018 |
| 10 | Succinate dehydrogenase (ubiquinone), flavoprotein subunit of complex II isoform 1 | gi\|74003064 | MS, MS/MS | 107/64 | 30/3 | 14/2 | 7.29 | 74.09 | 0.0410 ± 0.0074 | 0.0626 ± 0.0052 | 1.53 | 0.043 |
| 11 | ALB protein | gi\|74267962 | MS, MS/MS | 110/112 | 27/6 | 15/3 | 5.88 | 71.19 | 0.0507 ± 0.0083 | 0.0713 ± 0.0026 | 1.41 | 0.046 |
| 12 | Unidentified | – | – | – | – | – | – | – | 0.0102 ± 0.0030 | 0.0213 ± 0.0029 | 2.09 | 0.028 |
| 13 | Elongation protein 3 homolog (ELP3) isoform 1 | gi\|114619483 | MS/MS | –/36 | 7 | 2 | 8.93 | 61.03 | 0.0113 ± 0.0050 | 0.0268 ± 0.0031 | 2.37 | 0.030 |
| 14 | Methionine aminopeptidase 1 (MetAP1) | gi\|74002259 | MS | 52/– | 26 | 7 | 6.96 | 40.40 | 0.0695 ± 0.0087 | 0.0420 ± 0.0020 | 0.60 | 0.015 |
| 15 | Unidentified | – | – | – | – | – | – | – | 0.0486 ± 0.0041 | 0.0719 ± 0.0057 | 1.48 | 0.011 |
| 16 | Plakophilin 4 isoform CRA_g | gi\|119631836 | MS | 75/– | 17 | 11 | 9.11 | 10.10 | 0.0247 ± 0.0072 | 0.0484 ± 0.0062 | 1.95 | 0.038 |
| 17 | HSPC263, otubain1 | gi\|6841176 | MS, MS/MS | 106/48 | 46/9 | 11/2 | 4.90 | 31.95 | 0.0962 ± 0.0147 | 0.0545 ± 0.0088 | 0.57 | 0.041 |
| 18 | Unidentified | – | – | – | – | – | – | – | 0.0269 ± 0.0048 | 0.0395 ± 0.0023 | 1.47 | 0.046 |
| 19 | Parvalbumin | gi\|31980767 | MS | 84/– | 59 | 7 | 5.02 | 11.92 | 0.0329 ± 0.0018 | 0.0185 ± 0.0048 | 0.56 | 0.023 |
| 20 | Unidentified | – | – | – | – | – | – | – | 0.0000 ± 0.0000 | 0.0436 ± 0.0097 | DIV/0[b)] | 0.002 |

These altered proteins were then identified by Q-TOF MS and/or MS/MS analyses.

a) %Cov = %Sequence coverage [(number of the matched residues/total number of residues in the entire sequence) × 100%].

b) DIV/0 = divided by zero.

**Table 2.** Functional roles and subcellular localizations of the altered proteins identified from the COM-interacting MDCK cells

| Altered proteins | Subcellular localization | Function |
|---|---|---|
| **Proteins whose abundance levels were significantly increased during COM crystal adhesion** | | |
| Transcriptional repressor BSR/RACK7/PRKCBP1 | Nucleus | Transcription regulator |
| ARMC3 | Cytoplasm | Signal transduction |
| Lrpprc | Nucleus | RNA binding protein |
| MP 1 | Mitochondria | Metabolic enzyme |
| Minichromosome maintenance complex component 8 (MCM8) | Nucleus | DNA replication |
| Nuclear envelope 1 | Nuclear envelope | Nuclear membrane structure |
| Lamin A/C isoform 4 | Nuclear envelope | Nuclear membrane structure |
| Succinate dehydrogenase | Mitochondria | Metabolic enzyme |
| ALB protein | Secreted protein | Carrier protein |
| ELP3 isoform 1 | Nucleus | Transcription elongator |
| Plakophilin 4, isoform CRA_g | Adherens junctions | Cellular structure |
| **Proteins whose abundance levels were significantly decreased during COM crystal adhesion** | | |
| AlaRS | Cytoplasm | Protein biosynthesis |
| GRP94 | ER | Chaperone |
| MetAP 1 | Cytoplasm | Metabolic enzyme |
| HSPC263 | Cytoplasm | Metabolic enzyme |
| Parvalbumin | Cytoplasm | Enzyme activation and growth regulation |

GRP94 (also known as tumor rejection antigen 1 or gp96) is the most abundant chaperone located in the ER lumen, a place to restore or correct folding of the misfolded/misassembled proteins and target them for degradation by coupling to the proteasome [19, 20]. GRP94 regulates cellular homeostasis [21, 22] and apoptosis in several mammalian cell lines [23]. In the presence of various stresses, the final state or survival of cells may mainly depend on the ability of the cells to resist to the stresses. GRP94 regulates cell fate by maintaining the intracellular calcium balance among cytosol, ER, and mitochondria [24]. In the present study, we observed a marked decrease in abundance of GRP94 in the COM-interacting MDCK cells. The data obtained from 2-D Western blot analysis clearly confirmed the proteomic data (Fig. 5). However, it should be noted that Western blot analysis is more sensitive than the detection of protein spots by gel staining. Mechanisms of visualization of protein spots by antibody-chemiluminescence enhancement obviously differ from those of the detection by staining. These may explain the differential magnitudes of changes observed by these two different methods. The detection of another (smaller) GRP94 spot in Fig. 5 might be simply explained by the higher sensitivity of Western blot analysis. Our data were consistent with those obtained from a previous study, which showed significant down-regulation of heat shock protein 25 (HSP25), HSP 70, and heme oxygenase-1 expression in COM-treated MDCK cells [25]. The mechanistic basis for the decrease of these proteins during COM crystal adhesion remains unclear. Perhaps, the decreased levels of chaperones may simply reflect the damaged renal epithelial cells caused by COM-mediated ROS and decreased antioxidant glutathione concentrations [26].

HSPC263, also known as otubain 1, contained ubiquitin-interaction motifs and ubiquitin-associated domains, which are generally found in the proteins involved in the ubiquitin pathway [27, 28]. Otubain 1 is also a deubiquitinating enzyme cysteine protease, which precisely cleaves the polyubiquitin chains from the defective proteins [29]. Moreover, it has putative nuclear localization signals and a consensus LxxLL motif (where L is leucine and x is any amino acid), which is known to mediate the binding of transcriptional coactivators to liganded nuclear receptors [30]. The data from a previous study have suggested that otubain 1 may play a significant role in tumor necrosis factor (TNF) signaling pathway [29]. However, ubiquitination pathway has exerted in a wide spectrum of biological processes including cell cycle progression, transcriptional activation, signal transduction, apoptosis, and DNA repair [31, 32]. In our present study, HSPC263 protein was decreased in the COM-interacting cells. The role of decreased HSPC263 in MDCK cells during COM crystal adhesion remains unclear and deserves further investigation.

Transcriptional repressor BSR/RACK7/PRKCBP1 or protein kinase C (PKC)-binding protein 1 is a member of the receptors for activated C-kinase (RACK) family. Upon activation, most PKC isoenzymes are translocated to the cellular site of activity and bind to a specific receptor for RACK [33, 34]. The PKC-beta 1 interacts specifically with the carboxy-terminus of PRKCBP1 (protein kinase C binding protein 1) and increases both its phosphorylation and the duration of its activation. In the present study, we found that interactions

 

with COM crystals increased level of this PKC-binding protein, which is a specific receptor of activated PKC-beta 1 in MDCK cells. This cellular response was consistent with the data reported in several previous studies, which demonstrated that COM can induce up-regulation and/or activation of several signaling molecules; *i.e.*, PKC, c-Jun N-terminal kinase (JNK), p38, and mitogen-activated protein (MAP) kinase, as well as transcription factors, leading to the up-regulation of several genes and proteins, *i.e.*, OPN, fibronectin, and transforming growth factor beta-1 (TGF-$\beta_1$) [13, 35, 36].

Succinate dehydrogenase (SDH) or succinate-coenzyme Q reductase is an enzyme complex composed of four subunits, including SDHA, SDHB, SDHC, and SDHD. It is also known as complex II in an electron transport chain bound to the inner mitochondrial membrane [37–39]. SDHA acts by oxidizing succinate into fumarate, while passing electrons onto flavin adenine dinucleotide (FAD), which is then reduced to $FADH_2$ [37–39]. $FADH_2$ then passes its electrons onto the iron-sulfur centers found in the SDHB of the protein. After passing through the iron-sulfur centers, electrons are then passed into either a heme molecule or ubiquinone, which is bound to SDHC/SDHD dimer, where they are transported out of this complex and onto the next step of electron transport [37–39]. The fundamental role of SDH in the electron transport chain of mitochondria makes it vital in most multicellular organisms. Our present study identified a significant increase in SDH abundance in response to COM crystal adhesion. We have proposed that this increase is a cascade cellular response to the overproduction of ROS that is one of the most important effects of cell–crystal interactions [12].

In summary, we have identified a number of altered proteins in MDCK cells in response to COM crystal adhesion. These altered proteins included transcription/translation regulators, signal transduction proteins, metabolic enzymes, nuclear membrane proteins, carrier protein, cellular structural protein, chaperones, and proteins involved in biosynthesis, enzyme activation, and growth regulation. We have also proposed some molecular mechanisms underlying the cellular responses during COM crystal adhesion, which is probably the most crucial step in the pathogenic mechanisms of kidney stone formation. Together with the currently available knowledge that COM crystals adhere to the renal tubular cells via several crystal-binding molecules, *e.g.*, CD44, hyaluronan, OPN, annexin II, NRP, and sialic acid-containing glycoprotein [4–9], we have proposed Fig. 6 as a model to offer a clearer image of cellular responses to COM crystal adhesion. Further functional study on these altered proteins would lead to better understanding of the molecular mechanisms underlying kidney stone formation.

*We thank Dr. Sontana Siritantikorn and Department of Microbiology at Faculty of Medicine Siriraj Hospital for kindly providing the MDCK cells. This study was supported by The Thailand Research Fund, Commission on Higher Education, Mahidol University, the National Research Council of Thailand, Siriraj Grant for Research and Development, and the National Center for Genetic Engineering and Biotechnology (to V. Thongboonkerd), and by Siriraj Graduate Thesis Scholarship (to T. Semangoen).*

*The authors have declared no conflict of interest.*

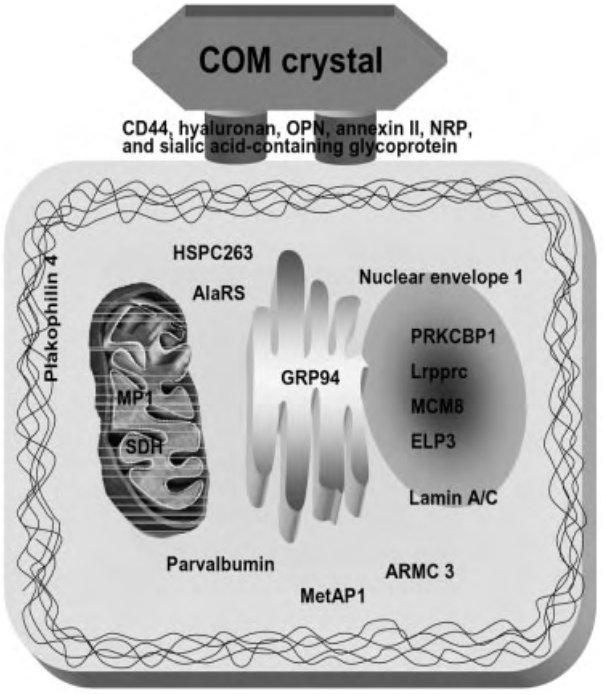


**Figure 6.** A model of cellular responses in MDCK cells during COM crystal adhesion, which has been proposed on the basis of currently available knowledge of crystal-binding molecules [4–9] together with the data obtained from our present study. After the COM crystals bind to these molecules (CD44, hyaluronan, OPN, annexin II, NRP, and sialic acid-containing glycoprotein) [4–9] the abundance levels of a set of cellular proteins are altered. These altered proteins include transcription/translation regulators, signal transduction proteins, metabolic enzymes, nuclear membrane proteins, carrier protein, cellular structural protein, chaperones, and proteins involved in biosynthesis, enzyme activation, and growth regulation (see also Table 2).

## 5 References

[1] Asplin, J. R., Parks, J. H., Chen, M. S., Lieske, J. C. *et al.*, Reduced crystallization inhibition by urine from men with nephrolithiasis. *Kidney Int.* 1999, *56*, 1505–1516.

[2] Tomazic, B. B., Nancollas, G. H., The dissolution of calcium oxalate kidney stones. A kinetic study. *J. Urol.* 1982, *128*, 205–208.

 

[3] Tomazic, B. B., Nancollas, G. H., A study of the phase transformation of calcium oxalate trihydrate-monohydrate. *Invest. Urol.* 1979, *16*, 329–335.

[4] Verkoelen, C. F., van der Boom, B. G., Romijn, J. C., Identification of hyaluronan as a crystal-binding molecule at the surface of migrating and proliferating MDCK cells. *Kidney Int.* 2000, *58*, 1045–1054.

[5] Verhulst, A., Asselman, M., Persy, V. P., Schepers, M. S. *et al.*, Crystal retention capacity of cells in the human nephron: Involvement of CD44 and its ligands hyaluronic acid and osteopontin in the transition of a crystal binding- into a nonadherent epithelium. *J. Am. Soc. Nephrol.* 2003, *14*, 107–115.

[6] Kumar, V., Farell, G., Deganello, S., Lieske, J. C., Annexin II is present on renal epithelial cells and binds calcium oxalate monohydrate crystals. *J. Am. Soc. Nephrol.* 2003, *14*, 289–297.

[7] Sorokina, E. A., Kleinman, J. G., Cloning and preliminary characterization of a calcium-binding protein closely related to nucleolin on the apical surface of inner medullary collecting duct cells. *J. Biol. Chem.* 1999, *274*, 27491–27496.

[8] Sorokina, E. A., Wesson, J. A., Kleinman, J. G., An acidic peptide sequence of nucleolin-related protein can mediate the attachment of calcium oxalate to renal tubule cells. *J. Am. Soc. Nephrol.* 2004, *15*, 2057–2065.

[9] Kramer, G., Steiner, G. E., Prinz-Kashani, M., Bursa, B. *et al.*, Cell-surface matrix proteins and sialic acids in cell-crystal adhesion; the effect of crystal binding on the viability of human CAKI-1 renal epithelial cells. *BJU Int.* 2003, *91*, 554–559.

[10] Lieske, J. C., Spargo, B. H., Toback, F. G., Endocytosis of calcium oxalate crystals and proliferation of renal tubular epithelial cells in a patient with type 1 primary hyperoxaluria. *J. Urol.* 1992, *148*, 1517–1519.

[11] Verkoelen, C. F., van der Boom, B. G., Schroder, F. H., Romijn, J. C., Cell cultures and nephrolithiasis. *World J. Urol.* 1997, *15*, 229–235.

[12] Huang, H. S., Ma, M. C., Chen, J., Chen, C. F., Changes in the oxidant-antioxidant balance in the kidney of rats with nephrolithiasis induced by ethylene glycol. *J. Urol.* 2002, *167*, 2584–2593.

[13] Koul, H. K., Menon, M., Chaturvedi, L. S., Koul, S. *et al.*, COM crystals activate the p38 mitogen-activated protein kinase signal transduction pathway in renal epithelial cells. *J. Biol. Chem.* 2002, *277*, 36845–36852.

[14] Umekawa, T., Chegini, N., Khan, S. R., Increased expression of monocyte chemoattractant protein-1 (MCP-1) by renal epithelial cells in culture on exposure to calcium oxalate, phosphate and uric acid crystals. *Nephrol. Dial. Transplant.* 2003, *18*, 664–669.

[15] Thongboonkerd, V., Semangoen, T., Chutipongtanate, S., Factors determining types and morphologies of calcium oxalate crystals: Molar concentrations, buffering, pH, stirring and temperature. *Clin. Chim. Acta* 2006, *367*, 120–131.

[16] O'Malley, R., Life's (more than) a BLAST. *Biochemist* 2002, *24*, 21–23.

[17] Yu, H., Sheikholeslami, R., Doherty, W. O. S., The effects of silica and sugar on the crystallographic and morphological properties of calcium oxalate. *J. Crystal Growth* 2004, *265*, 592–603.

[18] Donnet, M., Jongen, N., Lemaitre, J., Bowen, P., New morphology of calcium oxalate trihydrate precipitated in a segmented flow tubular reactor. *J. Mater. Sci. Lett.* 2000, *19*, 749–750.

[19] Macario, A. J., Heat-shock proteins and molecular chaperones: Implications for pathogenesis, diagnostics, and therapeutics. *Int. J. Clin. Lab. Res.* 1995, *25*, 59–70.

[20] Csermely, P., Schnaider, T., Soti, C., Prohaszka, Z. *et al.*, The 90-kDa molecular chaperone family: Structure, function, and clinical applications. A comprehensive review. *Pharmacol. Ther.* 1998, *79*, 129–168.

[21] Parsell, D. A., Taulien, J., Lindquist, S., The role of heat-shock proteins in thermotolerance. *Philos. Trans. R. Soc. Lond. B Biol. Sci.* 1993, *339*, 279–285.

[22] Parsell, D. A., Lindquist, S., The function of heat-shock proteins in stress tolerance: Degradation and reactivation of damaged proteins. *Annu. Rev. Genet.* 1993, *27*, 437–496.

[23] Kubota, H., Suzuki, T., Lu, J., Takahashi, S. *et al.*, Increased expression of GRP94 protein is associated with decreased sensitivity to X-rays in cervical cancer cell lines. *Int. J. Radiat. Biol.* 2005, *81*, 701–709.

[24] Liu, H., Miller, E., van de, W. B., Stevens, J. L., Endoplasmic reticulum stress proteins block oxidant-induced Ca2+ increases and cell death. *J. Biol. Chem.* 1998, *273*, 12858–12862.

[25] Patel, A. B., Robertson, W. G., Choong, S., Hothersall, J. S., Heat-shock protein 25 ameliorates calcium oxalate crystal-mediated oxidative stress in renal epithelial cells. *BJU Int.* 2006, *98*, 1094–1099.

[26] Khand, F. D., Gordge, M. P., Robertson, W. G., Noronha-Dutra, A. A. *et al.*, Mitochondrial superoxide production during oxalate-mediated oxidative stress in renal epithelial cells. *Free Radic. Biol. Med.* 2002, *32*, 1339–1350.

[27] Hofmann, K., Bucher, P., The UBA domain: A sequence motif present in multiple enzyme classes of the ubiquitination pathway. *Trends Biochem. Sci.* 1996, *21*, 172–173.

[28] Hofmann, K., Falquet, L., A ubiquitin-interacting motif conserved in components of the proteasomal and lysosomal protein degradation systems. *Trends Biochem. Sci.* 2001, *26*, 347–350.

[29] Balakirev, M. Y., Tcherniuk, S. O., Jaquinod, M., Chroboczek, J., Otubains: A new family of cysteine proteases in the ubiquitin pathway. *EMBO Rep.* 2003, *4*, 517–522.

[30] Heery, D. M., Kalkhoven, E., Hoare, S., Parker, M. G., A signature motif in transcriptional co-activators mediates binding to nuclear receptors. *Nature* 1997, *387*, 733–736.

[31] Baek, K. H., Conjugation and deconjugation of ubiquitin regulating the destiny of proteins. *Exp. Mol. Med.* 2003, *35*, 1–7.

[32] Wilkinson, K. D., Regulation of ubiquitin-dependent processes by deubiquitinating enzymes. *FASEB J.* 1997, *11*, 1245–1256.

[33] Mochly-Rosen, D., Smith, B. L., Chen, C. H., Disatnik, M. H. *et al.*, Interaction of protein kinase C with RACK1, a receptor for activated C-kinase: A role in beta protein kinase C mediated signal transduction. *Biochem. Soc. Trans.* 1995, *23*, 596–600.

[34] Mochly-Rosen, D., Localization of protein kinases by anchoring proteins: A theme in signal transduction. *Science* 1995, *268*, 247–251.

 

[35] Khan, S. R., Crystal-induced inflammation of the kidneys: Results from human studies, animal models, and tissue-culture studies. *Clin. Exp. Nephrol.* 2004, *8*, 75–88.

[36] Chaturvedi, L. S., Koul, S., Sekhon, A., Bhandari, A. *et al.*, Oxalate selectively activates p38 mitogen-activated protein kinase and c-Jun N-terminal kinase signal transduction pathways in renal epithelial cells. *J. Biol. Chem.* 2002, *277*, 13321–13330.

[37] Rustin, P., Munnich, A., Rotig, A., Succinate dehydrogenase and human diseases: New insights into a well-known enzyme. *Eur. J. Hum. Genet.* 2002, *10*, 289–291.

[38] Lancaster, C. R., Succinate:quinone oxidoreductases: An overview. *Biochim. Biophys. Acta* 2002, *1553*, 1–6.

[39] Briere, J. J., Favier, J., El, G. V., Djouadi, F. *et al.*, Succinate dehydrogenase deficiency in human. *Cell Mol. Life Sci.* 2005, *62*, 2317–2324.

 

research articles Journal of proteome research

# Altered Proteins in MDCK Renal Tubular Cells in Response to Calcium Oxalate Dihydrate Crystal Adhesion: A Proteomics Approach

**Theptida Semangoen,[†,‡] Supachok Sinchaikul,[§] Shui-Tein Chen,[§,||] and Visith Thongboonkerd*[,†]**

*Medical Proteomics Unit and Medical Molecular Biology Unit, Office for Research and Development, Faculty of Medicine Siriraj Hospital, Mahidol University, Bangkok, Thailand, Department of Immunology and Immunology Graduate Program, Faculty of Medicine, Siriraj Hospital, Mahidol University, Bangkok, Thailand, Institute of Biological Chemistry and Genomic Research Center, Academia Sinica, Taipei, Taiwan, and Institute of Biochemical Sciences, College of Life Science, National Taiwan University, Taipei, Taiwan*

**Received February 12, 2008**

The interaction between crystals and renal tubular cells has been proposed to be a crucial event that elicits subsequent cellular responses, leading to kidney stone formation. Nevertheless, the molecular mechanisms of these cellular responses remain poorly understood. We performed a gel-based differential proteomics study to examine cellular responses (as determined by altered protein expression) in Madin-Darby canine kidney (MDCK) cells, which were derived from dog kidney and exhibited distal renal tubule phenotype, during calcium oxalate dihydrate (COD) crystal adhesion. MDCK cells were grown in a medium without or with COD crystals (100 $\mu$g/ml) for 48 h. Crystal adhesion was illustrated by phase-contrast and scanning electron microscopy. Flow cytometry using annexin V/propidium iodide double staining showed that the percentage of cell death did not significantly differ between cells with and without COD crystal adhesion. Cellular proteins were then extracted, resolved with two-dimensional gel electrophoresis (2-DE), and visualized by SYPRO Ruby staining ($n = 5$ gels per group). Quantitative intensity analysis revealed 11 significantly altered proteins, 10 of which were successfully identified by quadrupole time-of-flight peptide mass fingerprinting (MS) and/or tandem MS (MS/MS), including metabolic enzymes, cellular structural protein, calcium-binding protein, adhesion molecule, protein involved in RNA metabolism, and chaperone. An increase in annexin II was confirmed by 2-D Western blot analysis. These data may lead to better understanding of the cellular responses in distal renal tubular cells during COD crystal adhesion.

**Keywords:** calcium oxalate • crystal adhesion • cellular response • proteomics • proteome • renal tubular cells • MDCK • kidney • stone

## Introduction

Kidney stones originate from the nucleation of microcrystals in renal tubular fluid followed by accumulation and retention of these crystals in the kidney.[1–3] The adhesion of crystals to renal tubular epithelial cells has been proposed as a critical process for kidney stone formation.[4,5] A number of crystal-binding molecules on surfaces of renal tubular epithelial cells that can promote crystal adhesion have been identified, including CD44,[6] hyaluronan,[6,7] osteopontin (OPN),[6] annexin II (Anx II),[8] nucleolin-related protein (NRP),[9] and sialic acid-containing glycoprotein.[10,11] Calcium oxalate (CaOx) is the major crystalline component of kidney stones. The interaction of CaOx crystals with renal tubular epithelial cells leads to the activation of intracellular responses, including overproduction of free radicals and reactive oxygen species (ROS), that is, superoxide ($O_2^{\bullet -}$), hydrogen peroxide ($H_2O_2$), and hydroxyl anions.[12] These molecules have the capacity to modify membrane lipids, DNA, mitochondria, and cytoskeletal elements. Furthermore, CaOx crystals can alter expression of several genes, for example, those encoding transcriptional activators, a regulator of extracellular matrix, and growth factors,[13] and of proteins such as OPN and monocyte chemoattractant protein-1 (MCP-1).[14]

Although few proteins are altered during CaOx crystal adhesion, it is likely that many remain unidentified. Moreover, previous studies examined changes in a fibroblast cell line,[14] whereas changes in distal renal tubular cells, which have direct contact with CaOx crystals, remain largely unknown. During the postgenomic era, proteomics offers many opportunities to explore the pathogenic mechanisms of several diseases. The aim of our present study therefore was to investigate responses

* To whom correspondence should be addressed. Visith Thongboonkerd, MD, FRCPT, Medical Proteomics Unit, 12th Floor Adulyadej Vikrom Building, 2 Prannok Road, Siriraj Hospital, Bangkoknoi, Bangkok 10700, Thailand. Phone/Fax: +66-2-4184973. E-mail: thongboonkerd@dr.com or vthongbo@yahoo.com.

† Medical Proteomics Unit and Medical Molecular Biology Unit, Mahidol University.

‡ Department of Immunology and Immunology Graduate Program, Mahidol University.

§ Academia Sinica.

|| National Taiwan University.

10.1021/pr800113k CCC: $40.75 



Published on Web 05/07/2008

(as determined by alterations in protein expression) in a distal renal tubular cell line during calcium oxalate dihydrate (COD) crystal adhesion. Madin-Darby canine kidney (MDCK) cells, which were derived from dog kidney and exhibited distal renal tubule phenotype,[15] were used in this study. A gel-based differential proteomics approach was employed to identify a set of proteins in MDCK cells that were altered during COD crystal adhesion. These altered proteins were then identified by quadrupole time-of-flight (Q-TOF) mass spectrometry (MS) and/or tandem MS (MS/MS) analyses. These data provide useful information for understanding the cellular responses in renal tubular epithelial cells in distal nephron during crystal adhesion and stone formation.

## Materials and Methods

**Preparation of COD Crystals.** COD crystals were prepared in an artificial urine as previously described.[16,17] Briefly, 125 mL of 25.08 mM $CaCl_2 \cdot 2H_2O$ was added into 250 mL of a buffer containing 19.26 mM trisodium citrate dihydrate ($C_6H_5Na_3O_7 \cdot 2H_2O$), 23.1 mM magnesium sulfate heptahydrate ($MgSO_4 \cdot 7H_2O$), and 127.4 mM potassium chloride (KCl). The pH of the solution was adjusted to 6.5 using HCl. The solution was then incubated at 25 °C for 15 min. Thereafter, 125 mL of 6.4 mM sodium oxalate ($Na_2C_2O_4$) was added under a continuous stirring. The solution was incubated further at 25 °C for 15 min. COD crystals were then harvested by centrifugation at 2000 × *g* for 5 min. Supernatant was discarded and the crystals were resuspended in methanol. After another centrifugation at 2000 × *g* for 5 min, methanol was discarded and the crystals were air-dried. The presence and purity of COD crystals were confirmed by phase-contrast and scanning electron microscopy (SEM). After crystal generation and harvesting, COD crystals were decontaminated with UV irradiation for 30 min. They were then added to a complete Eagle's minimum essential medium (MEM) (GIBCO, Invitrogen Corporation; Grand Island, NY) to achieve the final concentration of 100 $\mu$g of crystals/mL of medium.

**Cell Culture and COD Crystal Adhesion.** Approximately 3 × $10^6$ MDCK cells were inoculated in each 75 $cm^2$ tissue culture flask containing MEM supplemented with 10% fetal bovine serum (FBS), 1.2% penicillinG/ streptomycin, and 2 mM glutamine. The cultured cells were maintained in a humidified incubator at 37 °C with 5% $CO_2$ for 24 h. A total of 10 semiconfluent flasks were then divided into two groups ($n = 5$ per group), and the culture medium was replaced by either COD-containing (with 100 $\mu$g/mL COD crystals) or COD-free medium. For the COD-free medium, COD crystals with an equal amount of 100 $\mu$g/mL were added into the medium for 30 min but were finally removed from the medium (as to make the identical concentrations of free calcium and oxalate ions in the medium compared to those of COD-containing medium). The cells were grown for a further 48 h, and cell death was quantified by flow cytometry using annexin V/propidium iodide double staining. The adhesion of crystals to cell monolayer was also confirmed by phase-contrast microscopy and SEM.

**Cell Death Assay.** Apoptosis was detected by the determination of surface phosphatidylserine, which was translocated from the inner side of plasma membranes to outer layer of the cell during apoptotic cell death. After trypsinization, FITC-labeled annexin V, a calcium-dependent phospholipid-binding protein with a high affinity for phosphatidylserine, was added to discriminate healthy from apoptotic cells. Propidium iodide, a DNA stain, was added to simultaneously detect necrotic cells. MDCK cells from the monolayer were detached with 3 mL of 0.1% trypsin in 2.5 mM EDTA and resuspended in 10 mL MEM. The harvested cells were centrifuged at 500 × *g*, 4 °C for 5 min and washed with PBS. Cell pellets were resuspended with annexin V buffer (10 mM HEPES, 140 mM NaCl and 2.5 mM $CaCl_2.2H_2O$; pH 7.4) at a final concentration of 5 × $10^5$ cells/mL and then incubated with FITC-labeled annexin V (BD Biosciences; San Jose, CA) on ice for 15 min in the dark. Propidium iodide (BD Biosciences) (1 $\mu$L of 1 $\mu$g/$\mu$L) was added into the samples prior to analysis. The cells were then analyzed by flow cytometry (FACScan, Becton Dickinson Immunocytometry System; San Jose, CA), and a monolayer of MDCK cells treated with 2 $\mu$g/mL camptothecin was used as a positive control. This experiment was performed in triplicate. Percentage of cell death (% cell death) = [(number of both apoptotic and necrotic cells/number of all cells) × 100%].

**Confirmation of COD Crystal Adhesion by Phase-Contrast Microscopy and SEM.** COD crystal adhesion was confirmed by phase-contrast microscopy on an inverted light microscope (Olympus CKX41, Olympus Co. Ltd.; Tokyo, Japan) after three washes (with PBS) of the MDCK cells incubated with COD crystals (100 $\mu$g/mL) in 75 $cm^2$ tissue culture flasks, as mentioned above. For the evaluation by SEM, the cell culture and COD crystal adhesion were performed similar to that mentioned above but on coverslips, instead of culture flasks (with approximately 1 × $10^6$ cells per slide at an initial inoculation). After incubation with COD crystals (100 $\mu$g/mL), the coverslips were rinsed with normal saline solution (NSS) three times and fixed with 2% glutaraldehyde in NSS at room temperature for 2 h. The coverslips were then rinsed again with NSS three times and dehydrated by a graded ethanol series of 50, 70, 95, and 100% before being air-dried overnight. The coverslips were finally mounted on aluminum stubs and coated with gold particles. The crystal morphology and adhesion were then examined under a scanning electron microscope (JSM-25S, Jeol; Kyoto, Japan).

**Protein Extraction.** After incubation with or without COD crystals, the monolayer of MDCK cells was harvested by directly scraping into the tube containing 0.5 M EDTA in PBS to dissolve the adherent CaOx crystals. After incubation at 4 °C for 30 min, EDTA was removed by washing with PBS three times. Cell pellets were resuspended in a buffer containing 7 M urea, 2 M thiourea, 4% 3-[(3-cholamidopropyl) dimethyl-ammonio]-1-propanesulfonate (CHAPS), 120 mM dithiothreitol (DTT), 2% ampholytes (pH 3–10), and 40 mM Tris-HCl and further incubated at 4 °C for 30 min. Unsolubilized debris and particulate matter were removed by centrifugation at 9100 × *g* for 2 min. Protein concentrations were determined using the Bradford method.

**2-DE and Staining.** Samples (each of 200 $\mu$g total protein) derived from individual culture flasks ($n = 5$ for each group) were premixed with a rehydration buffer containing 7 M urea, 2 M thiourea, 2% CHAPS, 120 mM DTT, 40 mM Tris-base, 2% ampholytes (pH 3–10), and a trace of bromophenol blue to a final volume of 150 $\mu$L per sample. The mixtures were rehydrated onto Immobiline DryStrip (nonlinear pH gradient of 3–10, 7 cm long; GE Healthcare, Uppsala, Sweden) at room temperature for 10–15 h. The first dimensional separation or isoelectric focusing (IEF) was performed in Ettan IPGphor II IEF System (GE Healthcare) at 20 °C, using a stepwise mode to reach 9000 Vh. After completion of the IEF, the strips were first equilibrated for 15 min in an equilibration buffer containing 6 M urea, 130 mM DTT, 112 mM Tris-base, 4% SDS, 30% glycerol, and 0.002% bromophenol blue and then in another

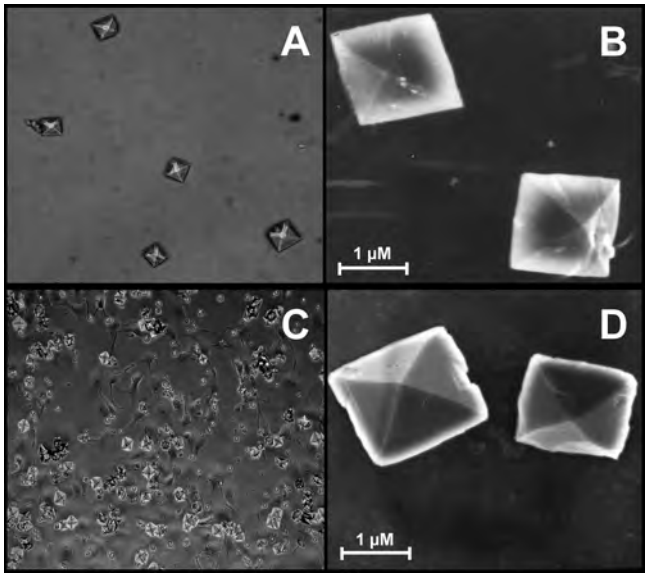


**Figure 1.** Typical tetragonal bipyramidal shape of COD crystals is shown in (A) and (B), whereas (C) and (D) illustrate interaction between MDCK cells and COD crystals (the disrupted or uneven borders of COD crystals were observed on the background of the MDCK monolayer). Images were taken by phase-contrast microscopy (A and C) and SEM (B and D). Original magnification powers were 100× in C, 400× in A, and 2000× in B and D.

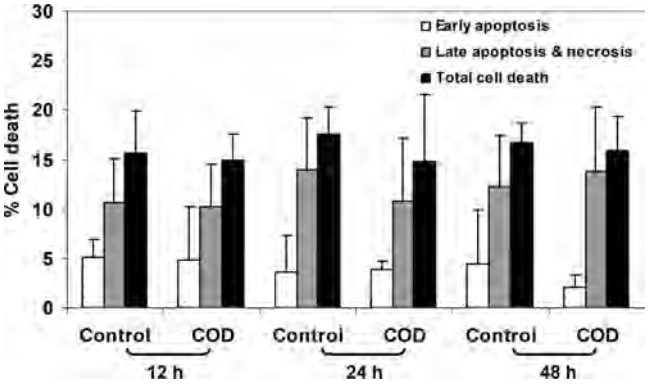


**Figure 2.** Time-course evaluation of cell death. The quantitation of cell death by flow cytometry using annexin V/propidium iodide double staining showed that there was no significant difference of % cell death in MDCK cells incubated with versus without COD crystals ($p$ values > 0.05 for the comparisons between the control and COD-interacting cells). The data are reported as mean (+SD) and each bar represents the results obtained from 3 independent experiments.

similar buffer, where DTT was replaced with 135 mM iodoacetamide, for a further 15 min. The second dimensional separation was performed in 12% polyacrylamide gel using SE260 mini-Vertical Electrophoresis Unit (GE Healthcare) at 150 V for approximately 2 h. Separated proteins were visualized with SYPRO Ruby fluorescence staining (Invitrogen - Molecular Probes; Eugene, OR). Gels were scanned using a Typhoon laser scanner (GE Healthcare).

**Matching and Analysis of Protein Spots.** Image Master 2D Platinum (GE Healthcare) software was used for matching and analysis of protein spots in 2-D gels. Parameters used for spot detection were (i) minimal area = 10 pixels; (ii) smooth factor = 2.0; and (iii) saliency = 2.0. A reference gel was created as a collection of all gel images. The reference gel was then used for matching the corresponding protein spots between gels. Background subtraction was performed and the intensity volume of each spot was normalized with total intensity volume (summation of the intensity volumes obtained from all spots within the same 2-D gel).

**Statistical Analysis.** Comparisons between the two sets of the samples (i.e., control vs COD-interacting cells) of % cell death and intensity levels of corresponding protein spots were performed using Mann–Whitney U test (SPSS software version 11.0). $P$ values less than 0.05 were considered statistically significant. Differentially expressed protein spots were subjected to in-gel tryptic digestion and identification by mass spectrometry.

**In-Gel Tryptic Digestion.** The protein spots whose intensity levels significantly differed between groups were excised from 2-D gels, washed twice with 200 $\mu$L of 50% acetonitrile (ACN)/25 mM $NH_4HCO_3$ buffer (pH 8.0) at room temperature for 15 min, and then washed once with 200 $\mu$L of 100% ACN. After washing, the solvent was removed, and the gel pieces were dried by a SpeedVac concentrator (Savant; Holbrook, NY) and rehydrated with 10 $\mu$L of 1% (w/v) trypsin (Promega; Madison, WI) in 25 mM $NH_4HCO_3$. After rehydration, the gel pieces were crushed and incubated at 37 °C for at least 16 h. Peptides were subsequently extracted twice with 50 $\mu$L of 50% ACN/5% trifluoroacetic acid (TFA); the extracted solutions were then combined and dried with the SpeedVac concentrator. The peptide pellets were resuspended with 10 $\mu$L of 0.1% TFA and purified using $ZipTip_{C18}$ (Millipore; Bedford, MA). The peptide solution was drawn up and down in the $ZipTip_{C18}$ 10 times and then washed with 10 $\mu$L of 0.1% formic acid by drawing up and expelling the washing solution three times. The peptides were finally eluted with 5 $\mu$L of 75% ACN/0.1% formic acid.

**Protein Identification by Q-TOF MS and MS/MS Analyses.** The proteolytic samples were premixed 1:1 with the matrix solution (5 mg/mL α-cyano-4-hydroxycinnamic acid (CHCA) in 50% ACN, 0.1% v/v TFA and 2% w/v ammonium citrate) and spotted onto the 96-well sample stage. The samples were analyzed by the Q-TOF Ultima™ mass spectrometer (Micromass; Manchester, UK), which was fully automated with predefined probe motion pattern and the peak intensity threshold for switching over from MS survey scanning to MS/MS, and from one MS/MS to another. Within each sample well, parent ions that met the predefined criteria (any peak within the $m/z$ 800–3000 range with intensity above 10 count ± include/exclude list) were selected for CID MS/MS using argon as the collision gas and a mass dependent ± 5 V rolling collision energy until the end of the probe pattern was reached. The LM and HM resolution of the quadrupole were both set at 10 to give a precursor selection window of about 4-Da wide.

The instrument was externally calibrated to <5 ppm accuracy over the mass range of $m/z$ 800−3000 using a sodium iodide and PEG 200, 600, 1000, and 2000 mixtures and further adjusted with Glu-Fibrinopeptide B as the near-point lock mass calibrant during data processing. At a laser firing rate of 10 Hz, individual spectra from 5-s integration periods acquired for each of the MS survey and MS/MS performed were combined, smoothed, deisotoped (fast option) and centroided using the ProteinLynx GlobalSERVER 2.0 data processing software (Micromass). This entailed the identification of the monoisotopic, carbon-12 peaks for MS data, and deconvolution of multiply charged spectra to their singly charged equivalents for MS/MS data. MaxEnt 3, a maximum-entropy-based technique, has been designed for this purpose and is an integral part of ProteinLynx GlobalSERVER 2.0.

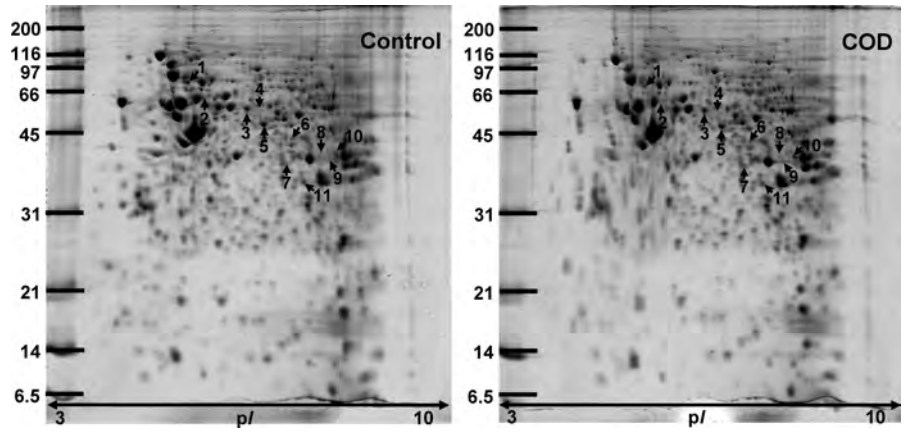


**Figure 3.** Representative 2-DE gel images of proteins derived from the control and COD-interacting MDCK cells. Proteins were resolved with 2-DE using a pH gradient of 3–10 (nonlinear) for the IEF and 12% polyacrylamide SDS-PAGE for the second dimensional separation. The resolved protein spots were then visualized with SYPRO Ruby stain. Each gel contained 200 $\mu$g total protein extracted from each culture flask ($n = 5$ for each group; total $n = 10$ gels were used for quantitative intensity analysis). The spots labeled with numbers are those whose intensity levels significantly differed between the two groups. These differentially expressed proteins were subsequently identified by Q-TOF MS and/or MS/MS analyses (see Table 1).

The combined MS and MS/MS ion meta data were searched in concert against the NCBI mammalian protein database using the ProteinLynx GlobalSERVER 2.0 workflow. Additionally, the MS and MS/MS data were extracted and outputted as the searchable *.txt* and *.pkl* files, respectively, for independent searches using the MASCOT search engine (http://www.matrixscience.com), assuming that peptides were monoisotopic, oxidized at methionine residues, and carbamidomethylated at cysteine residues. Only 1 missed trypsin cleavage was allowed, and peptide mass tolerances of 100 and 50 ppm were used for peptide mass fingerprinting (PMF) and MS/MS ions search, respectively.

**Immunoblotting.** To confirm the results of MS and/or MS/MS protein identification, 2-D Western blot analysis was performed. Proteins derived from MDCK cells (100 $\mu$g total protein for each sample; extraction was performed as for 2-DE analysis) were resolved by 2-DE and transferred onto nitrocellulose membranes (Whatman, Dassel, Germany) using a semi-dry transfer apparatus (Biorad, Milano, Italy) at 75 mA for 1 h. Nonspecific binding was blocked with 5% milk in PBS at room temperature for 1 h. The membranes were then incubated with goat polyclonal anti-Anx II antibody (Santa Cruz Biotechnology, Inc., Santa Cruz, CA) (1: 500 in 5% milk/PBS) at 4 °C overnight. After washing, the membranes were further incubated with rabbit antigoat IgG conjugated with horseradish peroxidase (Dako; FortCollins, CO) (1:1000 in 5% milk/PBS) at room temperature for 1 h. Immunoreactive protein spots were then visualized with SuperSignal West Pico chemiluminescence substrate (Pierce Biotechnology, Inc., Rockford, IL).

## Results and Discussion

The COD crystals were successfully produced with a typical morphology. Figure 1A and B shows phase-contrast and SEM images, respectively, of these COD crystals that were present uniformly as tetragonal bipyramidal shape (with symmetry counterparts). After an incubation of the COD crystals with MDCK cells for 48 h, these crystals remained on MDCK cell surfaces even with several washes using PBS. Figure 1C shows phase-contrast microscopic image of the COD crystals that adhered tightly onto the surface of MDCK cells. We also demonstrated the cell−crystal interaction using SEM. Figure 1D shows SEM image of the remaining COD crystals that adhered onto MDCK cell surfaces. Whereas the untreated COD crystals had sharp borders (Figure 1B), the MDCK-interacting crystals showed disrupted or uneven borders (Figure 1D), indicating cell−crystal interaction.

MDCK cell line has been recognized as one of the most suitable cell lines for the investigation of CaOx crystal adhesion and cell−crystal interaction.[11,18–21] To investigate the responses of MDCK cells during COD crystal adhesion, we demonstrated that effects of cell death, as a result of chemical toxicity, could be excluded. We performed a time-course study of cell death, comparing the MDCK cells incubated with COD crystals to those without crystals (control), using annexin V/propidium iodide double staining and flow cytometry. Figure 2 demonstrates that the percentage of cell death was comparable between the two groups at 12, 24, and 48 h incubation period ($p$ values $> 0.05$; $n = 3$ independent experiments for each condition). We did not extend the incubation period to longer than 48 h as the cells were completely confluent at the 48 h time-point and became overcrowded at later time-points. By light and phase-contrast microscopic examination, the morphological hallmarks of apoptotic and/or necrotic cell death (including condensed nuclei, rounding shape, large vacuoles in cytoplasm and floatation of cells) were not observed in any flasks of the cells incubated with COD crystals. Additionally, the COD-free medium was also incubated with an equal amount (100 $\mu$g/mL) of COD crystals (but these crystals were finally removed prior to the incubation with the control MDCK cells) to ensure that free calcium and oxalate ions that might be dissolved from the crystals would be the same between the experimental and control groups. These data convinced that alterations in protein expression were resulted solely from cell−crystal interaction, not from chemical-induced cytotoxicity.

2-DE-based differential proteomics study was performed to compare the cellular proteome of MDCK cells incubated with COD crystals with that of the control cells cultured without crystals. Cellular proteins derived from MDCK cells in each culture flask were resolved in each 2-DE gel ($n = 5$ gels derived from 5 individual flasks per group). Figure 3 shows representative 2-DE gel images of the cellular proteome of control and COD-interacting cells. Spot analysis using Image Master 2D

Platinum software revealed approximately 1000–1200 protein spots in each gel. Statistical analysis revealed 11 protein spots whose abundance levels were significantly altered during COD crystal adhesion (Figure 3 and Table 1). These altered proteins (6 were increased, whereas the other 5 were decreased) were then excised and subjected to in-gel tryptic digestion and identification by Q-TOF MS and/or MS/MS analyses.

Of these 11 altered protein spots, 10 proteins were successfully identified by Q-TOF MS and/or MS/MS analyses, whereas one altered protein remained unidentified (spot #7; Figure 3). This probably is due to the low-abundance level of this unidentified protein as it was observed as a very small and faint spot. Identities and other important information of all identified proteins are summarized in Table 1. These proteins included metabolic enzymes, cellular structural protein, calcium-binding protein, adhesion molecule, protein involved in RNA metabolism, and chaperone. Functional roles and predicted subcellular localizations of these 10 altered proteins identified by Q-TOF MS and/or MS/MS analyses are summarized in Table 2. Furthermore, 2-D Western blot analysis confirmed the markedly (4.59-fold) increased level of Anx II (spot #9) in COD-interacting MDCK cells (Figure 4).

We have successfully evaluated cellular responses of distal renal tubular cells during COD crystal adhesion, using a proteomics approach. We showed that an incubation of MDCK cells with 100 $\mu$g/mL COD crystals for 48 h did not significantly increase the percentage of cell death (Figure 2). Thus, the experimental conditions used herein were suitable for examining cellular responses to COD crystal adhesion. A gel-based differential proteomics revealed alterations in abundance levels of 11 proteins, 10 of which were successfully identified by MS and/or MS/MS analyses (Figure 3 and Table 1). The functional significance and potential roles of some of these altered proteins are highlighted as follows.

Anx II is a 36 kDa calcium-dependent phospholipids-binding protein that can be present in monomeric and heterotetrameric forms.[22] Anx II is involved in several cellular processes, that is, cell adhesion, endocytosis, exocytosis, cell motility, Actin assembly, cell-matrix interactions, and fibrinolysis.[22] In the present study, we observed a marked increase in abundance of Anx II in the COD-interacting MDCK cells. The data obtained from 2-D immunoblot analysis confirmed the proteomic data (Figure 4). Recently, Anx II has been identified as a CaOx crystal-binding molecule on the surface of MDCK cells.[8] These findings may imply that the increased level of Anx II may mediate the adhesion of COD crystals onto the surface of MDCK cells.

hnRNP H1 is a member of heterogeneous nuclear ribonucleoproteins (hnRNPs) family, which contains RNA recognition motifs and supplementary domains with atypical amino acid distributions.[23] The former motifs bind to pre-mRNA, whereas the latter domains contribute to various functions, including annealing and splicing of RNA.[24] More than 20 proteins have been identified as the members in the hnRNPs family and are designated with letters from A to U.[25] Among these, hnRNP H1 plays an essential role in manipulating gene expression. Previous studies have shown that hnRNP H1 participates in alternative splicing of genes encoding $\beta$-tropomyosin and thyroid hormone receptor.[26,27] Alterations in hnRNP H1 expression levels are associated with various cell differentiation processes. Additionally, hnRNP H1 acts as a gene regulatory protein and represses the expression of certain genes in mesenchymal cells. Throughout the differentiation process of

**Table 1.** Summary of Differentially Expressed Proteins, Whose Abundance Levels Were Significantly Altered during COD Crystal Adhesion[a]

| spot no. | protein | NCBI[b] ID | identified by | matching scores (MS, MS/MS | %cov[c] (MS, MS/MS) | no. of matched Peptides (MS, MS/MS) | p*I* | MW (kDa) | intensity levels (arbitrary unit) control (mean ± SEM) | intensity levels (arbitrary unit) COD (mean ± SEM) | ratio (COD/ control) | *P* values |
|---|---|---|---|---|---|---|---|---|---|---|---|---|
| 1 | Lamin B | gi\|293689 | MS, MS/MS | 71, 44 | 18, 5 | 14, 2 | 5.14 | 66.95 | 0.1423 ± 0.0094 | 0.0913 ± 0.0114 | 0.64 (↓) | 0.016 |
| 2 | Chaperonin isoform 4 | gi\|114582392 | MS, MS/MS | 92, 244 | 34, 15 | 10, 4 | 8.13 | 50.73 | 0.0361 ± 0.0039 | 0.0200 ± 0.0036 | 0.55 (↓) | 0.032 |
| 3 | Heterogeneous nuclear ribonucleoprotein H1 (hnRNP H1) | gi\|5031753 | MS, MS/MS | 97, 280 | 39, 14 | 11, 4 | 5.89 | 49.48 | 0.0466 ± 0.0036 | 0.0833 ± 0.0142 | 1.79 (↑) | 0.032 |
| 4 | Cytokeratin 7 (CK 7) | gi\|73996579 | MS | 70 | 29 | 11 | 6.21 | 51.65 | 0.0212 ± 0.0025 | 0.0131 ± 0.0014 | 0.62 (↓) | 0.032 |
| 5 | Ornithine aminotransferase (OAT), mitochondrial precursor isoform 1 | gi\|73998800 | MS, MS/MS | 195, 315 | 51, 16 | 16, 5 | 6.44 | 48.75 | 0.2715 ± 0.0291 | 0.3817 ± 0.0211 | 1.41 (↑) | 0.032 |
| 6 | Branched-chain-amino-acid aminotransferase (Placental protein 18) (PP18) | gi\|73948032 | MS | 114 | 35 | 11 | 7.14 | 44.93 | 0.0483 ± 0.0097 | 0.0949 ± 0.0160 | 1.97 (↑) | 0.032 |
| 7 | Unidentified | – | – | – | – | – | – | – | 0.0421 ± 0.0174 | 0.0987 ± 0.0125 | 2.34 (↑) | 0.032 |
| 8 | Alcohol dehydrogenase (ADH) | gi\|73977957 | MS, MS/MS | 70, 59 | 29, 7 | 11, 2 | 7.12 | 36.90 | 0.0352 ± 0.0010 | 0.0544 ± 0.0052 | 1.55 (↑) | 0.008 |
| 9 | Annexin A2 (Anx II) | gi\|50950177 | MS, MS/MS | 159, 55 | 48, 4 | 15, 1 | 6.92 | 38.92 | 0.0146 ± 0.0064 | 0.0670 ± 0.0143 | 4.59 (↑) | 0.008 |
| 10 | Glyceraldehyde-3-phosphate dehydrogenase (G3PDH) | gi\|50978862 | MS, MS/MS | 87, 162 | 19, 12 | 10, 4 | 8.20 | 36.07 | 0.1969 ± 0.0176 | 0.1244 ± 0.0240 | 0.63 (↓) | 0.032 |
| 11 | Galactose-specific lectin | gi\|114653156 | MS/MS | 83 | 7 | 2 | 8.26 | 37.99 | 0.2723 ± 0.0161 | 0.2022 ± 0.0200 | 0.74 (↓) | 0.032 |

[a] These altered proteins were then identified by Q-TOF MS and/or MS/MS analyses. [b] NCBI = National Center for Biotechnology Information. [c] %cov = %sequence coverage [(number of the matched residues/total number of residues in the entire sequence) × 100%].

**Table 2.** Functional Roles and Subcellular Localizations of the Altered Proteins Identified from the COD-Interacting MDCK Cells

| altered proteins | subcellular localization | function |
|---|---|---|
| proteins whose abundance levels were significantly increased during COD crystal adhesion | | |
| hnRNP H1 | nucleus | RNA metabolism |
| OAT, mitochondrial precursor isoform 1 | mitochondria | metabolic enzyme |
| PP 18 | mitochondria | metabolic enzyme |
| ADH | mitochondria | metabolic enzyme |
| Anx II | cytosol (monomeric)/nucleus (heteromeric) | calcium-binding protein |
| proteins whose abundance levels were significantly decreased during COD crystal adhesion | | |
| Lamin B | intermediate filament | cellular structure |
| Chaperonin isoform 4 | mitochondria | chaperone |
| CK 7 | intermediate filament | cellular structure |
| G3PDH | cytoplasm | metabolic enzyme |
| Galactose-specific lectin | cell membrane | adherence molecule |

smooth muscle cells, the decreased expression level of hnRNP H1 leads to the increased expression of smooth muscle cell proteins, that is, α-Actin, desmin, and myosin.[28] Our present study found that the level of hnRNP H1 protein was significantly increased in the COD-interacting cells. This finding might implicate the central function of hnRNP H1 in regulation of expression of genes and their products during COD crystal adhesion. However, the precise role of hnRNP H1 in kidney stone formation remains unknown and deserves further investigation.

The 48 kDa OAT is well characterized as a mitochondrial matrix enzyme that is normally present in liver and kidney tissues.[29] The OAT enzymatic activity reversibly converts L-ornithine to α-ketoglutarate, producing glutamic-γ-semialdehyde and glutamate. OAT plays an essential role in driving L-ornithine to the oxidative pathway for energy production via the TCA cycle.[30] L-ornithine is a pivotal molecule in several metabolic pathways in L-proline, L-glutamate, L-glutamine, L-citrulline, and L-arginine biosynthesis. Our present study identified a significant increase in OAT protein in response to COD crystal adhesion. We hypothesize that the increase in this mitochondrial protein is involved in altered metabolism as a response to COD crystal adhesion. Nevertheless, the precise role of increased OAT in the COD-interacting cells needs to be elucidated.

Lectins are sugar-binding proteins that bind to sugar molecules, which are highly specific for their sugar moieties.[31] These proteins are present on cell surfaces of mammalian cells and can mediate cell-cell interactions by combining with complementary carbohydrates on apposing cells.[31] In addition to cell-cell interactions, they also play role in other several cellular functions including glycoprotein synthesis. One type of lectins specifically recognizes galactose residues on cell surface and functions to remove particular type of glycoproteins from the circulation. Unlike Anx II, which is a crystal-binding protein that had increased level during COD crystal adhesion, we found that a galactose-specific lectin (Gal-specific lectin) was significantly decreased in the COD-interacting cells. The mechanism of this decrease during COD crystal adhesion remains unknown. A recent study showed that lipopolysaccharide antigen can suppress the expression of Gal/GalNAc-specific lectin, which acts as an endocytosis receptor of macrophage.[32] The data suggested that the decrease in lectin level may drive a negative signal to balance the lipopolysaccharide-stimulated signals mediated by proinflammatory cytokines.[32] Based on this assumption, we propose that, perhaps, the engagement of COD crystal may elicit a negative signal that results to the decreased expression level of the Gal-specific lectin as well. Moreover, as lectins play important role in cell-cell interactions, we also hypothesize that COD crystals, while reducing the level of a lectin in renal tubular cells, may somehow disrupt interactions of the affected renal tubular cell to the adjacent cells. However, further functional study is required to unravel this mysterious pathogenic mechanism.

In summary, we identified 10 proteins that were significantly altered in MDCK cells during COD crystal adhesion. Although

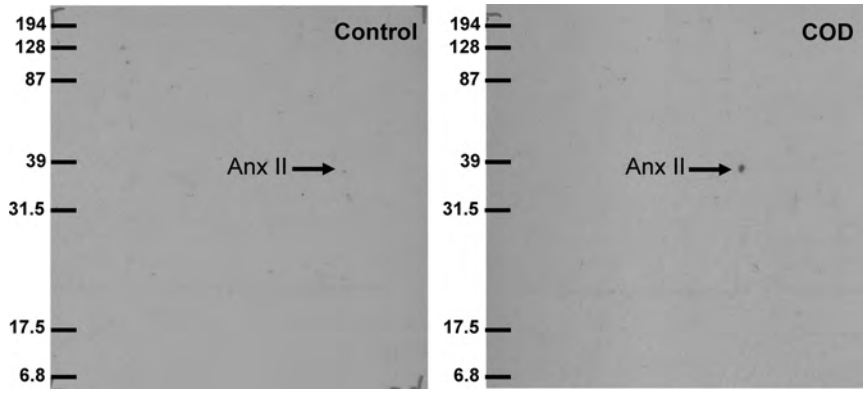


**Figure 4.** Validation of the proteomic data by 2-D Western blot analysis. Proteins derived from MDCK cells (100 μg total protein for each sample) were resolved by 2-DE and transferred onto nitrocellulose membranes. After blocking nonspecific binding, the membranes were incubated with goat polyclonal anti-Anx II antibody and then with rabbit antigoat IgG conjugated with horseradish peroxidase. Immunoreactive protein spots were then visualized with chemiluminescence substrate. The 2-D Western blot data confirmed that Anx II level was markedly increased in the COD-interacting cells.

these proteins are well-known to be involved in several cellular functions, their precise roles in kidney stone formation remain poorly understood. Further functional characterizations of these altered proteins in association with crystal adhesion are required and will definitely lead to better understanding of the cellular responses of distal renal tubular cells during COD crystal adhesion and of the pathogenic mechanisms of kidney stone formation. It should be noted that CaOx monohydrate (COM) is the most common crystalline composition found in kidney stones with a frequency of up to 78%,[33] whereas COD is the second most common found with a frequency of up to 43%.[33] Although previous studies have shown that COD can nucleate and adhere to renal tubular epithelial cells,[34–36] several lines of evidence have indicated that COM has more potent adhesive capability and can induce toxic effects to renal tubular epithelial cells.[37–40] It would be very interesting to evaluate also the altered proteome in distal renal tubular epithelial cells during COM crystal adhesion. These two sets of data obtained from experimental models of COD and COM crystal adhesion would thus be complementary to create a clearer image of the pathogenic mechanisms of kidney stone disease.

**Abbreviations:** 2-DE, two-dimensional gel electrophoresis; ACN, acetonitrile; ADH, alcohol dehydrogenase; Anx II, annexin 2; CaOx, calcium oxalate; CHAPS, 3-[(3-cholamidopropyl) dimethyl-amino]-1-propanesulfonate; CHCA, cyano-4-hydroxycinnamic acid; CK 7, cytokeratin 7; COD, calcium oxalate dihydrate; COM, calcium oxalate monohydrate; DTT, dithiothreitol; EDTA, ethylene diamine tetraacetic acid; FBS, fetal bovine serum; G3PDH, glyceraldehyde-3-phosphate dehydrogenase; hnRNP H1, heterogeneous nuclear ribonucleoprotein H1; IEF, isoelectric focusing; MDCK, Madin-Darby canine kidney; MCP-1, monocyte chemoattractant protein-1; MEM, Eagle's minimum essential medium; MS, mass spectrometry; MS/MS, tandem mass spectrometry; NRP, nucleolin-related protein; NSS, normal saline solution; OAT, ornithine aminotransferase; OPN, osteopontin; PP18, placental protein 18; Q-TOF, quadrupole time-of-flight; RNA, ribonucleic acid; ROS, reactive oxygen species; SEM, scanning electron microscopy; TFA, trifluoroacetic acid.

**Acknowledgment.** We thank Dr. Sontana Siritantikorn and Department of Microbiology at Faculty of Medicine Siriraj Hospital for kindly providing the MDCK cells. This study was supported by The Thailand Research Fund, Commission on Higher Education, Mahidol University, the National Research Council of Thailand, Siriraj Grant for Research and Development, and the National Center for Genetic Engineering and Biotechnology (to V.T.), and by Siriraj Graduate Thesis Scholarship (to T.S.).

## References

(1) Coe, F. L.; Evan, A.; Worcester, E. Kidney stone disease. *J. Clin. Invest.* **2005**, *115*, 2598–2608.
(2) Evan, A. P.; Coe, F. L.; Lingeman, J. E.; Worcester, E. Insights on the pathology of kidney stone formation. *Urol. Res.* **2005**, *33*, 383–389.
(3) Robertson, W. G. Kidney models of calcium oxalate stone formation. *Nephron Physiol.* **2004**, *98*, 21–30.
(4) Wesson, J. A.; Ward, M. D. Role of crystal surface adhesion in kidney stone disease. *Curr. Opin. Nephrol. Hypertens.* **2006**, *15*, 386–393.
(5) Khan, S. R. Calcium oxalate crystal interaction with renal tubular epithelium, mechanism of crystal adhesion and its impact on stone development. *Urol. Res.* **1995**, *23*, 71–79.
(6) Verhulst, A.; Asselman, M.; Persy, V. P.; Schepers, M. S.; Helbert, M. F.; Verkoelen, C. F.; De Broe, M. E. Crystal retention capacity of cells in the human nephron: involvement of CD44 and its ligands hyaluronic acid and osteopontin in the transition of a crystal binding- into a nonadherent epithelium. *J. Am. Soc. Nephrol.* **2003**, *14*, 107–115.
(7) Verkoelen, C. F.; van der Boom, B. G.; Romijn, J. C. Identification of hyaluronan as a crystal-binding molecule at the surface of migrating and proliferating MDCK cells. *Kidney Int.* **2000**, *58*, 1045–1054.
(8) Kumar, V.; Farell, G.; Deganello, S.; Lieske, J. C. Annexin II is present on renal epithelial cells and binds calcium oxalate monohydrate crystals. *J. Am. Soc. Nephrol.* **2003**, *14*, 289–297.
(9) Sorokina, E. A.; Wesson, J. A.; Kleinman, J. G. An acidic peptide sequence of nucleolin-related protein can mediate the attachment of calcium oxalate to renal tubule cells. *J. Am. Soc. Nephrol.* **2004**, *15*, 2057–2065.
(10) Kramer, G.; Steiner, G. E.; Prinz-Kashani, M.; Bursa, B.; Marberger, M. Cell-surface matrix proteins and sialic acids in cell−crystal adhesion; the effect of crystal binding on the viability of human CAKI-1 renal epithelial cells. *BJU Int.* **2003**, *91*, 554–559.
(11) Verkoelen, C. F.; van der Boom, B. G.; Kok, D. J.; Romijn, J. C. Sialic acid and crystal binding. *Kidney Int.* **2000**, *57*, 1072–1082.
(12) Huang, H. S.; Ma, M. C.; Chen, J.; Chen, C. F. Changes in the oxidant-antioxidant balance in the kidney of rats with nephrolithiasis induced by ethylene glycol. *J. Urol.* **2002**, *167*, 2584–2593.
(13) Hammes, M. S.; Lieske, J. C.; Pawar, S.; Spargo, B. H.; Toback, F. G. Calcium oxalate monohydrate crystals stimulate gene expression in renal epithelial cells. *Kidney Int.* **1995**, *48*, 501–509.
(14) Umekawa, T.; Iguchi, M.; Uemura, H.; Khan, S. R. Oxalate ions and calcium oxalate crystal-induced up-regulation of osteopontin and monocyte chemoattractant protein-1 in renal fibroblasts. *BJU Int.* **2006**, *98*, 656–660.
(15) Saier, M. H., Jr. Growth and differentiated properties of a kidney epithelial cell line (MDCK). *Am. J. Physiol.* **1981**, *240*, C106–C109.
(16) Thongboonkerd, V.; Semangoen, T.; Chutipongtanate, S. Factors determining types and morphologies of calcium oxalate crystals: Molar concentrations, buffering, pH, stirring and temperature. *Clin. Chim. Acta* **2006**, *367*, 120–131.
(17) Egan, T. J.; Rodgers, A. L.; Siele, T. Nucleation of calcium oxalate crystals on an imprinted polymer surface from pure aqueous solution and urine. *J. Biol. Inorg. Chem.* **2004**, *9*, 195–202.
(18) Lieske, J. C.; Swift, H.; Martin, T.; Patterson, B.; Toback, F. G. Renal epithelial cells rapidly bind and internalize calcium oxalate monohydrate crystals. *Proc. Natl. Acad. Sci. U.S.A.* **1994**, *91*, 6987–6991.
(19) Lieske, J. C.; Huang, E.; Toback, F. G. Regulation of renal epithelial cell affinity for calcium oxalate monohydrate crystals. *Am. J. Physiol. Renal Physiol.* **2000**, *278*, F130–F137.
(20) Verkoelen, C. F.; van der Boom, B. G.; Houtsmuller, A. B.; Schroder, F. H.; Romijn, J. C. Increased calcium oxalate monohydrate crystal binding to injured renal tubular epithelial cells in culture. *Am. J. Physiol.* **1998**, *274*, F958–F965.
(21) Khan, S. R.; Byer, K. J.; Thamilselvan, S.; Hackett, R. L.; McCormack, W. T.; Benson, N. A.; Vaughn, K. L.; Erdos, G. W. Crystal-cell interaction and apoptosis in oxalate-associated injury of renal epithelial cells. *J. Am. Soc. Nephrol.* **1999**, *10* (14), S457–S463.
(22) Gerke, V.; Moss, S. E. Annexins: from structure to function. *Physiol. Rev.* **2002**, *82*, 331–371.
(23) Krecic, A. M.; Swanson, M. S. hnRNP complexes: composition, structure, and function. *Curr. Opin. Cell Biol.* **1999**, *11*, 363–371.
(24) Biamonti, G.; Riva, S. New insights into the auxiliary domains of eukaryotic RNA binding proteins. *FEBS Lett.* **1994**, *340*, 1–8.
(25) Dreyfuss, G.; Matunis, M. J.; Pinol-Roma, S.; Burd, C. G. hnRNP proteins and the biogenesis of mRNA. *Annu. Rev. Biochem.* **1993**, *62*, 289–321.
(26) Chen, C. D.; Kobayashi, R.; Helfman, D. M. Binding of hnRNP H to an exonic splicing silencer is involved in the regulation of alternative splicing of the rat beta-tropomyosin gene. *Genes Dev.* **1999**, *13*, 593–606.
(27) Hastings, M. L.; Wilson, C. M.; Munroe, S. H. A purine-rich intronic element enhances alternative splicing of thyroid hormone receptor mRNA. *RNA* **2001**, *7*, 859–874.
(28) Liu, J.; Beqaj, S.; Yang, Y.; Honore, B.; Schuger, L. Heterogeneous nuclear ribonucleoprotein-H plays a suppressive role in visceral myogenesis. *Mech. Dev.* **2001**, *104*, 79–87.
(29) Dhanakoti, S. N.; Brosnan, M. E.; Herzberg, G. R.; Brosnan, J. T. Cellular and subcellular localization of enzymes of arginine metabolism in rat kidney. *Biochem. J.* **1992**, *282* (2), 369–375.
(30) Mezl, V. A.; Knox, W. E. Properties and analysis of a stable derivative of pyrroline-5-carboxylic acid for use in metabolic studies. *Anal. Biochem.* **1976**, *74*, 430–440.
(31) Sharon, N.; Lis, H. Lectins as cell recognition molecules. *Science* **1989**, *246*, 227–234.

(32) Ma, B. Y.; Kaihama, M.; Nonaka, M.; Oka, S.; Kawasaki, N.; Kawasaki, T. LPS suppresses expression of asialoglycoprotein-binding protein through TLR4 in thioglycolate-elicited peritoneal macrophages. *Glycoconj. J.* **2007**, *24*, 243–249.
(33) Schubert, G. Stone analysis. *Urol. Res.* **2006**, *34*, 146–150.
(34) Lieske, J. C.; Toback, F. G.; Deganello, S. Face-selective adhesion of calcium oxalate dihydrate crystals to renal epithelial cells. *Calcif. Tissue Int.* **1996**, *58*, 195–200.
(35) Lieske, J. C.; Toback, F. G.; Deganello, S. Direct nucleation of calcium oxalate dihydrate crystals onto the surface of living renal epithelial cells in culture. *Kidney Int.* **1998**, *54*, 796–803.
(36) Lieske, J. C.; Toback, F. G.; Deganello, S. Sialic acid-containing glycoproteins on renal cells determine nucleation of calcium oxalate dihydrate crystals. *Kidney Int.* **2001**, *60*, 1784–1791.
(37) Tomazic, B. B.; Nancollas, G. H. The dissolution of calcium oxalate kidney stones. A kinetic study. *J. Urol.* **1982**, *128*, 205–208.
(38) Guo, C.; McMartin, K. E. The cytotoxicity of oxalate, metabolite of ethylene glycol, is due to calcium oxalate monohydrate formation. *Toxicology* **2005**, *208*, 347–355.
(39) McMartin, K. E.; Wallace, K. B. Calcium oxalate monohydrate, a metabolite of ethylene glycol, is toxic for rat renal mitochondrial function. *Toxicol. Sci.* **2005**, *84*, 195–200.
(40) Khan, S. R. Crystal-induced inflammation of the kidneys: results from human studies, animal models, and tissue-culture studies. *Clin. Exp. Nephrol.* **2004**, *8*, 75–88.

PR800113K

research articles Journal of proteome research

# Proteomic Analysis of Calcium Oxalate Monohydrate Crystal-Induced Cytotoxicity in Distal Renal Tubular Cells

**Visith Thongboonkerd,*,† Theptida Semangoen,†,‡ Supachok Sinchaikul,§ and Shui-Tein Chen§,||**

*Medical Proteomics Unit & Medical Molecular Biology Unit, Office for Research and Development, Faculty of Medicine Siriraj Hospital, Mahidol University, Bangkok, Thailand, Department of Immunology and Immunology Graduate Program, Faculty of Medicine Siriraj Hospital, Mahidol University, Bangkok, Thailand, Institute of Biological Chemistry and Genomic Research Center, Academia Sinica, Taipei, Taiwan, and Institute of Biochemical Sciences, College of Life Science, National Taiwan University, Taipei, Taiwan*

**Received April 1, 2008**

Calcium oxalate monohydrate (COM) is the major crystalline component found in kidney stones and its adhesion to renal tubular cells provokes tubular injury, which in turn enhances COM crystal adhesion. However, COM-induced toxic effects in these tubular cells remain largely unknown. We performed a proteomics study to characterize changes in the cellular proteome in MDCK distal renal tubular cells after an exposure to high-dose (1000 $\mu$g/mL) COM crystals for 48 h, at which percentage of cell death was significantly increased. Proteins were extracted from MDCK cells cultured with COM-containing or COM-free medium ($n = 5$ individual flasks per group), resolved in individual 2-D gels, and stained with SYPRO Ruby fluorescence dye. Quantitative and statistical analyses revealed 53 proteins whose abundance levels were altered (25 were increased, whereas other 28 were decreased) by COM-induced toxicity. Among these, 50 were successfully identified by quadrupole time-of-flight (Q-TOF) mass spectrometry (MS) and/or tandem MS (MS/MS) analyses. The proteomic data were clearly confirmed by 2-D Western blot analysis. While three chaperones (GRP78, Orp150 and Hsp60) were increased, other proteins involved in protein biosynthesis, ATP synthesis, cell cycle regulator, cellular structure, and signal transduction were decreased. These data provide some novel mechanistic insights into the molecular mechanisms of COM crystal-induced tubular toxicity.

**Keywords:** Calcium oxalate • Cellular responses • Crystal adhesion • Kidney • Proteome • Proteomics • Stone • Tubular toxicity

## Introduction

Kidney stone disease (nephrolithiasis) remains a common health problem worldwide.[1,2] Among all types of kidney stones, calcium oxalate monohydrate (COM) is the major crystalline compound found in the stone mass (with a frequency of up to 77.5%).[3] In addition to crystallization, crystal growth and crystal aggregation, the other crucial mechanism for COM kidney stone formation is adhesion of COM crystals to renal tubular epithelial cells.[4,5] Adhesion of COM crystals can induce injury and apoptosis of renal tubular epithelial cells, and vice versa, COM-induced cellular injury can facilitate COM crystal adhesion.[6−9] This vicious cycle therefore accelerates kidney stone formation. Understanding alterations in renal tubular cells induced by COM crystals may lead to an identification of molecular targets for the prevention of kidney stone formation. However, changes in renal tubular epithelial cells during COM crystal-induced toxicity remain largely unknown. Several previous studies, which had dissected this vicious cycle, unfortunately focused mainly on redox or oxidative stress pathways,[9−11] particularly in mitochondria.[12,13] Clearer image of global changes in COM crystal-induced renal tubular toxicity is thus required.

During the postgenomic era, proteomics has become one of the most promising tools in nephrology and urology fields to unravel pathogenic mechanisms underlying renal and urological diseases.[14−16] The advantage of the proteomics approach is that both the previously determined and undetermined proteins that are involved in the disease mechanisms can be simultaneously examined. In the present study, we employed a classical proteomics approach to identify changes in the cellular proteome as a response to COM crystal-induced toxicity in MDCK distal renal tubular cells. The rationale of using MDCK cell line was that it exhibits several features of tubular cells in the distal nephron,[17] which has been thought to be the primary site of kidney stone formation. Moreover, MDCK cell line has been frequently used in several of previous

* To whom correspondence should be addressed. Visith Thongboonkerd, M.D., FRCPT, Medical Proteomics Unit, Office for Research and Development, 12th Floor Adulyadej Vikrom Building, 2 Prannok Road, Siriraj Hospital, Bangkoknoi, Bangkok 10700, Thailand. Phone/Fax: +66-2-4184973. E-mail: thongboonkerd@dr.com or vthongbo@yahoo.com

† Medical Proteomics Unit & Medical Molecular Biology Unit, Mahidol University.

‡ Department of Immunology and Immunology Graduate Program, Mahidol University.

§ Institute of Biological Chemistry and Genomic Research Center, Academia Sinica.

|| Institute of Biochemical Sciences, National Taiwan University.

10.1021/pr8002408 CCC: $40.75 



Published on Web 10/14/2008

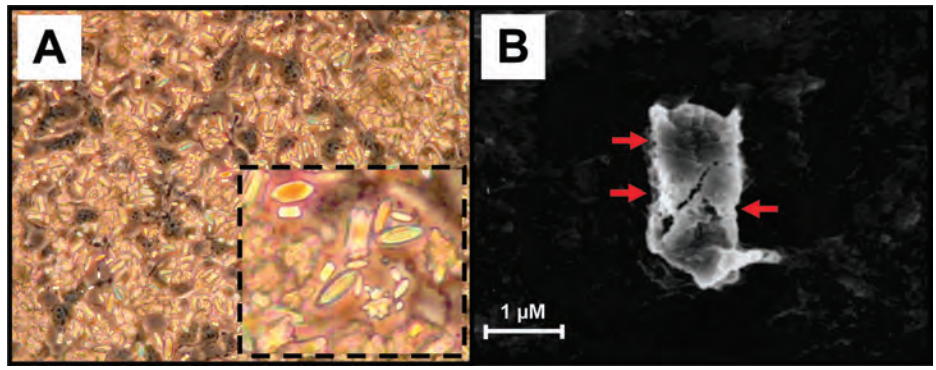


**Figure 1.** COM crystal adhesion and cell-crystal interactions. Images were taken using phase-contrast microscopy (A) and scanning electron microscopy (SEM) (B) after an incubation of COM crystals (1000 $\mu$g/mL) with MDCK cells for 48 h. An inset in (A) is a zoom-in phase-contrast microscopic image demonstrating the COM crystals adhered on the MDCK cell monolayer. SEM image in (B) shows blurred or interrupted borders (illustrated with arrows) of COM crystals (which indicate cell-crystal interactions) with the background of the monolayer of MDCK cells. Original magnification power was 100× in (A) and 2000× in (B).

studies on COM crystal-induced renal tubular cell injury.[18] A high-dose (1000 $\mu$g/mL) of COM crystals used in the present study caused significantly increased cell death at 48-h after the exposure to the crystals. Two-dimensional electrophoresis (2-DE) followed by quadrupole time-of-flight (Q-TOF) mass spectrometry (MS) and/or tandem MS (MS/MS) analyses revealed significant changes in abundance levels of several proteins in these COM-induced toxic MDCK cells compared to controls. The functional roles and subcellular localizations of these altered proteins indicated that these changes were related, at least in part, to COM crystal-induced tubular injury and ultimately to kidney stone formation.

## Materials and Methods

**Preparation of COM Crystals.** COM crystals were prepared as previously described.[19] Briefly, 10 mM calcium chloride dihydrate ($CaCl_2 \cdot 2H_2O$) was mixed with 10 mM sodium oxalate ($Na_2C_2O_4$) to make final concentrations of 5 mM and 0.5 mM, respectively, in Tris buffer containing 90 mM NaCl (pH 7.4). The mixture was incubated at 25 °C overnight and COM crystals were harvested by centrifugation at 3000 rpm for 5 min. Supernatant was discarded and the crystals were resuspended in methanol. After another centrifugation at 3000 rpm for 5 min, methanol was discarded and the crystals were dried at 37 °C overnight. COM crystals were then decontaminated by UV light radiation for 30 min. They were then added to a complete Eagle's minimum essential medium (MEM) (GIBCO, Invitrogen Corporation; Grand Island, NY) to achieve the final concentration of 1000 $\mu$g/mL. These *in vitro* COM crystals had similar size and shape as those of *in vivo* samples found in the urine of kidney stone patients.

**Cell Culture and COM Crystal Adhesion.** Approximately 3 × $10^6$ MDCK cells were inoculated in each 75 $cm^2$ tissue culture flask containing MEM supplemented with 10% fetal bovine serum (FBS), 1.2% penicillinG/streptomycin and 2 mM glutamine. The cultured cells were maintained in a humidified incubator at 37 °C with 5% $CO_2$ for 24 h. A total of 10 semiconfluent flasks were then divided into two groups ($n = 5$ per group) and the culture medium was replaced by either COM-containing (with 1000 $\mu$g/mL COM crystals) or COM-free medium. For the COM-free medium, COM crystals with an equal amount of 1000 $\mu$g/mL were added into the medium for 30 min, but were finally removed from the medium by centrifugation at 3000 rpm for 5 min.

**Imaging by Phase-Contrast Microscopy and Scanning Electron Microscopy (SEM).** Phase-contrast microscopy was simply performed on an inverted light microscope (Olympus CKX41, Olympus Co. Ltd.; Tokyo, Japan) after three washes (with PBS) of the MDCK cells incubated with COM crystals (1000 $\mu$g/mL) in 75 $cm^2$ tissue culture flasks, as mentioned above. For the evaluation by SEM, the cell culture and COM crystal adhesion were performed exactly the same as aforementioned, but on coverslips, instead of culture flasks (with approximately 1 × $10^6$ cells per slide at an initial inoculation). After incubation with COM crystals (1000 $\mu$g/mL), the coverslips were rinsed with normal saline solution (NSS) three times and fixed with 2% glutaraldehyde in NSS at room temperature for 2 h. The coverslips were then rinsed again with NSS three times and dehydrated by a graded ethanol series of 50%, 70%, 95% and 100% before being air-dried overnight. The coverslips were finally mounted on aluminum stubs and coated with gold particles. The crystal morphology and adhesion were then examined under a scanning electron microscope (JSM-25S, Jeol; Kyoto, Japan).

**Cell Death Assay.** Apoptosis was detected by the determination of surface phosphatidylserine, which was translocated from the inner side of plasma membranes to outer layer of the cell during apoptotic cell death. After trypsinization, FITC-labeled annexin V, a calcium-dependent phospholipid-binding protein with a high affinity for phosphatidylserine, was added to discriminate healthy from apoptotic cells. Additionally, propidium iodide, a DNA stain, was used simultaneously to detect necrotic cells. MDCK cells from the monolayer were detached with 0.1% trypsin in 2.5 mM EDTA and resuspended in 10 mL of MEM. The harvested cells were centrifuged at 1500 rpm, 4 °C for 5 min, and washed with PBS. Cell pellets were resuspended with annexin V buffer (10 mM HEPES, 140 mM NaCl and 2.5 mM $CaCl_2 \cdot 2H_2O$; pH 7.4) at a final concentration of 5 × $10^5$ cells/mL and then incubated with FITC-labeled annexin V (BD Biosciences; San Jose, CA) on ice for 15 min in the dark. Propidium iodide (BD Biosciences) was added into the samples at a final concentration of 10 $\mu$L/mL prior to analysis. The cells were then analyzed by flow cytometry (FACScan, Becton Dickinson Immunocytometry System; San

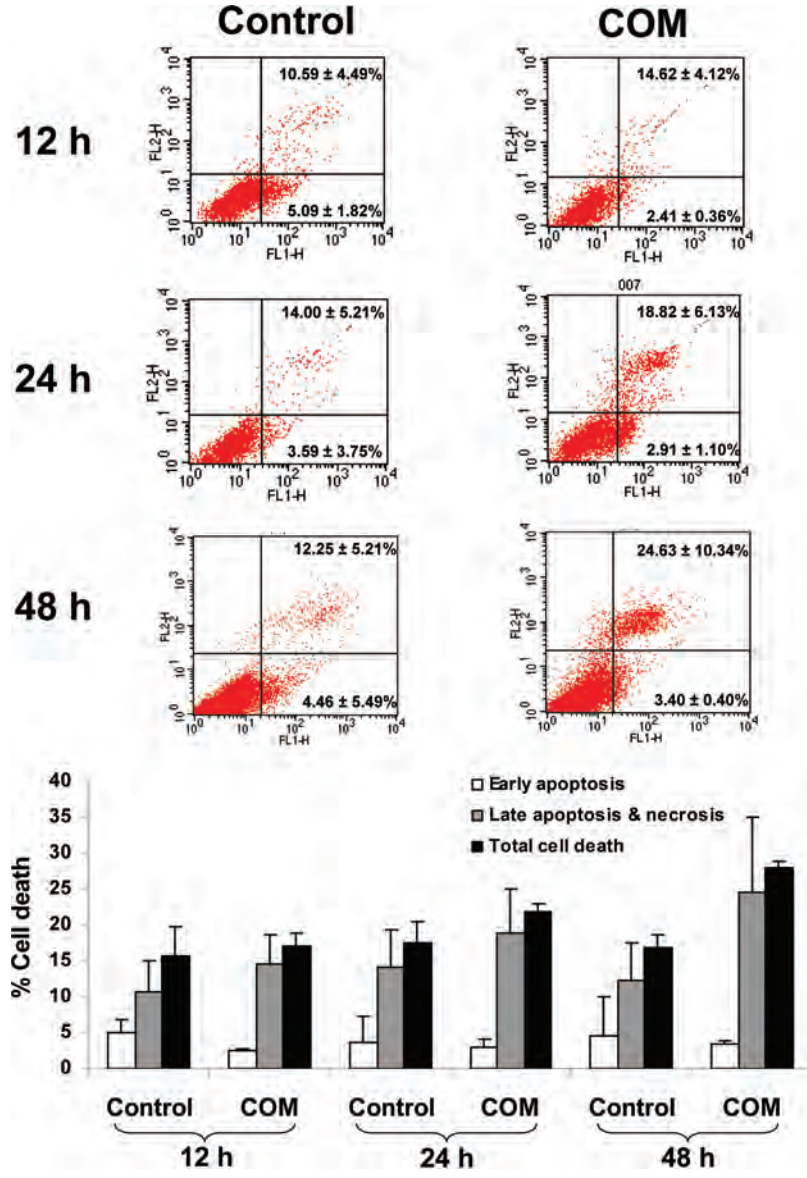


**Figure 2.** Flow cytometric data of cell death during exposure to COM crystals. MDCK cells were cultured without (control) or with COM crystals (1000 $\mu$g/mL). Apoptosis and necrosis of these cells were evaluated using annexin V (FL1-H)/propidium iodide (FL2-H) double staining. The percentage of cell death was determined by a summation of the number of cells in the right upper quadrant (late apoptotic cells and/or necrotic cells), left upper quadrant (necrotic cells), and right lower quadrant (early apoptotic cells) compared to total cell count in all four quadrants. Lower panel shows Mean (+SD) of cell death data obtained from 3 independent experiments.

Jose, CA) and a monolayer of MDCK cells treated with 2 $\mu$g/mL camptothecin was used as a positive control. This experiment was performed in triplicates. Percentage of cell death (% cell death) = [(number of both apoptotic and necrotic cells/number of all cells) × 100%].

**Protein Extraction.** After incubation with or without COM crystals, the monolayer of MDCK cells was harvested by directly scraping into the tube containing 0.5 M EDTA in PBS to dissolve the adherent CaOx crystals followed by an incubation at 4 °C for 30 min. EDTA was then removed by washing with PBS three times. After a centrifugation at 10 000 rpm for 2 min, the cell pellet was washed with PBS three times and was then resuspended in a buffer containing 7 M urea, 2 M thiourea, 4% 3-[(3-cholamidopropyl) dimethyl-ammonio]-1-propanesulfonate (CHAPS), 120 mM dithiothreitol (DTT), 2% ampholytes (pH 3−10) and 40 mM Tris-HCl, and further incubated at 4 °C for 30 min. Unsolubilized debris and particulate matters were removed by centrifugation at 10 000 rpm for 2 min. Protein concentrations were determined using the Bradford method.

**2-DE and Staining.** Protein solutions (each of 200 $\mu$g total protein) derived from individual culture flasks ($n = 5$ for each group) were premixed with a rehydration buffer containing 7 M urea, 2 M thiourea, 2% CHAPS, 120 mM DTT, 40 mM Tris-base, 2% ampholytes (pH 3−10) and a trace of bromophenol blue to make the final volume of 150 $\mu$L per sample. The mixtures were rehydrated onto Immobiline DryStrip (nonlinear pH gradient of 3−10, 7 cm long; GE Healthcare, Uppsala, Sweden) at room temperature for 10−15 h. The first-dimensional separation or isoelectric focusing (IEF) was performed in Ettan IPGphor II IEF System (GE Healthcare) at 20 °C, using a stepwise mode to reach 9000 Vh. After completion of the IEF, the strips were first equilibrated for 15 min in an equilibration buffer containing 6 M urea, 130 mM DTT, 112 mM Tris-base, 4% SDS, 30% glycerol and 0.002% bromophenol blue, and then

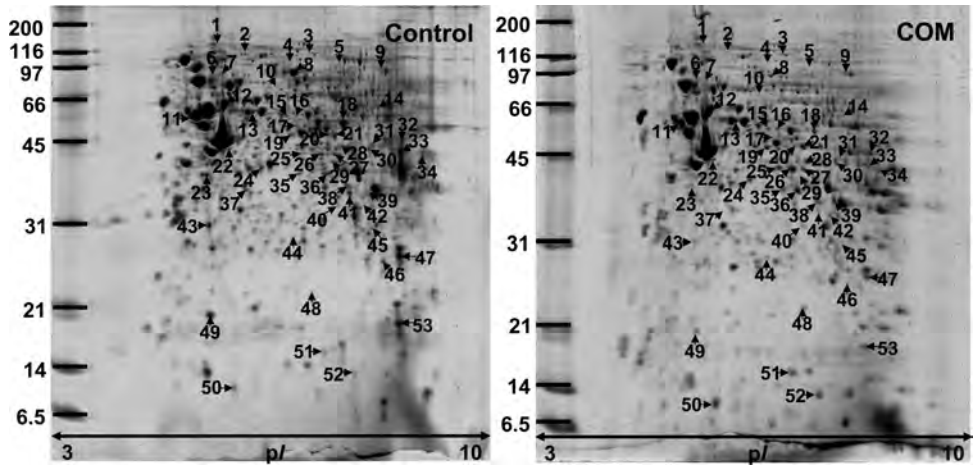


**Figure 3.** Representative 2-D gel images of proteins derived from the control and COM-exposed MDCK cells. Proteins were resolved with 2-DE using a pH gradient of 3−10 (nonlinear) for the IEF and 12% polyacrylamide SDS-PAGE for the second-dimensional separation. The resolved protein spots were then visualized with SYPRO Ruby stain. Each gel contained 200 $\mu$g of total protein extracted from each culture flask ($n = 5$ for each group; total $n = 10$ gels were used for quantitative intensity analysis). The spots labeled with numbers are those whose intensity levels significantly differed between the two groups. These differentially expressed proteins were subsequently identified by Q-TOF MS and/or MS/MS analyses (see Table 1).

in another similar buffer, which replaced DTT with 135 mM iodoacetamide, for further 15 min. The second-dimensional separation or SDS-PAGE was performed in 12% polyacrylamide gel using SE260 mini-Vertical Electrophoresis Unit (GE Healthcare) at 150 V for approximately 2 h. Separated proteins were visualized with SYPRO Ruby fluorescence staining (Invitrogen-Molecular Probes; Eugene, OR). Gel images were taken using a Typhoon laser scanner (GE Healthcare).

**Matching and Analysis of Protein Spots.** Image Master 2D Platinum (GE Healthcare) software was used for matching and analysis of protein spots in 2-D gels. Parameters used for spot detection were (i) minimal area = 10 pixels; (ii) smooth factor = 2.0; and (iii) saliency = 2.0. A reference gel was created from an artificial gel combining all of the (common and uncommon) spots presenting in different gels into one image. This reference gel was then used for matching the corresponding protein spots among all different gels within the same group ($n = 5$ gels per group) and between the two different groups (i.e., control vs COM-exposed cells). The spots were automatically aligned and matched using some selected landmarks, which were the well-defined spots that were present in all gels. However, each of the matched spots by this automatic option was then confirmed or edited manually. Background subtraction was performed and the intensity volume of each spot was normalized with total intensity volume (summation of the intensity volumes obtained from all spots within the same 2-D gel).

**Statistical Analysis.** Comparisons between the two sets of the samples (i.e., control vs COM-exposed cells) of % cell death and intensity levels of corresponding protein spots were performed using unpaired Student's $t$ test. $P$-values less than 0.05 were considered statistically significant. Differentially expressed protein spots, which were statistically significant, were subjected to in-gel tryptic digestion and identification by mass spectrometry.

**In-Gel Tryptic Digestion.** The protein spots whose intensity levels significantly differed between groups were excised from 2-D gels, washed twice with 200 $\mu$L of 50% acetonitrile (ACN)/25 mM $NH_4HCO_3$ buffer (pH 8.0) at room temperature for 15 min, and then washed once with 200 $\mu$L of 100% ACN. After washing, the solvent was removed, and the gel pieces were dried by a SpeedVac concentrator (Savant; Holbrook, NY) and rehydrated with 10 $\mu$L of 1% (w/v) trypsin (Promega; Madison, WI) in 25 mM $NH_4HCO_3$. After rehydration, the gel pieces were crushed with siliconized blue stick and incubated at 37 °C for at least 16 h. Peptides were subsequently extracted twice with 50 $\mu$L of 50% ACN/5% trifluoroacetic acid (TFA); the extracted solutions were then combined and dried with the SpeedVac concentrator. The peptide pellets were resuspended with 10 $\mu$L of 0.1% TFA and purified using $ZipTip_{C18}$ (Millipore; Bedford, MA). The peptide solution was drawn up and down in the $ZipTip_{C18}$ 10 times and then washed with 10 $\mu$L of 0.1% formic acid by drawing up and expelling the washing solution three times. The peptides were finally eluted with 5 $\mu$L of 75% ACN/0.1% formic acid.

**Protein Identification by MALDI-Q-TOF MS and MS/MS Analyses.** The proteolytic samples were premixed 1:1 with the matrix solution (5 mg/mL α-cyano-4-hydroxycinnamic acid (CHCA) in 50% ACN, 0.1% (v/v) TFA and 2% (w/v) ammonium citrate) and spotted onto the 96-well sample stage. The samples were analyzed by the Q-TOF Ultima mass spectrometer (Micromass; Manchester, U.K.), which was fully automated with predefined probe motion pattern and the peak intensity threshold for switching over from MS survey scanning to MS/MS, and from one MS/MS to another. Within each sample well, parent ions that met the predefined criteria (any peak within the $m/z$ 800−3000 range with intensity above 10 count ± include/exclude list) were selected for CID MS/MS using argon as the collision gas and a mass dependent ±5 V rolling collision energy until the end of the probe pattern was reached. The LM and HM resolution of the quadrupole were both set at 10 to give a precursor selection window of about 4-Da wide. Manual acquisition and optimization for individual samples or peaks was also possible.

The instrument was externally calibrated to <5 ppm accuracy over the mass range of $m/z$ 800−3000 using a sodium iodide and PEG 200, 600, 1000 and 2000 mixtures and further adjusted with Glu-Fibrinopeptide B as the near-point lock mass calibrant during data processing. At a laser firing rate of 10 Hz, individual spectra from 5-s integration period acquired for each of the MS survey and MS/MS performed were combined,

**Table 1.** Summary of Differentially Expressed Proteins, Whose Abundance Levels Were Significantly Altered after an Exposure to 1000 μg/mL COM Crystals[a]

| spot no. | protein | NCBI[b] ID | identified by | PMF[c], MS/MS ions scores | %cov[d] (MS, MS/MS) | no. of matched peptides (MS, MS/MS) | p*I* | MW (kDa) | intensity levels (pixel unit) (mean ± SEM) control | intensity levels (pixel unit) (mean ± SEM) COM | ratio (COM/control) | *p*-values |
|---|---|---|---|---|---|---|---|---|---|---|---|---|
| 1 | 150 kDa oxygen-regulated protein precursor (Orp150) | XP_536547 | MS/MS | NA, 34 | NA, 1 | NA, 1 | 5.46 | 122.21 | 0.0155 ± 0.0098 | 0.0531 ± 0.0117 | 3.42 | 0.038 |
| 2 | Major vault protein (MVP) | XP_536910 | MS | 78, NA | 20, NA | 12, NA | 5.50 | 99.42 | 0.0498 ± 0.0050 | 0.0287 ± 0.0066 | 0.57 | 0.033 |
| 3 | Cingulin isoform CRA_b | EAW53435 | MS | 57, NA | 15, NA | 11, NA | 5.58 | 120.30 | 0.0188 ± 0.0060 | 0.0389 ± 0.0034 | 2.07 | 0.019 |
| 4 | Progesterone-induced blocking factor 1 (PIBF1) | AAL37481 | MS | 74, NA | 20, NA | 15, NA | 5.77 | 90.00 | 0.0347 ± 0.0021 | 0.0112 ± 0.0051 | 0.32 | 0.003 |
| 5 | Glutaminyl-tRNA synthetase (GlnRS) isoform 9 | XP_862570 | MS | 83, NA | 22, NA | 15, NA | 6.38 | 88.71 | 0.0291 ± 0.0037 | 0.0161 ± 0.0040 | 0.55 | 0.044 |
| 6 | 78 kDa glucose-regulated protein precursor (GRP78) isoform 5 | XP_863385 | MS | 91, NA | 26, NA | 13, NA | 5.09 | 72.25 | 0.0085 ± 0.0085 | 0.0629 ± 0.0131 | 7.40 | 0.008 |
| 7 | CG1550-PA | XP_531703 | MS, MS/MS | 119, 142 | 29, 5 | 15, 3 | 5.22 | 74.48 | 0.0738 ± 0.0059 | 0.0510 ± 0.0078 | 0.69 | 0.049 |
| 8 | Ezrin (Cytovillin) (Villin-2) isoform 5 | XP_862432 | MS, MS/MS | 104, 93 | 33, 3 | 18, 3 | 5.90 | 70.86 | 0.5208 ± 0.0462 | 0.2588 ± 0.0752 | 0.50 | 0.018 |
| 9 | Aconitase 2, mitochondrial isoform 7 | XP_858265 | MS, MS/MS | 101, 140 | 23, 5 | 15, 3 | 8.61 | 85.64 | 0.0416 ± 0.0059 | 0.0902 ± 0.0133 | 2.17 | 0.010 |
| 10 | Meningioma expressed antigen 6 (Mgea6) (Ctage5) protein | AAH24076 | MS | 73, NA | 26, NA | 11, NA | 5.17 | 65.34 | 0.0443 ± 0.0033 | 0.0269 ± 0.0053 | 0.61 | 0.024 |
| 11 | Beta tubulin | CAA43197 | MS, MS/MS | 114, 211 | 32, 7 | 20, 4 | 4.85 | 50.11 | 1.0862 ± 0.0634 | 0.6589 ± 0.0886 | 0.61 | 0.004 |
| 12 | 60 kDa heat shock protein (Hsp60) | XP_857240 | MS, MS/MS | 139, 310 | 38, 13 | 18, 5 | 5.47 | 57.84 | 0.8067 ± 0.0523 | 1.4488 ± 0.1902 | 1.80 | 0.012 |
| 13 | Cytokeratin 8 (CK 8) | XP_543639 | MS, MS/MS | 118, 120 | 40, 9 | 15, 3 | 5.94 | 49.14 | 0.0951 ± 0.0079 | 0.0093 ± 0.0086 | 0.10 | <0.001 |
| 14 | ATP synthase, H+ transporting, mitochondrial F1 complex, alpha subunit precursor | NP_004037 | MS/MS | NA, 142 | NA, 7 | NA, 3 | 9.16 | 59.83 | 0.0672 ± 0.0117 | 0.0333 ± 0.0050 | 0.50 | 0.029 |
| 15 | Hypothetical protein LOC533555 | NP_001095628 | MS | 71, NA | 23, NA | 12, NA | 7.02 | 63.12 | 0.0287 ± 0.0024 | 0.0442 ± 0.0051 | 1.54 | 0.026 |
| 16 | Cytokeratin 7 (CK 7) | XP_534795 | MS, MS/MS | 82, 36 | 28, 2 | 11, 1 | 6.21 | 51.65 | 0.0356 ± 0.0073 | 0.0683 ± 0.0120 | 1.92 | 0.047 |
| 17 | Cyclin A1 | XP_600212 | MS | 54, NA | 23, NA | 7, NA | 5.73 | 48.16 | 0.0437 ± 0.0041 | 0.0131 ± 0.0064 | 0.30 | 0.004 |
| 18 | Alpha enolase (Enolase 1) isoform 9 | XP_859439 | MS, MS/MS | 119, 180 | 37, 7 | 13, 3 | 6.63 | 47.68 | 0.5842 ± 0.0273 | 0.3343 ± 0.0604 | 0.57 | 0.005 |
| 19 | Unidentified | – | – | – | – | – | – | – | 0.0990 ± 0.0124 | 0.2176 ± 0.0417 | 2.20 | 0.026 |
| 20 | Alpha-centractin (centractin) (Actin-related protein) | XP_001499674 | MS, MS/MS | 58, 61 | 26, 6 | 7, 2 | 6.40 | 48.86 | 0.0858 ± 0.0059 | 0.0606 ± 0.0089 | 0.71 | 0.046 |
| 21 | Tu translation elongation factor (EF-Tu), mitochondrial | XP_536924 | MS, MS/MS | 139, 349 | 38, 13 | 18, 5 | 9.03 | 63.60 | 0.2163 ± 0.0176 | 0.3604 ± 0.0552 | 1.67 | 0.038 |
| 22 | Stomatin-like protein 2 (SLP-2) isoform 1 | XP_531986 | MS, MS/MS | 47, 108 | 22, 12 | 7, 3 | 6.88 | 38.66 | 0.0692 ± 0.0033 | 0.0841 ± 0.0054 | 1.22 | 0.046 |
| 23 | Elongation factor 1 (EF-1 delta) isoform 3 | XP_856555 | MS, MS/MS | 61, 104 | 33, 16 | 6, 3 | 4.94 | 30.328 | 0.1489 ± 0.0222 | 0.0749 ± 0.0168 | 0.50 | 0.029 |
| 24 | Annexin A1 (Anx I) (Lipocortin I) (Calpactin II) | XP_533524 | MS, MS/MS | 141, 289 | 49, 16 | 13, 4 | 5.84 | 38.887 | 0.5712 ± 0.0439 | 0.3555 ± 0.0742 | 0.62 | 0.037 |
| 25 | Casein kinase 1 (CK1), delta isoform 2 | XP_533137 | MS | 63, NA | 27, NA | 11, NA | 9.54 | 45.39 | 0.0555 ± 0.0150 | 0.2040 ± 0.0339 | 3.68 | 0.004 |
| 26 | Nebulin-related anchoring protein (NRAP) isoform C | NP_006166 | MS | 76, NA | 15, NA | 21, NA | 9.25 | 193.79 | 0.0884 ± 0.0150 | 0.3783 ± 0.0839 | 4.28 | 0.009 |
| 27 | Branched-chain-amino-acid aminotransferase (BCAT(m)) (placenta protein 18) (PP18) | XP_541509 | MS | 47, NA | 20, NA | 8, NA | 7.14 | 44.93 | 0.1139 ± 0.0137 | 0.1711 ± 0.0130 | 1.50 | 0.016 |
| 28 | Alpha-N-acetylgalactosaminide alpha-2,6-sialyltransferase 5 (GalNAc alpha-2,6-sialyltransferase V) | XP_345319 | MS | 56, NA | 30, NA | 8, NA | 8.53 | 43.79 | 0.0789 ± 0.0200 | 0.0045 ± 0.0045 | 0.06 | 0.007 |
| 29 | Heterogeneous nuclear ribonucleoprotein H3 (hnRNP-H3) isoform 6 | XP_860502 | MS, MS/MS | 56, 59 | 40, 4 | 8, 1 | 6.37 | 38.76 | 0.0504 ± 0.0049 | 0.0242 ± 0.0064 | 0.48 | 0.012 |

**Table 1.** Continued

| spot no. | protein | NCBI[b] ID | identified by | PMF[c], MS/MS ions scores | %cov[d] (MS, MS/MS) | no. of matched peptides (MS, MS/MS) | p*I* | MW (kDa) | intensity levels (pixel unit) (mean ± SEM) control | intensity levels (pixel unit) (mean ± SEM) COM | ratio (COM/control) | *p*-values |
|---|---|---|---|---|---|---|---|---|---|---|---|---|
| 30 | Mitochondrial import receptor subunit TOM40 homologue (translocase of outer membrane 40 kDa subunit homologue) isoform 1 (TOMM40) | XP_852633 | MS/MS | NA, 96 | NA, 7 | NA, 2 | 6.79 | 37.99 | 0.0838 ± 0.0097 | 0.1444 ± 0.0238 | 1.72 | 0.046 |
| 31 | Proteasome subunit p42 | BAA11338 | MS, MS/MS | 114, 37 | 41, 3 | 15, 1 | 7.10 | 44.42 | 0.0871 ± 0.0062 | 0.0416 ± 0.0143 | 0.48 | 0.019 |
| 32 | Ubiquinol-cytochrome-c reductase complex core protein 2, mitochondrial precursor (Complex III subunit II) isoform 1 | XP_536942 | MS, MS/MS | 44, 81 | 23, 7 | 8, 2 | 9.04 | 48.41 | 0.1203 ± 0.0182 | 0.2232 ± 0.0402 | 1.86 | 0.048 |
| 33 | Fructose-bisphosphate aldolase A (aldolase A) isoform 2 | XP_849434 | MS, MS/MS | 107, 100 | 37, 13 | 13, 3 | 8.30 | 39.94 | 0.3415 ± 0.0411 | 0.0665 ± 0.0202 | 0.19 | <0.001 |
| 34 | Aspartate aminotransferase (AST) isoform 2 | XP_851273 | MS, MS/MS | 77, 28 | 30, 3 | 10, 1 | 9.10 | 43.76 | 0.0080 ± 0.0080 | 0.0978 ± 0.0281 | 12.25 | 0.015 |
| 35 | Eukaryotic translation initiation factor C2, 2 protein (Eif2c2) isoform 2 | XP_001143064 | MS | 69, NA | 26, NA | 11, NA | 9.29 | 56.53 | 0.0601 ± 0.0079 | 0.1464 ± 0.0193 | 2.44 | 0.003 |
| 36 | Cell division cycle 2 (CDC2), G1 to S and G2 to M | AAI10152 | MS | 68, NA | 38, NA | 7, NA | 8.38 | 34.06 | 0.1975 ± 0.0131 | 0.3729 ± 0.0729 | 1.89 | 0.045 |
| 37 | Annexin A8 (Anx VIII) (Vascular anticoagulant-beta) isoform 1 | XP_536412 | MS, MS/MS | 159, 97 | 63, 6 | 17, 2 | 5.53 | 36.83 | 0.1547 ± 0.0176 | 0.0977 ± 0.0130 | 0.63 | 0.031 |
| 38 | Uridine phosphorylase 1 (UPP1) | XP_537889 | MS, MS/MS | 85, 53 | 39, 11 | 10, 2 | 6.59 | 34.50 | 0.1722 ± 0.0267 | 0.3016 ± 0.0361 | 1.75 | 0.020 |
| 39 | Porin | AAA60145 | MS, MS/MS | 74, 171 | 35, 19 | 7, 3 | 5.87 | 35.62 | 0.0675 ± 0.0107 | 0.2257 ± 0.0490 | 3.34 | 0.014 |
| 40 | Proteasome alpha 1 subunit | XP_001379009 | MS, MS/MS | 69, 147 | 36, 15 | 8, 3 | 7.64 | 33.61 | 0.1166 ± 0.0095 | 0.0717 ± 0.0127 | 0.62 | 0.022 |
| 41 | Unnamed protein product | BAC05344 | MS | 70, NA | 37, NA | 8, NA | 5.91 | 31.63 | 0.2460 ± 0.0255 | 0.1514 ± 0.0234 | 0.62 | 0.026 |
| 42 | Adenylate kinase isoenzyme 2 (Ak2) | XP_535321 | MS, MS/MS | 43, 61 | 36, 7 | 7, 2 | 6.54 | 26.78 | 0.0682 ± 0.0139 | 0.1218 ± 0.0126 | 1.78 | 0.021 |
| 43 | Rho GDP dissociation inhibitor alpha (RhoGDI alpha) | XP_849933 | MS, MS/MS | 112, 90 | 63, 19 | 13, 3 | 5.12 | 23.44 | 0.2278 ± 0.0134 | 0.1255 ± 0.0210 | 0.55 | 0.003 |
| 44 | Peroxiredoxin 3 (PRDX3) | NP_776857 | MS/MS | NA, 114 | NA, 9 | NA, 2 | 7.15 | 28.41 | 0.1159 ± 0.0056 | 0.0667 ± 0.0137 | 0.58 | 0.011 |
| 45 | Triosephosphate isomerase (TIM) isoform 5 | XP_867371 | MS, MS/MS | 55, 89 | 40, 16 | 6, 2 | 8.29 | 23.18 | 0.2064 ± 0.0242 | 0.0452 ± 0.0205 | 0.22 | 0.001 |
| 46 | Phosphatidylethanolamine binding protein 1 (PEBP1) | NP_001041557 | MS | 67, NA | 50, NA | 7, NA | 7.10 | 21.08 | 0.1870 ± 0.0167 | 0.0866 ± 0.0199 | 0.46 | 0.005 |
| 47 | Transgelin 2 (TAGLN2) | NP_003555 | MS, MS/MS | 78, 7 | 38, 7 | 10, 1 | 8.41 | 22.55 | 0.7400 ± 0.1872 | 0.2654 ± 0.0657 | 0.36 | 0.044 |
| 48 | Heterogeneous nuclear ribonucleoprotein M isoform (hnRNP-M) isoform 12 | XP_868371 | MS | 61, NA | 24, NA | 12, NA | 8.74 | 75.93 | 0.0289 ± 0.0078 | 0.1182 ± 0.0151 | 4.09 | 0.001 |
| 49 | Eukaryotic translation initiation factor 5A-1 (eIF-5A1) | P10160 | MS, MS/MS | 40, 101 | 43, 8 | 7, 2 | 5.08 | 16.98 | 0.4196 ± 0.0478 | 0.2217 ± 0.0336 | 0.53 | 0.010 |
| 50 | TGF beta receptor type I (TGFR1) | BAC66064 | MS | 69, NA | 57, NA | 5, NA | 6.36 | 13.86 | 0.1719 ± 0.0169 | 0.3219 ± 0.0545 | 1.87 | 0.030 |
| 51 | Ribosomal protein L12 (RPL12) isoform 1 | XP_001143119 | MS/MS | NA, 48 | NA, 30 | NA, 2 | 9.15 | 14.60 | 0.1729 ± 0.0250 | 0.2618 ± 0.0269 | 1.51 | 0.042 |
| 52 | Polyubiquitin | XP_851119 | MS/MS | NA, 86 | NA, 19 | NA, 2 | 5.31 | 12.82 | 0.1408 ± 0.0166 | 0.2519 ± 0.0135 | 1.79 | 0.001 |
| 53 | Peptidylprolyl isomerase A (PPIA) | BAC56500 | MS, MS/MS | 77, 178 | 47, 29 | 6, 3 | 8.46 | 17.09 | 0.9448 ± 0.1487 | 0.5269 ± 0.0932 | 0.56 | 0.044 |

[a] These altered proteins were then identified by Q-TOF MS and/or MS/MS analyses. NA = Not applicable. [b] NCBI = National Center for Biotechnology Information. [c] PMF = Peptide mass fingerprinting. [d] %Cov = %Sequence coverage [(number of the matched residues/total number of residues in the entire sequence) × 100%].

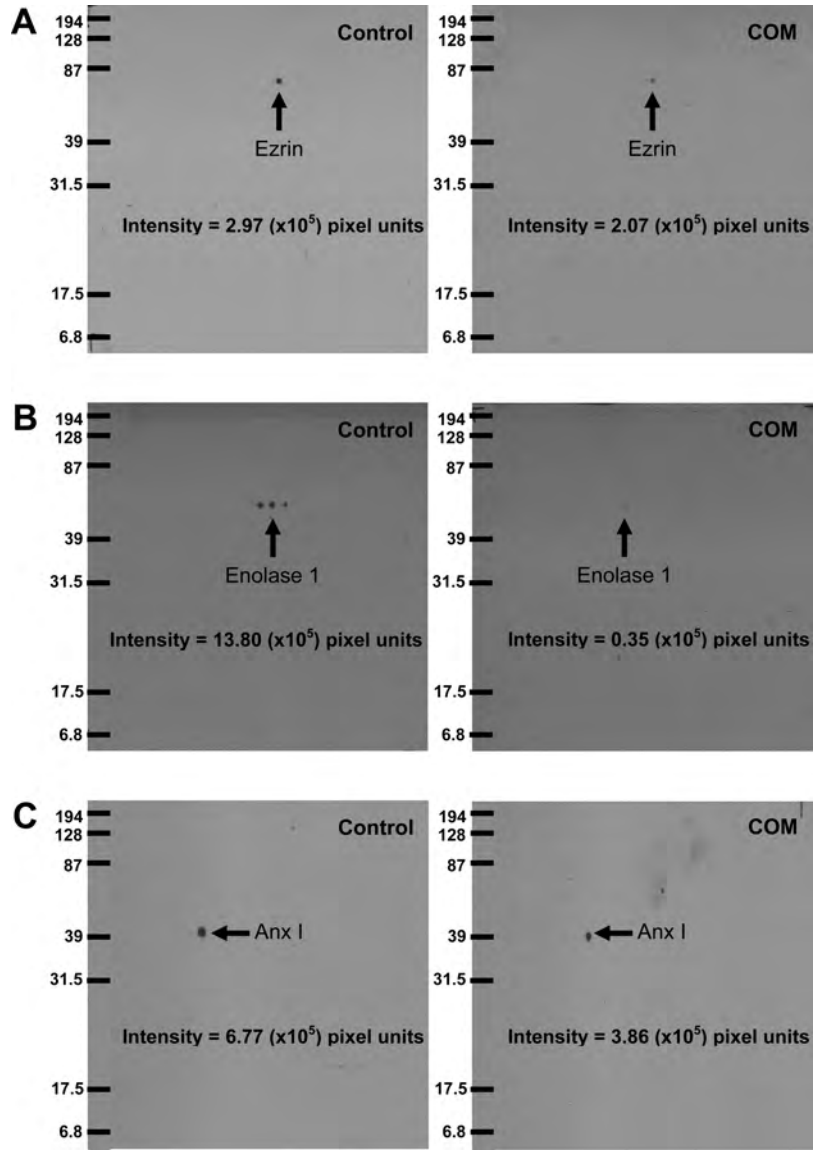


**Figure 4.** Validation of the proteomic data by 2-D Western blot analysis. Proteins derived from MDCK cells (100 $\mu$g of total protein for each sample; extraction was performed as for 2-DE analysis) were resolved with 2-DE and transferred onto nitrocellulose membranes. After blocking nonspecific bindings, the membranes were incubated with mouse polyclonal anti-ezrin (A), rabbit polyclonal anti-enolase 1 (B), and mouse monoclonal anti-Anx I (C) primary antibodies, and then with their respective secondary antibodies conjugated with horseradish peroxidase. Immunoreactive protein spots were then visualized with chemiluminescence substrate.

smoothed, deisotoped (fast option) and centroided using the ProteinLynx GlobalSERVER 2.0 data processing software (Micromass). The MS and MS/MS data were extracted and outputted as the searchable *.txt* and *.pkl* files, respectively, for independent searches using the public MASCOT search engine (http://www.matrixscience.com). The data were searched against the NCBI mammalian protein database (with approximately $5.7 \times 10^6$ entries) assuming that peptides were monoisotopic. Fixed modification was carbamidomethylation at cysteine residues, whereas variable modification was oxidation at methionine residues. Only 1 missed trypsin cleavage was allowed, and peptide mass tolerances of 100 and 50 ppm were allowed for peptide mass fingerprinting and MS/MS ions search, respectively.

**2-D Western Blotting.** To confirm the results of MS and/or MS/MS protein identification, 2-D Western blot analysis was performed. Proteins derived from MDCK cells (100 $\mu$g of total protein for each sample; extraction was performed as for 2-DE analysis) were resolved by 2-DE (as described above) and transferred onto nitrocellulose membranes (Whatman, Dassel, Germany) using a semidry transfer apparatus (Bio-Rad, Milano, Italy) at 75 mA for 1 h. Nonspecific bindings were blocked with 5% milk in PBS at room temperature for 1 h. The membranes were then incubated with mouse polyclonal anti-ezrin (1:500 in 5% milk/PBS) (Santa Cruz Biotechnology, Inc., Santa Cruz, CA), rabbit polyclonal anti-enolase 1 (1:200 in 5% milk/PBS) (Santa Cruz Biotechnology, Inc.) and mouse monoclonal anti-Anx I (1:500 in 5% milk/PBS) (CHEMICON International, Inc., Temecula, CA) primary antibodies at 4 °C overnight. After washing, the membranes were further incubated with respective secondary antibodies conjugated with horseradish peroxidase (with dilutions of 1:2000 to 1:5000 in 5% milk/PBS) at room temperature for 1 h. Immunoreactive protein spots were then visualized with SuperSignal West Pico chemiluminescence substrate (Pierce Biotechnology, Inc., Rockford, IL).

**Table 2.** Functional Roles and Subcellular Localizations of the Altered Proteins Identified from the COM-Exposed MDCK Cells[a]

| altered proteins | subcellular localization | function |
|---|---|---|
| *Proteins Whose Abundance Levels Were Significantly Increased during COM Crystal Adhesion* | | |
| Aconitase2, mitochondrial isoform 7 | Mitochondria | Metabolic enzyme |
| Ak 2 isoform 1 | Mitochondrial intermembrane space | Metabolic enzyme |
| AST isoform 2 | Mitochondria | Metabolic enzyme |
| BCAT(m) | Mitochondria | Metabolic enzyme |
| CDC2 | Nucleus | Metabolic enzyme |
| Cingulin isoform CRA_b | Tight junction | Cellular structure |
| CK1delta isoform 2 | Cytosol-Golgi and ER-Golgi transport vesicles | Vesicular trafficking |
| CK7 | Intermediate filament | Cellular structure |
| EF-Tu | Cytoplasm | Protein biosynthesis |
| Eif2c2 isoform 2 | Cytoplasm | Protein biosynthesis |
| GRP78 | ER | Chaperone |
| hnRNP-M, a isoform 12 | Nucleus | RNA metabolism |
| Hsp60 | Mitochondria | Chaperone |
| NRAP isoform C | Cell membrane | Cellular structure |
| Orp150 | ER | Chaperone |
| Polyubiquitin | Cytoplasm | Protein degradation |
| Porin | Cell membrane | Channel |
| RPL 12 isoform 1 | Large ribosomal subunit | Translation |
| SLP-2 isoform 1 | Cell membrane | Cellular structure |
| TGFR1 | Cell membrane | Receptor for TGF-beta |
| TOMM40 isoform 1 | Mitochondrial outer membrane | Import of protein precursors |
| Ubiquinol-cytochrome-c reductase | Mitochondria | Metabolic enzyme |
| UPP1 | Cytoplasm | Metabolic enzyme |
| Proteins Whose Abundance Levels Were Significantly Decreased during COM Crystal Adhesion | | |
| Annexin A8 isoform 1 | Cell membrane | Signal transduction |
| Annexin A1 | Cell membrane | Signal transduction |
| ATP synthase alpha subunit precursor | Mitochondria | ATP synthesis |
| Beta tubulin | Microtubule | Cellular structure |
| Centractin (Actin-related protein) | Associated with centrosome, cytosol | Cellular structure |
| CG1550-PA | Cytoplasm | Metabolic enzyme |
| CK8 | Intermediate filament | Cellular structure |
| Cyclin A1 | Nucleus | Cell cycle regulator |
| EF-1, delta isoform 3 | Cytoplasm | Protein biosynthesis |
| eIF-5A1 | Cytoplasm | Protein biosynthesis |
| Enolase 1 | Cytoplasm | Metabolic enzyme |
| Ezrin isoform 5 | Cell membrane | Cellular structure |
| Fructose-bisphosphate aldolase A isoform 2 | Cytoplasm | Metabolic enzyme |
| GalNAc alpha-2,6-sialyltransferase | Golgi apparatus membrane | Metabolic enzyme |
| GlnRS isoform 9 | Cytoplasm | Protein biosynthesis |
| hnRNP-H3, a isoform 6 | Nucleus | RNA metabolism |
| Mgea6 (Ctage5) protein | Cell membrane | Signal transduction |
| MVP | Nucleus/Cytosol | Nucleocytoplasmic transport |
| PEBP1 | Cytoplasm | Signal transduction |
| PIBF1 | Nucleus | Immune response |
| PPIA | Cytoplasm | Protein biosynthesis |
| PRDX3 | Mitochondrial membrane | Antioxidant enzyme |
| Proteasome alpha 1 subunit | Cytoplasm | Protein degradation |
| Proteasome subunit p42 | Cytoplasm | Protein degradation |
| RhoGDI alpha | Cytoplasm | Inhibitor of Rho protein degradation |
| TAGLN2 | Cytoplasm | Cellular structure |
| TIM isoform 5 | Cytoplasm | Metabolic enzyme |

[a] Three altered proteins: hypothetical protein (spot no. 15), unnamed protein product (spot no. 41), and unidentified protein (spot no. 19), of which function remains unknown are not included.

## Results

Approximately 3-million MDCK cells were inoculated in each culture flask and maintained for 24 h. A total of 10 semiconfluent flasks were then divided into two groups ($n = 5$ per group) and the culture medium was replaced by either COM-containing (with 1000 $\mu$g/mL COM crystals) or COM-free medium. The cells were grown further for 48 h. Crystal adhesion on the cell surface was clearly demonstrated using phase-contrast microscopy (Figure 1A) and SEM (Figure 1B). These crystals adhered tightly onto the cells as they remained adherent even after several washes with PBS. Interestingly, the borders of these crystals became blurred or interrupted, which indicated cell−crystal interactions. In a parallel experiment, time-course cell death assay using annexin V/propidium iodide double staining showed that % cell death was gradually increased in MDCK cells exposed to COM crystals. At 48 h, % cell death was significantly greater in the COM-exposed MDCK cells compared to the control MDCK cells (28.04 ± 0.89 vs 16.71 ± 1.89%, $p < 0.001$) (Figure 2).

After the culture with or without COM crystals for 48 h, MDCK cells were harvested from individual flasks and cellular proteins from each flask were extracted and resolved in each 2-D gel ($n = 5$ gels per group). The resolved proteins were then visualized by SYPRO Ruby fluorescence stain and the visualized spots were analyzed by Image Master 2D Platinum (GE Healthcare) software, as detailed in Materials and Methods. From approximately 1200−1400 spots visualized in each 2-D gel, quantitative intensity analysis and statistics revealed significant changes in abundance levels of totally 53 protein spots in the COM-exposed cells (Figure 3). These altered proteins were then identified by Q-TOF MS (peptide mass fingerprinting; PMF) and/or MS/MS (peptide sequencing). Table 1 summarizes

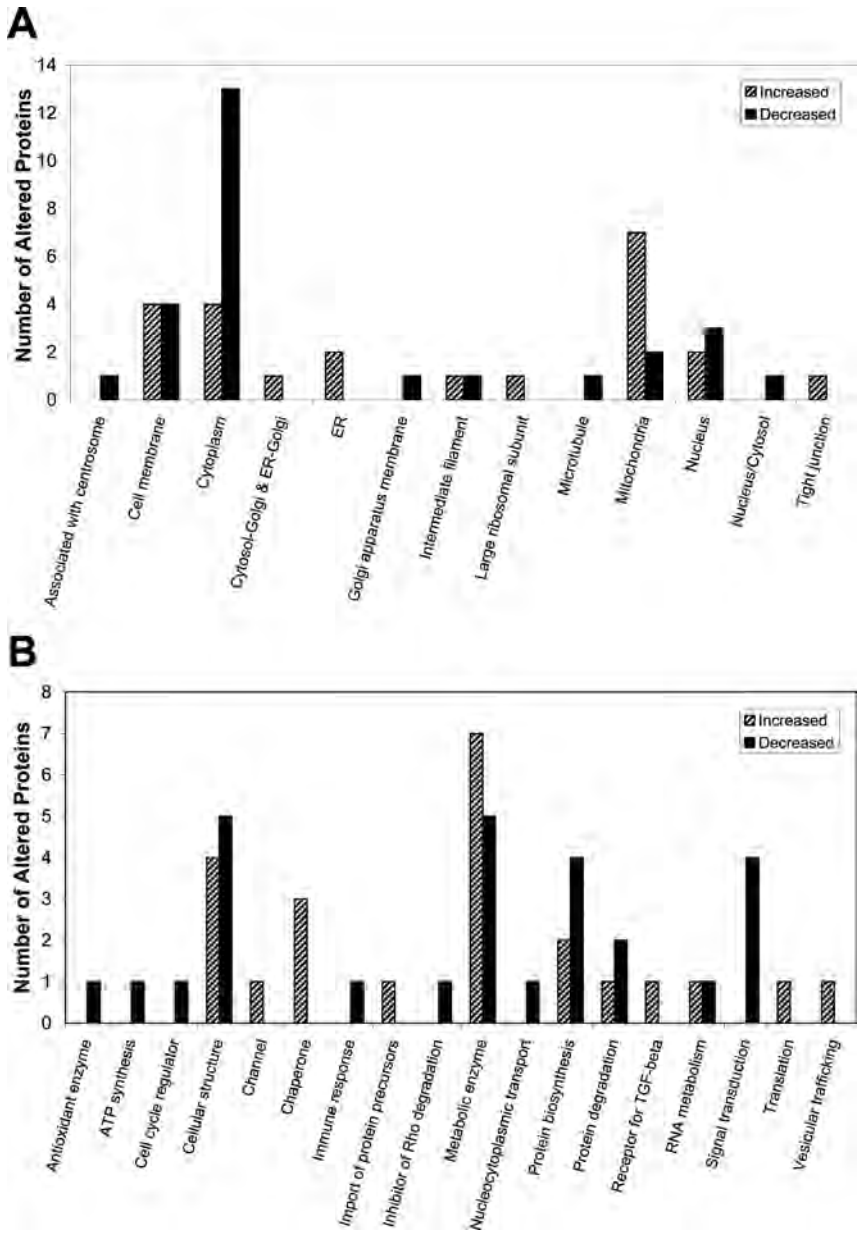


**Figure 5.** Numbers of the altered proteins in MDCK cells treated with COM crystals (1000 $\mu$g/mL) with respect to individual subcellular compartments (A) and functional categories (B).

identities, identification scores and other information related to protein identification and changes in their abundance levels. 2-D Western blot analysis was performed on randomly selected altered proteins to confirm the proteomic data. Figure 4 illustrates that the decreased levels in ezrin, enolase 1, and annexin A1 (Anx I) were clearly confirmed by 2-D Western blot analysis.

In addition, bioinformatic analysis using the Swiss-Prot protein knowledgebase and TrEMBL computer-annotated supplement to Swiss-Prot (http://www.expasy.org/sprot/) was performed to obtain additional information (specifically, subcellular localization and functional significance) of the altered proteins; (Table 2). Numbers of the altered proteins, with respect to individual subcellular compartments and functional categories, are summarized in Figure 5, panels A and B, respectively.

## Discussion

We demonstrated that COM crystals could adhere tightly to MDCK cells with subsequent detrimental effects to the cells (Figures 1 and 2). Exposure to COM crystals for 48 h (which might be considered as an acute phase response *in vivo*) caused increased cell death and alterations in abundance levels of several cellular proteins (25 proteins were increased, whereas other 28 were decreased). These data clearly indicate that COM crystals are toxic to distal renal tubular cells. Table 2 provides functional insights and subcellular localizations of these altered proteins. Regarding function, proteins involved in metabolic enzymatic pathways were mostly affected (7 proteins were increased, whereas 5 were decreased) (Figure 5B). The second and third most common functional groups affected by COM-induced toxicity included those involved in cell structure and cytoskeletal assembly (4 proteins were increased, whereas 5

were decreased) and those involved in protein biosynthesis (2 proteins were increased, whereas 4 were decreased), respectively (Figure 5B). Regarding subcellular localization, the most affected compartment was cytoplasm (4 proteins were increased, whereas 13 were decreased) (Figure 5A). Mitochondria (7 proteins were increased, whereas 2 were decreased) and cell membrane (4 proteins were increased, whereas 4 were decreased) were the second and third most common compartments, respectively, affected by COM-induced toxicity (Figure 5A). Our data on subcellular compartments of renal tubular cells that were frequently affected by COM crystal-induced toxicity were consistent with those reported in other previous studies.[12,20,21] The functional significance and potential roles of some of these altered proteins in the renal tubular toxicity induced by COM crystals are highlighted as follows.

Three chaperones (GRP78, Orp150 and Hsp60) had increased levels in MDCK cells after the exposure to COM crystals. GRP78 (or immunoglobulin-binding protein, BiP) is an ER luminal chaperone that can be activated by unfolded/misfolded proteins in the ER.[22] Orp150, another ER chaperone, belongs to Hsp70 family and can be triggered by oxygen deprivation or hypoxia.[23] While GRP78 and Orp150 are ER chaperones, Hsp60 (or mitochondrial matrix protein P1) is a mitochondrial chaperone that can prevent misfolding of proteins and promote refolding and proper assembly of unfolded/misfolded proteins in the mitochondrial matrix.[24] Numerous studies have demonstrated an important role of these chaperones in defense mechanism against cellular toxicity and apoptosis.[23,25−31] Our present study identified increased levels of these three chaperones in response to COM crystal adhesion, suggesting that their increases might be for protecting further cellular damage induced by COM crystals. However, the time-course cell death study implicated that their increases were not sufficient to protect COM crystal-induced cellular injury as the cell death was progressively increased when the exposure time was prolonged (Figure 2) and there were too many detrimental changes in cellular proteins that counterbalanced and finally overcame the protecting effects of these three chaperones (Table 2 and Figure 5B).

COM crystals caused several detrimental effects in MDCK cells. In particular, four proteins involved in protein biosynthesis [glutaminyl-tRNA synthetase (GlnRS) isoform 9, elongation factor 1 (EF-1) delta isoform 3, eukaryotic translational initiator factor 5A-1 (eIF-5A1), and peptidylprolyl isomerase A (PPIA)], a protein involved in ATP synthesis (ATP synthase alpha subunit precursor), and a cellular cycle regulator (cyclin A1) were significantly decreased after the exposure to COM crystals. These detrimental changes might clearly explain the reason that the three chaperones with increased levels (GRP78, Orp150 and Hsp60) could not completely protect the cells from further injury or apoptosis/necrosis induced by COM crystal adhesion.

Moreover, several proteins involved in cellular structure [beta tubulin, centractin, cytokeratin 8 (CK8), ezrin isoform 5, and transgelin 2 (TAGLN2)] were also decreased. While tubulin[32,33] and centractin[34,35] are very important for cell cycle and division, ezrin[36−38] and transgelin 2[39,40] are essential for other several cellular functions. The decreases in these proteins involved in cellular structure can definitely reduce cell integrity and also induce cellular vulnerability to stimuli or toxicants. Ezrin (also known as p81, cytovillin and villin-2) is a PDZ-domain phosphoprotein, belongs to an ezrin/radixin/moesin (ERM) family, and is a linker protein for the association between plasma membrane and actin cytoskeleton assembly.[36] These ERM proteins govern cellular function through the Rho GTPase pathway.[41,42] Ezrin also participates in other signal transduction pathways.[37,38] Additionally, our data also showed the coordinated changes in several proteins involved in signal transduction, including RhoGDI alpha, meningioma expressed antigen 6 (Mgea6), annexin A1 (Anx I), annexin A8 (Anx VIII) isoform 1, and phosphatidyl ethanolamine binding protein 1 (PEBP1), all of which were also decreased. All these decreases were likely to worsen the cellular toxicity induced by COM crystals.

While several proteins involved in cellular structure and cytoskeletal assembly were decreased, some of these proteins on the other hand were increased. The mechanism underlying these disparate results remains unclear. Interestingly, most of these increased cellular structure proteins were plasma membrane [nebulin-related anchoring protein (NRAP) isoform C, and stomatin-like protein 2 (SLP-2) isoform 1] and tight junction (cingulin isoform CRA_b) proteins. Perhaps, these proteins might play important role in facilitating crystal binding or serve as adhesion molecules to bind with COM crystals. However, further investigation is required to confirm our hypothesis.

Interestingly, one antioxidative protein [peroxiredoxin 3 (PRDX3)] was significantly decreased during COM crystal adhesion. PRDX3 is a mitochondrial protein involved in the redox pathway and can protect cells from oxidative damage. Its reduction can decline the threshold of cells to the oxidative stress.[43] This finding was consistent with the results reported in previous studies, which indicated that COM can induce oxidative damage to renal tubular epithelial cells.[44−46] The decrease in PRDX3 might explain tubular oxidative injury induced by COM crystals.

It should be noted that we evaluated changes in the cellular proteome in MDCK cells after 48-h exposure to a high dose (1000 $\mu$g/mL) of COM crystals. Although we successfully identified several proteins that were altered in this setting, evaluation of changes in the cellular proteome induced by lower doses of COM crystals and at earlier time-points would lead to an understanding of "early responses" in distal renal tubular cells during cell−crystal interactions. Moreover, the study of proteome changes in proximal renal tubular cells would provide more insights into the molecular mechanisms of COM crystal-induced tubulotoxicity.

In summary, we successfully identified a set of proteins in MDCK cells that were altered by COM crystal-induced toxicity. Alterations in several of these proteins could explain the mechanistic pathways of COM crystal-induced toxicity in renal tubular epithelial cells. However, the functional significance of some altered proteins remains unclear and should be further elucidated to better understand the detrimental changes and adaptive responses in these cells during COM crystal adhesion, and to unravel the pathogenic mechanisms of kidney stone disease.

**Abbreviations:** 2-DE, two-dimensional electrophoresis; ACN, acetonitrile; Ak2, adenylate kinase isoenzyme 2; Anx I, annexin A1; Anx VIII, annexin A8; AST, aspartate aminotransferase; BCAT(m), branched-chain-amino-acid aminotransferase; CDC2, cell division cycle 2; CHAPS, 3-[(3-cholamidopropyl) dimethylamino]-1-propanesulfonate; CHCA, cyano-4-hydroxycinnamic acid; CK1, casein kinase 1; CK 7, cytokeratin 7; CK 8, cytokeratin 8; COM, calcium oxalate monohydrate; DTT, dithiothreitol; EDTA, ethylene diamine tetraacetic acid; EF-1, elongation factor 1; EF-Tu, Tu translation elongation factor; Eif2c2, eukaryotic

translation initiation factor C2, 2 protein; eIF-5A1, eukaryotic translation initiation factor 5A-1; FBS, fetal bovine serum; GalNAG, alpha-*N*-acetylgalactosaminide; GlnRS, glutaminyl-tRNA synthetase; GRP78, 78 kDa glucose-regulated protein; hnRNP-H3, heterogeneous nuclear ribonucleoprotein H3; hnRNP-M, heterogeneous nuclear ribonucleoprotein M isoform; Hsp60, 60 kDa heat shock protein; IEF, isoelectric focusing; MDCK, Madin-Darby Canine Kidney; MEM, Eagle's minimum essential medium; Mgea6, meningioma expressed antigen 6; MS, mass spectrometry; MS/MS, tandem mass spectrometry; MVP, major vault protein; NRAP, nebulin-related anchoring protein; Orp150, 150 kDa oxygen-regulated protein precursor; PEBP1, phosphatidylethanolamine binding protein 1; PIBF1, progesterone-induced blocking factor 1; PMF, peptide mass fingerprinting; PPIA, peptidylprolyl isomerase A; PRDX3, peroxiredoxin 3; Q-TOF, quadrupole time-of-flight; RhoGDI alpha, Rho GDP dissociation inhibitor alpha; RPL12, ribosomal protein L12; SEM, scanning electron microscopy; SLP-2, stomatin-like protein 2; TAGLN2, transgelin 2; TFA, trifluoroacetic acid; TGFR1, TGF beta receptor type I; TIM, triosephosphate isomerase; TOMM40, translocase of outer membrane 40 kDa subunit; UPP1, uridine phosphorylase 1; UPR, unfolded protein response.

**Acknowledgment.** This study was supported by The Thailand Research Fund, Commission on Higher Education, Mahidol University, the National Research Council of Thailand, Siriraj Grant for Research and Development, and the National Center for Genetic Engineering and Biotechnology (to V. Thongboonkerd), and by Siriraj Graduate Thesis Scholarship (to T. Semangoen). We are also grateful to the Core Facilities for Proteomics and Structural Biology Research, Institute of Biological Chemistry, Academia Sinica, Taiwan.

## References

(1) Coe, F. L.; Evan, A.; Worcester, E. Kidney stone disease. *J. Clin. Invest.* **2005**, *115*, 2598–2608.
(2) Amato, M.; Lusini, M. L.; Nelli, F. Epidemiology of nephrolithiasis today. *Urol. Int.* **2004**, *72 Suppl 1*, 1–5.
(3) Schubert, G. Stone analysis. *Urol. Res.* **2006**, *34*, 146–150.
(4) Sheng, X.; Ward, M. D.; Wesson, J. A. Crystal surface adhesion explains the pathological activity of calcium oxalate hydrates in kidney stone formation. *J. Am. Soc. Nephrol.* **2005**, *16*, 1904–1908.
(5) Rabinovich, Y. I.; Esayanur, M.; Daosukho, S.; Byer, K. J.; El Shall, H. E.; Khan, S. R. Adhesion force between calcium oxalate monohydrate crystal and kidney epithelial cells and possible relevance for kidney stone formation. *J. Colloid Interface Sci.* **2006**, *300*, 131–140.
(6) Khan, S. R. Crystal-induced inflammation of the kidneys: results from human studies, animal models, and tissue-culture studies. *Clin. Exp. Nephrol.* **2004**, *8*, 75–88.
(7) Khan, S. R.; Byer, K. J.; Thamilselvan, S.; Hackett, R. L.; McCormack, W. T.; Benson, N. A.; Vaughn, K. L.; Erdos, G. W. Crystal-cell interaction and apoptosis in oxalate-associated injury of renal epithelial cells. *J. Am. Soc. Nephrol.* **1999**, *10 Suppl 14*, S457−S463.
(8) Asselman, M.; Verhulst, A.; De Broe, M. E.; Verkoelen, C. F. Calcium oxalate crystal adherence to hyaluronan-, osteopontin-, and CD44-expressing injured/regenerating tubular epithelial cells in rat kidneys. *J. Am. Soc. Nephrol.* **2003**, *14*, 3155–3166.
(9) Muthukumar, A.; Selvam, R. Renal injury mediated calcium oxalate nephrolithiasis: role of lipid peroxidation. *Renal Failure* **1997**, *19*, 401–408.
(10) Habibzadegah-Tari, P.; Byer, K.; Khan, S. R. Oxalate induced expression of monocyte chemoattractant protein-1 (MCP-1) in HK-2 cells involves reactive oxygen species. *Urol. Res.* **2005**, *33*, 440–447.
(11) Thamilselvan, S.; Khan, S. R.; Menon, M. Oxalate and calcium oxalate mediated free radical toxicity in renal epithelial cells: effect of antioxidants. *Urol. Res.* **2003**, *31*, 3–9.
(12) McMartin, K. E.; Wallace, K. B. Calcium oxalate monohydrate, a metabolite of ethylene glycol, is toxic for rat renal mitochondrial function. *Toxicol. Sci.* **2005**, *84*, 195–200.
(13) Khand, F. D.; Gordge, M. P.; Robertson, W. G.; Noronha-Dutra, A. A.; Hothersall, J. S. Mitochondrial superoxide production during oxalate-mediated oxidative stress in renal epithelial cells. *Free Radical Biol. Med.* **2002**, *32*, 1339–1350.
(14) Thongboonkerd, V. Proteomics in nephrology: current status and future directions. *Am. J. Nephrol.* **2004**, *24*, 360–378.
(15) Thongboonkerd, V.; Malasit, P. Renal and urinary proteomics: Current applications and challenges. *Proteomics* **2005**, *5*, 1033–1042.
(16) Thongboonkerd, V. Proteomic analysis of renal diseases: Unraveling the pathophysiology and biomarker discovery. *Expert Rev. Proteomics* **2005**, *2*, 349–366.
(17) Saier, M. H., Jr. Growth and differentiated properties of a kidney epithelial cell line (MDCK). *Am. J. Physiol.* **1981**, *240*, C106−C109.
(18) Tsujihata, M. Mechanism of calcium oxalate renal stone formation and renal tubular cell injury. *Int. J. Urol.* **2008**, *15*, 115–120.
(19) Thongboonkerd, V.; Semangoen, T.; Chutipongtanate, S. Factors determining types and morphologies of calcium oxalate crystals: Molar concentrations, buffering, pH, stirring and temperature. *Clin. Chim. Acta* **2006**, *367*, 120–131.
(20) Jonassen, J. A.; Cao, L. C.; Honeyman, T.; Scheid, C. R. Intracellular events in the initiation of calcium oxalate stones. *Nephron Exp. Nephrol.* **2004**, *98*, e61−e64.
(21) Meimaridou, E.; Jacobson, J.; Seddon, A. M.; Noronha-Dutra, A. A.; Robertson, W. G.; Hothersall, J. S. Crystal and microparticle effects on MDCK cell superoxide production: oxalate-specific mitochondrial membrane potential changes. *Free Radical Biol. Med.* **2005**, *38*, 1553–1564.
(22) Li, J.; Lee, A. S. Stress induction of GRP78/BiP and its role in cancer. *Curr. Mol. Med.* **2006**, *6*, 45–54.
(23) Ozawa, K.; Kuwabara, K.; Tamatani, M.; Takatsuji, K.; Tsukamoto, Y.; Kaneda, S.; Yanagi, H.; Stern, D. M.; Eguchi, Y.; Tsujimoto, Y.; Ogawa, S.; Tohyama, M. 150-kDa oxygen-regulated protein (ORP150) suppresses hypoxia-induced apoptotic cell death. *J. Biol. Chem.* **1999**, *274*, 6397–6404.
(24) Bukau, B.; Horwich, A. L. The Hsp70 and Hsp60 chaperone machines. *Cell* **1998**, *92*, 351–366.
(25) Miyake, H.; Hara, I.; Arakawa, S.; Kamidono, S. Stress protein GRP78 prevents apoptosis induced by calcium ionophore, ionomycin, but not by glycosylation inhibitor, tunicamycin, in human prostate cancer cells. *J. Cell Biochem.* **2000**, *77*, 396–408.
(26) Yu, Z.; Luo, H.; Fu, W.; Mattson, M. P. The endoplasmic reticulum stress-responsive protein GRP78 protects neurons against excitotoxicity and apoptosis: suppression of oxidative stress and stabilization of calcium homeostasis. *Exp. Neurol.* **1999**, *155*, 302–314.
(27) Bando, Y.; Tsukamoto, Y.; Katayama, T.; Ozawa, K.; Kitao, Y.; Hori, O.; Stern, D. M.; Yamauchi, A.; Ogawa, S. ORP150/HSP12A protects renal tubular epithelium from ischemia-induced cell death. *FASEB J.* **2004**, *18*, 1401–1403.
(28) Kitao, Y.; Ozawa, K.; Miyazaki, M.; Tamatani, M.; Kobayashi, T.; Yanagi, H.; Okabe, M.; Ikawa, M.; Yamashima, T.; Stern, D. M.; Hori, O.; Ogawa, S. Expression of the endoplasmic reticulum molecular chaperone (ORP150) rescues hippocampal neurons from glutamate toxicity. *J. Clin. Invest.* **2001**, *108*, 1439–1450.
(29) Ozawa, K.; Kondo, T.; Hori, O.; Kitao, Y.; Stern, D. M.; Eisenmenger, W.; Ogawa, S.; Ohshima, T. Expression of the oxygen-regulated protein ORP150 accelerates wound healing by modulating intracellular VEGF transport. *J. Clin. Invest.* **2001**, *108*, 41–50.
(30) Gupta, S.; Knowlton, A. A. HSP60, Bax, apoptosis and the heart. *J. Cell Mol. Med.* **2005**, *9*, 51–58.
(31) Ghosh, J. C.; Dohi, T.; Kang, B. H.; Altieri, D. C. Hsp60 regulation of tumor cell apoptosis. *J. Biol. Chem.* **2008**, *283*, 5188–5194.
(32) Verhey, K. J.; Gaertig, J. The tubulin code. *Cell Cycle* **2007**, *6*, 2152–2160.
(33) Pellegrini, F.; Budman, D. R. Review: tubulin function, action of antitubulin drugs, and new drug development. *Cancer Invest.* **2005**, *23*, 264–273.
(34) Clark, S. W.; Meyer, D. I. Centractin is an actin homologue associated with the centrosome. *Nature* **1992**, *359*, 246–250.
(35) Clark, I. B.; Meyer, D. I. Overexpression of normal and mutant Arp1alpha (centractin) differentially affects microtubule organization during mitosis and interphase. *J. Cell Sci.* **1999**, *112 (Pt 20)*, 3507–3518.
(36) Algrain, M.; Turunen, O.; Vaheri, A.; Louvard, D.; Arpin, M. Ezrin contains cytoskeleton and membrane binding domains accounting for its proposed role as a membrane-cytoskeletal linker. *J. Cell Biol.* **1993**, *120*, 129–139.

(37) Tsukita, S.; Yonemura, S. ERM (ezrin/radixin/moesin) family: from cytoskeleton to signal transduction. *Curr. Opin. Cell Biol.* **1997**, *9*, 70–75.
(38) Naba, A.; Reverdy, C.; Louvard, D.; Arpin, M. Spatial recruitment and activation of the Fes kinase by ezrin promotes HGF-induced cell scattering. *EMBO J.* **2008**, *27*, 38–50.
(39) Yu, H.; Konigshoff, M.; Jayachandran, A.; Handley, D.; Seeger, W.; Kaminski, N.; Eickelberg, O. Transgelin is a direct target of TGF-{beta}/Smad3-dependent epithelial cell migration in lung fibrosis. *FASEB J.* **2008**, *22*, 1778–1789.
(40) Shapland, C.; Hsuan, J. J.; Totty, N. F.; Lawson, D. Purification and properties of transgelin: a transformation and shape change sensitive actin-gelling protein. *J. Cell Biol.* **1993**, *121*, 1065–1073.
(41) Mackay, D. J.; Esch, F.; Furthmayr, H.; Hall, A. Rho- and rac-dependent assembly of focal adhesion complexes and actin filaments in permeabilized fibroblasts: an essential role for ezrin/radixin/moesin proteins. *J. Cell Biol.* **1997**, *138*, 927–938.
(42) D'Angelo, R.; Aresta, S.; Blangy, A.; Del Maestro, L.; Louvard, D.; Arpin, M. Interaction of ezrin with the novel guanine nucleotide exchange factor PLEKHG6 promotes RhoG-dependent apical cytoskeleton rearrangements in epithelial cells. *Mol. Biol. Cell* **2007**, *18*, 4780–4793.
(43) Mukhopadhyay, S. S.; Leung, K. S.; Hicks, M. J.; Hastings, P. J.; Youssoufian, H.; Plon, S. E. Defective mitochondrial peroxiredoxin-3 results in sensitivity to oxidative stress in Fanconi anemia. *J. Cell Biol.* **2006**, *175*, 225–235.
(44) Meimaridou, E.; Lobos, E.; Hothersall, J. S. Renal oxidative vulnerability due to changes in mitochondrial-glutathione and energy homeostasis in a rat model of calcium oxalate urolithiasis. *Am. J. Physiol.: Renal Physiol.* **2006**, *291*, F731−F740.
(45) Patel, A. B.; Robertson, W. G.; Choong, S.; Hothersall, J. S. Heat-shock protein 25 ameliorates calcium oxalate crystal-mediated oxidative stress in renal epithelial cells. *BJU Int.* **2006**, *98*, 1094–1099.
(46) Byer, K.; Khan, S. R. Citrate provides protection against oxalate and calcium oxalate crystal induced oxidative damage to renal epithelium. *J. Urol.* **2005**, *173*, 640–646.

PR8002408